Studies on ruthenium and osmium clusters containing chiral phosphorus and nitrogen compounds.

A thesis submitted to the
University of London
in partial fulfilment of the requirements for the degree of
Doctor of Philosophy

by

Marc Stchedroff

Department of Chemistry
University College London
August 1999

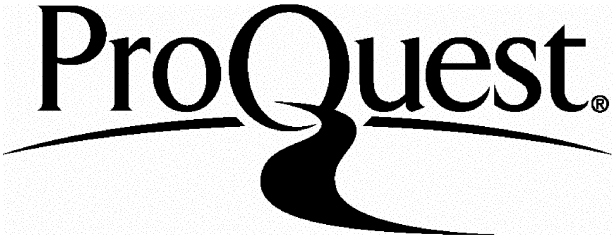

For my mother

Abstract

Ruthenium and osmium clusters containing chiral phosphorus and nitrogen compounds.

This thesis describes the synthesis, structure (based on IR, MS, NMR and XRD methods) and reactions of novel triosmium and triruthenium carbonyl clusters containing diphosphine and monophosphine ligands, several of which are chiral. Fluxional behaviour (where this is accessible) has been studied, where appropriate aided by ^{13}CO enrichment.

The ligand (R)-2,2'-bis(diphenylphosphino)-1,1'-binaphthyl (BINAP) reacts with $[Ru_3(CO)_{12}]$ in the presence of trimethylamine-*N*-oxide (Me_3NO) to form $[Ru_3(OH)_2(CO)_8(\mu\text{-BINAP})]$, rather than the expected product $[Ru_3(CO)_{10}(BINAP)]$. Direct thermal reaction of $[Ru_3(CO)_{12}]$ with BINAP leads to an orthometallated product $[Ru_3(\mu\text{-H})(CO)_9(\mu_3\text{-BINAP-H})]$. The cluster $[Ru_3(OH)_2CO)_8(\mu\text{-BINAP})]$ notably contains the first example of the important ligand BINAP bridging two metal centres and exhibits restricted rotation of two of the four phenyl groups which are graphitically aligned with the naphthyl rings (VT NMR studies). This behaviour appears to be characteristic of the bridging rather than the chelating BINAP ligand.

The ligand BINAP reacts with $[Os_3(CO)_{12}]$ to give $[Os_3(CO)_{11}(BINAP)]$, $[Os_3(CO)_{10}(BINAP)]$ and $[Os_3(\mu\text{-}H)(CO)_8(BINAP\text{-}H)]$. The product $[Os_3(CO)_{11}(BINAP)]$ exhibits dynamic exchange of two conformers (dynamic ^{31}P NMR evidence). X-ray structures are reported for $[Os_3(CO)_{11}(BINAP)]$ and $[Os_3(\mu\text{-}H)(CO)_8(BINAP\text{-}H)]$.

The 4-tolyl analogue of BINAP (tolBINAP) reacts with $[Os_3(\mu\text{-}H)_2(CO)_{10}]$ to give $[Os_3(\mu\text{-}H)_2(CO)_8(\mu\text{-}tolBINAP)]$ which was compared with the corresponding 1,2-bis(diphenylphosphino)ethane (dppe), bis(diphenylphosphino)methane (dppm) and related complexes. The X-ray structures of $[Os_3(\mu\text{-}H)_2(CO)_8(\mu\text{-}tolBINAP)]$ and $[Os_3(\mu\text{-}H)_2(CO)_8(\mu\text{-}dppm)]$ are compared in the context of the chain length of the diphosphine ligand.

(R)(+)-4-pyridylethanol reacts with $[Ru_3(CO)_{10}(MeCN)_2]$ and $[Os_3(CO)_{10}(MeCN)_2]$ to give the products $[M_3(\mu\text{-}H)(\mu\text{-}C_5H_3NCHMeOH)(CO)_{10}]$ (M = Ru or Os) formed by the orthometallation of the pyridine ring. For comparative purposes the known pyridine analogue has been reprepared. The chiral pyridine leads to a diastereomeric mixture which was separated by HPLC and analysed by NMR methods which demonstrate a rigid non-dynamic co-ordination of the organic ligand. An analogous reaction with (S)(-)-nicotine has also been studied and separation by HPLC of the two positional isomers and the diastereomers of each positional isomer achieved. All six chiral clusters prepared have been analysed by CD spectroscopy to establish their relative configurations and the determination of the X-ray structure of one isomer of

$[Os_3(\mu\text{-}H)(CO)_{10}(C_5H_3NCHMeOH)]$ has allowed their absolute stereochemistry to be determined.

The reactivities of the metal hydride in $[Os_3(\mu\text{-}H)_2(CO)_8(\mu\text{-tolBINAP})]$ has been compared with that of the parent dihydride $[Os_3(\mu\text{-}H)_2(CO)_{10}]$. In particular the ability of unsaturated molecules to add and then insert reversibly into the Os-H bonds has been assessed by the exchange of the hydride ligands with materials such as styrene-d_8 by isotope labelling methods.

A novel means of determining the chemical shifts of ^{187}Os in trinuclear osmium clusters via $^1J_{H\text{-}Os}$ and $^1J_{P\text{-}Os}$ has been developed and tested on a series of compounds at high resolution. These methods enable detection of the least sensitive spin ½ nucleus in sample sizes of 50 mg in reasonable experimental times of less than one hour on relatively standard equipment. Significant chemical shift differences have been observed. These methods have only previously been attempted with mononuclear species.

Contents

Acknowledgements

I would like to thank my supervisor Professor A. J. Deeming for his help, guidance and support during the course of this research. I would also like to thank Dr A. E. Aliev for his friendship, advice and help and Dr Alex Arce for an enjoyable and highly productive stay at IVIC, Venezuela.

Drs I. P Jones, E. Curzon and A. Gibbs of Bruker UK provided much valuable help with the setting up of the new NMR instrumentation. My thanks to Mr Andrew Cadman of Bruker Switzerland for the construction of the special probe used for the triple resonance experiments in Chapter 7 and for many fascinating insights into probe design and construction.

Dave Knapp and Joe Knolan rate a special thank you for their rebuild of the autoclave used to synthesise the $[Os_3(CO)_{12}]$ as well as to Dick Waymark for his patience and ability and to John Hill and Steve Corker for mass spectrometric work and HPLC advice and coffee. Thank you.

To all those in Laboratory 301M who provided so much entertainment and were a pleasure to work with, again a special thank you.

Chapter 1 Reactions of $[Ru_3(CO)_{12}]$ and $[Os_3(CO)_{12}]$

1.1 Introduction

$[Os_3(CO)_{12}]$ is synthesised by the reaction of OsO_4 and CO under pressure and at elevated temperature usually in an ethanolic solution. The ethanol and probably also CO are oxidised by the OsO_4, but the stoichiometry and the mechanism of this reaction are unknown and apparently unstudied. The carbonyl compound is obtained as yellow plate-like crystals in yields of up to 90%.[1] Earlier methods of synthesising $[Os_3(CO)_{12}]$ used solvents such as xylene and gave comparatively low yields as well as contamination with $[Os_4O_4(CO)_{12}]$.[2] $[Ru_3(CO)_{12}]$ is synthesised from $RuCl_3$, using Zn dust as a reducing agent in this case, again by carbonylation at pressure and is obtained as orange crystals.[3] Both the trinuclear clusters are highly stable in air at room temperature. However solid $[Ru_3(CO)_{12}]$ darkens on exposure to sunlight and air over prolonged periods. $[Ru_3(CO)_{12}]$ photolyses (THF solution) in sunlight to give an insoluble material of apparent formula $[\{Ru(CO)_4\}_n]$, which has not been fully characterised and no uses for it have been developed.[4]

The molecule $[Os_3(CO)_{12}]$ has approximate D_{3h} symmetry in its crystalline form with six *axial* carbonyl ligands perpendicular to the plane of the metal triangle and six *equatorial* CO ligands in the Os_3 plane.[5] Such CO distribution is analogous to that of chemisorbed CO on metal (111) surfaces.[6] The average Os-Os bond is 2.833(3) Å, the average *axial* Os-C bond being 1.946(6) Å and the average *equatorial* Os-C bond being 1.912(7) Å. Being coordinatively saturated the cluster

generally requires CO loss to form uncharged derivative with the exception of halogenation, in which case $[Os_3(CO)_{12}]$ reacts with Cl_2 to form $[Os_3Cl_2(CO)_{12}]$.[39]

In general osmium clusters do not adopt structures with bridging CO, whereas ruthenium is much more likely to form bridging structures and iron cluster have a strong tendency to form carbonyl bridges such as in $[Fe_3(CO)_{12}]$.[59] This difference could be electronic in origin, but simple steric considerations could also account for this.

The interest in trinuclear chemistry focuses on the following features:[7]-

a) Robustness, especially of osmium clusters.
b) Ability to introduce organic ligands and subsequently transform these materials without changing the cluster nuclearity.
c) The clusters are easy to work with and generally produce air stable derivatives.
d) Ability to make and break metal-metal bonds during a reaction according to electronic requirements without affecting cluster nuclearity.
e) There is a huge chemistry with terminal, μ_2 and μ_3 organic and inorganic ligands.
f) There is the possibility of highly specific chiral interactions because of cluster shape and bulk.

Clusters may be defined in a variety of ways but they are generally considered to be compounds containing three of more metal atoms with metal-metal bonding.[7] Trinuclear clusters such as those formed by iron, ruthenium and osmium of the

form $M_3(CO)_{12}$ are amongst the simplest clusters. Higher nuclearity clusters are also much studied but the scope of this review is limited to M_3 clusters.

An early stimulus to cluster chemistry was the surface analogy in which it was proposed that cluster chemistry would mimic surface chemistry of the metals and in particular surface defects could be easily replicated.[9] There has been much discussion as to the extent to which metal clusters model these bulk properties.[9] It has been proposed[8] that the reasons for a difference in behaviour between clusters and surfaces are:-

a) With increase in the number of metal atoms in an array, the energy levels of the atoms overlap to form energy bands which do not exist in small clusters. Therefore there will be intrinsically different electron structure between the two systems.
b) In large metal particles there may be many types of metal surfaces, whereas in clusters, there may only be a few. It is still relatively difficult to ascribe a certain type of reaction to a particular surface structure.

On the other hand others, have argued that the specificity of metal surface type found in large clusters is an asset.[9] Rather than depending on the random occurrence of a specific type of surface or surface defect, in principle such a surface or defect can be exclusively reproduced within a cluster, thereby increasing the specificity and catalytic potential of, thus far hypothetical, clusters. A problem with the geometric design of clusters is that the shape is unlikely to be carried through the catalytic chemistry it was designed for, particularly if extreme temperature and pressure are used.

1.2 Reactivity

1.2.1 Thermolysis

Both $[Ru_3(CO)_{12}]$ and $[Os_3(CO)_{12}]$ are susceptible to thermolytic reactions, with $[Ru_3(CO)_{12}]$ being considerably more so than $[Os_3(CO)_{12}]$. The M-M bond enthalpies of the triruthenium and triosmium clusters are 78 kJ mol^{-1} and 94 kJ mol^{-1} respectively and M-CO bond enthalpies change similarly.[10] Thermally driven reactions are therefore much more likely to lead to cluster reorganisation with triruthenium than with triosmium clusters. The difficulty of handling only thermally robust materials initially limited the scope of triosmium chemistry, but once labile derivatives were developed the scope of chemistry enlarged to enable thermally less stable ligands to be used. For instance, the thermal reaction of BINAP with $[Os_3(CO)_{12}]$ leads to an orthometallated species, whereas the reaction of BINAP with $[Os_3(CO)_{10}(MeCN)_2]$ leads to displacement of the MeCN ligands and a straightforward disubstituted product.[11]

Three principle modes of coordination are encountered:-

a) To a single metal centre: e.g. monodentate ligands or bidentate ligands. Ligands such as PPh_3 and $P(OMe)_3$ added in stoichiometric quantities to $[M_3(CO)_{12}]$ or to $[M_3(CO)_{11}(MeCN)]$ readily react to give the substituted derivatives $[M_3(CO)_{11}L]$ where L = PPh_3 or $P(OMe)_3$.[12] It is also possible for the cluster to form $[M_3(CO)_{11}L]$ where L is a bidentate ligand (e.g. dppm) which is coordinated in a monodentate manner. Equally possible is bidentate ligand chelation as in 1,1-$[M_3(CO)_{10}L]$.[7]

b) Across two metal centres: e.g. bidentate ligands. Bidentate ligands in the series dppm, dppe, dppp and dppb all preferentially bridge the M_3 framework.[7] Reactions of the series dppm, dppe, dppp and dppb with 1,2-$[Os_3(CO)_{10}(MeCN)_2]$ generate the 1,2-isomer in preference to 1,1-$[Os_3(CO)_{10}L]$ except that dppm does not form the 1,1 isomer under any circumstances, presumably for steric reasons.[13]

c) Face capping by bonding to three metal atoms: e.g. orthometallation of dangling cyclic appendages of bidentate ligands. Orthometallation is common with the dangling phenyl groups that are frequently attached to tertiary phosphines. Typically a hydrogen atom detaches from the phenyl ring to form a bridging hydride with the phenyl ring σ-bonded and sometimes also π-bonded to the metal triangle. An example from our work is the orthometallation of 1,1-$[Os_3(CO)_{10}(BINAP)]$ to form 1,1-$[Os_3(\mu\text{-}H)(CO)_9\{BINAP\text{-}H\}]$.[14] However, BINAP reacts with $[Ru_3(CO)_{12}]$ under some circumstances with metallation to form 1,2-$[Ru_3(\mu\text{-}H)(CO)_8\{BINAP\text{-}H\}]$.[11]

There are, of course, other modes of bonding than those outlined above.

1.2.2 Clusters with labile ligands

$[Os_3(CO)_{10}(MeCN)_2]$, $[Os_3(CO)_{11}(MeCN)]$ and $[Os_3(\mu\text{-}H)_2(CO)_{10}]$ are the starting materials of choice for triosmium chemistry.[7] These clusters are fairly robust and can be stored indefinitely in cool conditions away from sunlight. By contrast for triruthenium chemistry $[Ru_3(CO)_{10}(MeCN)_2]$ and $[Ru_3(CO)_{11}(MeCN)]$ are readily prepared but there is no bulk analogue to $[Os_3(\mu\text{-}H)_2(CO)_{10}]$.[15] Attempts to

hydrogenate $[Ru_3(CO)_{12}]$ lead to the cluster $[Ru_4H_4(CO)_{12}]$[16] and not to $[Ru_3(\mu\text{-}H)_2(CO)_{10}]$, which is unknown in bulk but has been observed spectroscopically.[17] $[Ru_4H_4(CO)_{12}]$ is itself reactive substitutionally with a variety of phosphines and forms clusters such as $[Ru_4H_4(CO)_{10}(dppe)]$.[18]

$[M_3(CO)_{10}(MeCN)_2]$, $[M_3(CO)_{11}(MeCN)]$ (where M = Os or Ru) and $[Os_3(\mu\text{-}H)_2(CO)_{10}]$, although robust enough to be stored are all highly reactive species and, with the majority of soft ligands, will react at room temperature. Historically the cyclooctene substituted triosmium cluster $[Os_3(cyclooctene)_2(CO)_{10}]$ was used as a starting material, but it does not store as well as the bis-acetonitrile or dihydride derivatives and has to be kept in cyclooctene solution.[19] The preparation of $[Ru_3(CO)_9(MeCN)_3]$, has been reported[20] and its reaction with monosubstituted alkynes leads to $[Ru_3H(CO)_9(C_2R)]$ where R = alkyl. The reaction of disubstituted alkynes RC_2R' with $[Ru_3(CO)_9(MeCN)_3]$ leads to $[Ru_3(CO)_9(\mu_3\text{-}\eta^2\text{:}\eta^2\text{:}\eta^2\text{-}C_6R_3R'_3)]$,[21] complexes containing an aromatic ligand face-capping the cluster, formed by way of a [2+2+2] cyclotrimerization.[22] Similar face-capping systems have been reported for the triosmium analogue although the synthetic route was more involved.[23, 24] The main interest in this chemistry is that the M_3 cluster acts as a template for the cyclotrimerization.

The compound $[Os_3(CO)_{10}(MeCN)_2]$ and the butadiene derivative $[Os_3(CO)_{10}(\eta^4\text{-}cis\text{-}C_4H_6)]$ both react stoichiometrically with dppp to give $[Os_3(CO)_{10}(\mu\text{-dppp})]$. This cluster reacts with more dppp to give $[Os_3(CO)_9(\mu\text{-dppp})(\eta^1\text{-dppp})]$. This is in contrast to $[Os_3(CO)_{10}(\mu\text{-dppm})]$ which on further reaction with dppm forms $[Os_3(CO)_8(\mu\text{-dppm})_2]$.[25] It is accepted that

dppm cannot easily chelate for steric reasons presumably whereas dppe, dppb and dppp can either bridge or chelate in clusters with ease.[25]

The butadiene cluster $[Os_3(C_4H_6)(CO)_{10}]$ has two isomeric forms, those with bridging and chelating butadiene respectively. These mixed isomers react with diphos, where diphos = $Ph_2P(CH_2)_nPPh_2$ [dppm (n = 1), dppe (n = 2), dppp (n = 3) and dppb (n = 4)] to give mixtures of the isomers of the form 1,1-$[Os_3(CO)_{10}$(diphos)] and 1,2-$[Os_3(CO)_{10}$(diphos)] which are readily separable by TLC.[26]

The reactions of $[Os_3(CO)_{11}(MeCN)]$ are an interesting contrast giving rise to a series of compounds $[Os_3(CO)_{11}$(diphosphine)] with one co-ordinated phosphorus and one free phosphorus as well as the di-cluster compound $[Os_6(CO)_{22}$(diphosphine)] with the two $[Os_3(CO)_{11}]$ sub-units linked by the ligand. The cluster $[Os_3(CO)_{11}$(dppm)] readily undergoes decarbonylation on exposure to sunlight to give the 1,2-$[Os_3(CO)_{10}$(dppm)], while the other compounds in the series do not decarbonylate under the same mild conditions but decarbonylate readily in the presence of Me_3NO to give the bridging but not the chelating isomers.[26] Interestingly Pöe found that the rate of formation of chelate complexes is governed by the rate at which the first donor atom enters the coordination sphere. The entry of the remaining donor atoms (in the same ligand, in this case dppm) is usually then very much faster as the effective local concentration is high.

Figure 1.2 Structure of $[Os_3(CO)_{10}(MeCN)_2]$

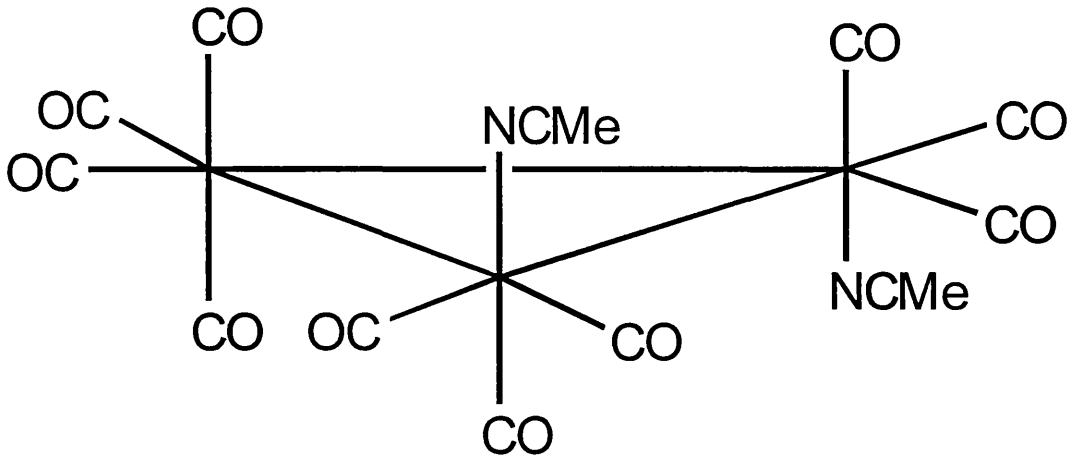

Figure 1.3 Structure of $[Os_3(CO)_{10}\{\mu\text{-dppm}\}]$

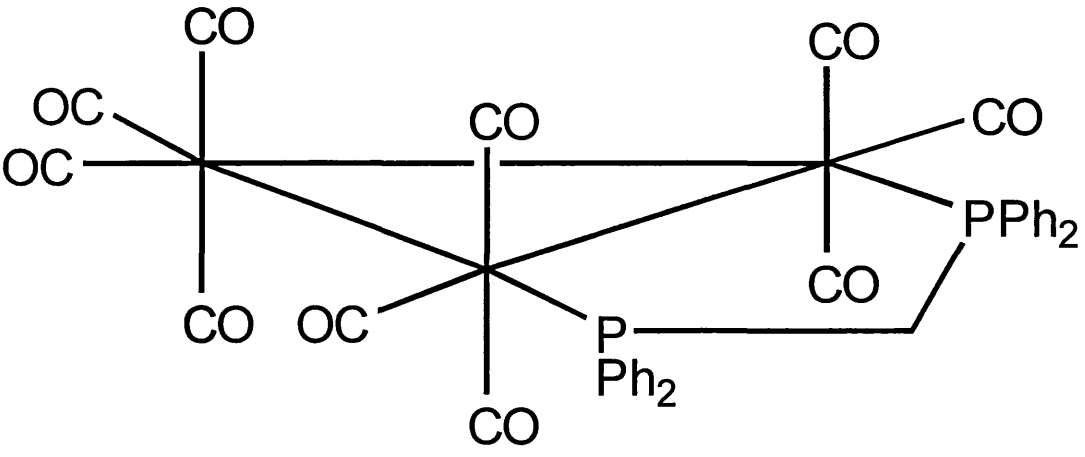

Pöe studied these mechanisms by following the thermal conversion of the monodentate forms of potentially bidentate ligands into the bidentate form by the loss of a CO ligand. This was shown to be an intramolecular process. Pöe also demonstrated that the rate of the second substitution (chelating ring closure) is independent of the concentration of both CO and dppm.[27]

Extensive studies have been carried out on further substitution reactions of cluster $[Os_3(CO)_{10}(dppm)]$. Decarbonylation of this cluster was found to give $[Os_3(\mu\text{-}H)(CO)_8\{Ph_2PCH_2P(Ph)C_6H_4\}]$. Refluxing $[Os_3(\mu\text{-}H)(CO)_8(Ph_2PCH_2P(Ph)C_6H_4)]$ with CO passing through the solution reforms the cluster $[Os_3(CO)_{10}(dppm)]$ showing that the hydrogen migration from the phenyl ring to hydride is reversible.[28]

When the cluster $[Os_3(\mu\text{-}H)(CO)_8\{Ph_2PCH_2P(Ph)C_6H_4\}]$ is treated with diphenylacetylene, the cluster $[Os_3(CO)_7(\mu^3\text{-}\eta^2\text{-}PhC_2Ph)(Ph_2PCH_2PPh_2)]$ is formed. Addition of CO to this cluster gives $[Os_3(CO)_7(\mu\text{-}CO)(PhC_2Ph)(Ph_2PCH_2PPh_2)]$ in which the alkyne is still bonded $\mu_3\text{-}\eta^2$, but has to be rotated by 30° into the parallel form from a perpendicular orientation.[29]

The butadiene clusters $[Os_3(CO)_{10}\{\eta^4\text{-s-}cis\text{-}C_4H_6\}]$ and $[Os_3(CO)_{10}\{\mu\text{-s-}trans\text{-}C_4H_6\}]$ react with PMe_2Ph at ambient temperature to give both $[Os_3(CO)_{10}(PMe_2Ph)_2]$ and $[Os_3(CO)_9(PMe_2Ph)_3]$ as mixed isomers. The compound $[Os_3(CO)_{10}(PMe_2Ph)_2]$ separates by TLC to give isomers 1,1 and 1,2-$[Os_3(CO)_{10}(PMe_2Ph)_2]$. These isomers are non-interconverting at room

temperature although the 1,2-isomer does exist in two rapidly interconverting forms as shown by ^{13}C and ^{31}P NMR evidence.[26]

The clusters $[Os_3(\mu\text{-}C_6H_6)(CO)_9]$[30] and $[Ru_3(\mu\text{-}C_6H_6)(CO)_9]$[31] in which the benzene ligands are face-capping have been prepared and characterised by single crystal X-ray diffraction. The CO ligands align *equatorial*ly or facing away from the benzene ligand such that the benzene plane appears to be floating parallel to the metal triangle. There is some evidence for alternating C-C bond lengths, that there is a distortion into a Kekulé-type structure with long 1.45(1) Å and short 1.40(2) Å bond lengths alternating around the ring. However the errors in these lengths do not allow a clear distinction between long and short bonds but an accumulation of data from different structures supports the idea. The ^{13}C NMR spectrum of the benzene moeity shows a δ 90 upfield shift on coordination which also might imply some loss of aromatic character.

The reaction of the 48-electron cluster $[Os_3(\mu\text{-}H)(CO)_{10}(CF_3CCHCF_3)]$ with PEt_3 at room temperature leads to the formation of the 50-electron cluster $[Os_3(\mu\text{-}H)(CO)_{10}(PEt_3)(CF_3CCHCF_3)]$ as the major product in the form of a linear chain. This was the first example of the reaction of a two electron donor that lead to M-M bond cleavage room temperature. The effect of addition of a 2-electron donor is equivalent in many ways to a 2-electron reduction. In this case the conversion of a 48 to a 50-electron cluster leads to the opening of a triangular cluster to an open linear one.[32]

Figure 1.4 X-ray structure of $[HOs_3(CO)_{10}(PEt_3)(CF_3CCHCF_3)]$ reproduced from reference 32.

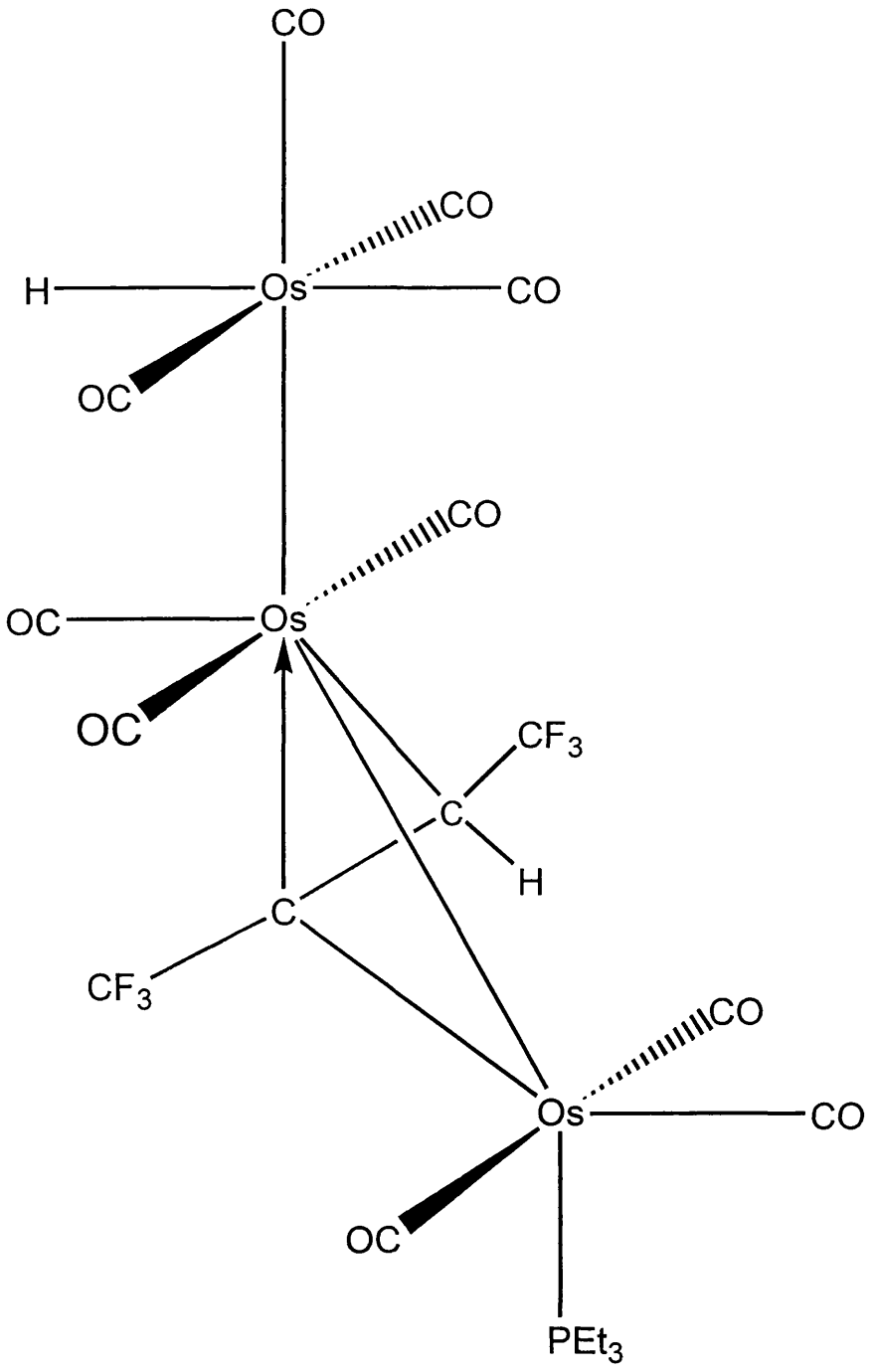

1.2.3 Reactions with electron acceptors: protonation and halogenation

There is extensive evidence of protonation of metal-metal bonds to produce bridging hydrides across two metal centres. HCl, H_2SO_4 and trifluoroacetic acid have commonly been used in addition to other protonating agents. Electrophilic addition at metal centres should not require any alteration to the metal framework as there is no change in the number of electrons associated with the cluster. This is particularly true in the case of higher nuclearity clusters (M_{3+}) although higher clusters can adopt different geometries without any change in their valence electron count.

In polynuclear metal clusters the metal framework is a potential source of electron density and therefore a fruitful site for protonation. Most cluster compounds react readily with strong acids with protonation at metal centres as long as there are no other strongly basic centres.[33]

As an extreme example the weakly basic clusters $[M_3(CO)_{12}]$ (M = Ru or Os) are protonated in 98% H_2SO_4 to give cationic $[M_3H(CO)_{12}]^+$ which are remarkably stable in this medium.[34,35]

Figure 1.5 Structures of some protonated triosmium species showing that steric restrictions of the μ-dppm (top) do not allow the protons to bridge the phosphine bridged edge of the metal triangle. Whereas these steric restrictions do not apply to μ-dppe.[42]

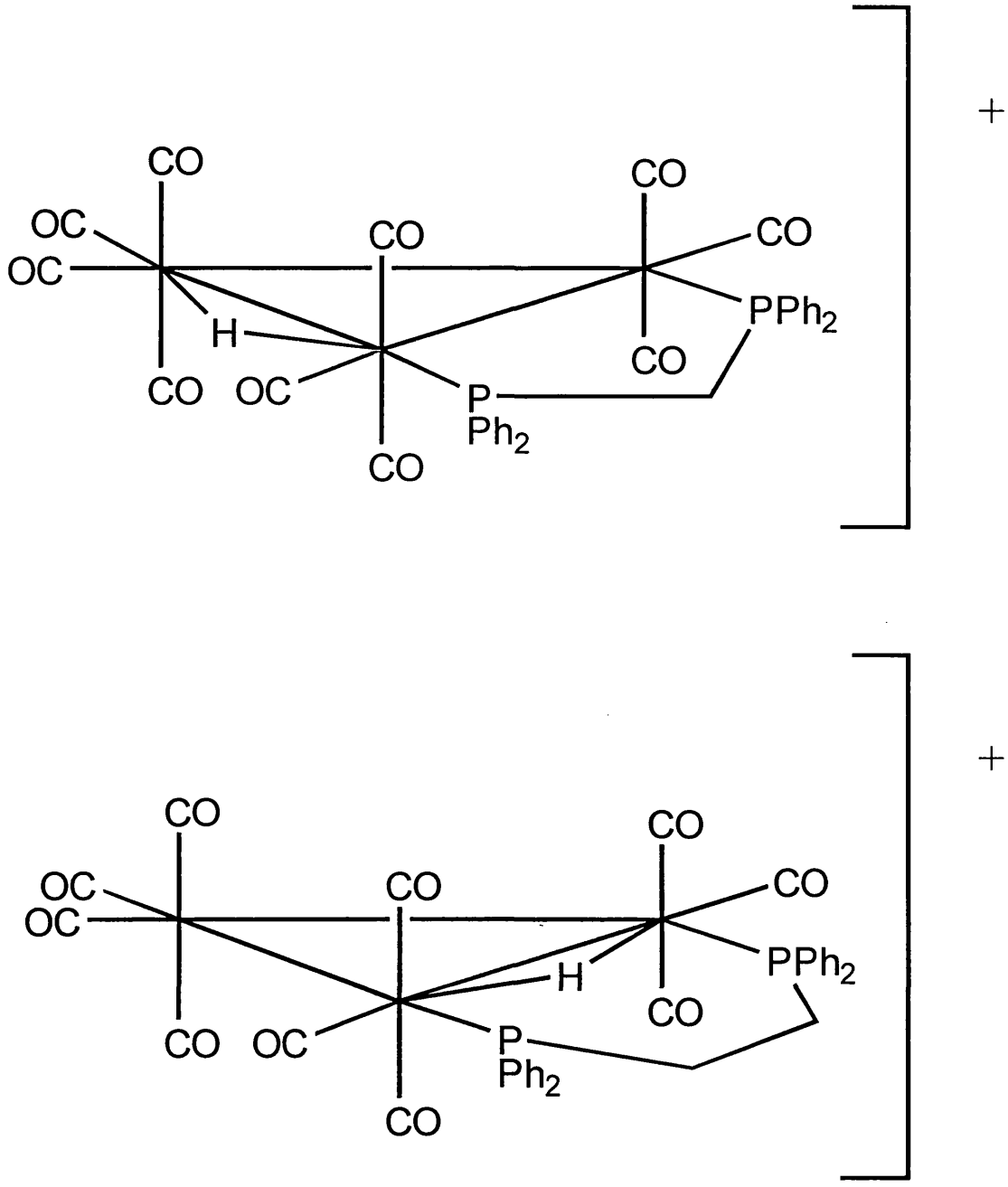

Trifluoroacetic acid is more readily miscible in standard NMR solvents and so is more frequently used: the protonation of the series of more basic clusters $[Os_3(CO)_{10}(diphos)]$ where diphos = $Ph_2P(CH_2)_nPPh_2$ [dppm (n = 1), dppe (n = 2), dppp (n = 3) and dppb (n = 4)] shows differences in reactivity towards H^+.[36] A sixteen fold excess of trifluoroacetic acid leads to $[Os_3(\mu\text{-}H)(CO)_{10}(diphos)]^+$, with the hydride ligands bridging the same, electron rich, osmium atoms as the diphos ligand where diphos is dppe, dppp, dppb.[37] By contrast the hydride and the dppm bridge different edges of the cluster triangle in $[Os_3(\mu\text{-}H)(CO)_{10}(dppm)]^+$, most probably on account of steric factors (figure 1.5). Ruthenium clusters behave similarly. Two interconverting isomers are observed, in solution, for the dppe hydrido triruthenium cluster corresponding to the hydride sharing the same metal centres as the dppm bridge and another where dppm and hydride bridge different metal edges.[25]

In nearly all cases the hydrido-ligands occupy a bridging position in the cluster. There is good evidence that the rates of protonation and deprotonation of clusters are very much less than the rates of intramolecular hydride exchange. Various workers have reported that there is no coalescence of hydride and protonating agent signals in the ^1H NMR spectra, which indicates that the intermolecular hydride exchange is slow on the NMR timescale. It is believed that a two step process for protonation might be in some cases involved: (i) the addition of H^+ into one site and (ii) a subsequent intramolecular exchange between the two available sites. However, there is no exchange between the two metal hydrides

and the solvent (in the case of the $D_2SO_4/[Os_3D(SPh)(CO)_{10}]$ system) until the D_2SO_4 is diluted with D_2O.[34]

The clusters $[Os_3(\mu\text{-}H)_2(CO)_{10}]$ and some of its simple substituted derivatives add protons to a metal-metal bond to give $[Os_3(\mu\text{-}H)_3(CO)_{10}]^+$ and $[Os_3(\mu\text{-}H)_3(CO)_9L]^+$ respectively where (L = PPh_3, PEt_3, or $AsPh_3$).[38]

An other important example of electrophilic addition is halogenation. The reaction of $[Os_3(CO)_{12}]$ with chlorine or bromine yields ultimately the, molecules $[Os_3(CO)_{12}(X)_2]$ (where X = Cl or Br) containing open metal chains whereas the corresponding reaction with iodine gives $[Os_3(CO)_{12}(I)][I_3]$ and the ^{13}C NMR spectra of $[Os_3(CO)_{12}(I)_2]$ formed by I^- addition to the cluster indicates a linear structure with the iodine ligands in the *cis* position to the chain on different terminal osmium atoms.[39] This observation prompted an examination of the mechanism of the halogenation of metal clusters that concluded that initially the di*equatorial* isomer of $[Os_3(CO)_{12}(Cl)_2]$ is formed and then over time forms the *axial/equatorial* isomer. A similar system is observed for the reaction of bromine with $[Os_3(CO)_{12}]$ except that the transformation between the di*equatorial* and the *axial/equatorial* isomer is slower. The situation for the reaction of iodine with $[Os_3(CO)_{12}]$ appears to be completely different and from elemental analysis the product seems to be $[Os_3(CO)_{12}I_4]$ which, on the basis of the similarity of the ^{13}C NMR spectrum to that of $[Os_3(CO)_{12}(H)][PF_6]$, is described as the ionic derivative $[Os_3(CO)_{12}(I)][I_3]$ which in solution over a period of hours rearranges to *equatorial/equatorial* isomer of $[Os_3(CO)_{12}(I)_2]$.[39] Whether the differences in the reaction pathways are real and can be ascribed to steric factors or whether the

differences observed are purely the result of decreasing electrophilicity of the halogen series Cl_2 to I_2 leading to the observed intermediates is not at all clear.

Figure 1.6 Linear chain triosmium compounds made from the reaction of $[Os_3(CO)_{12}]$ with chlorine or bromine. Reproduced from reference 39.

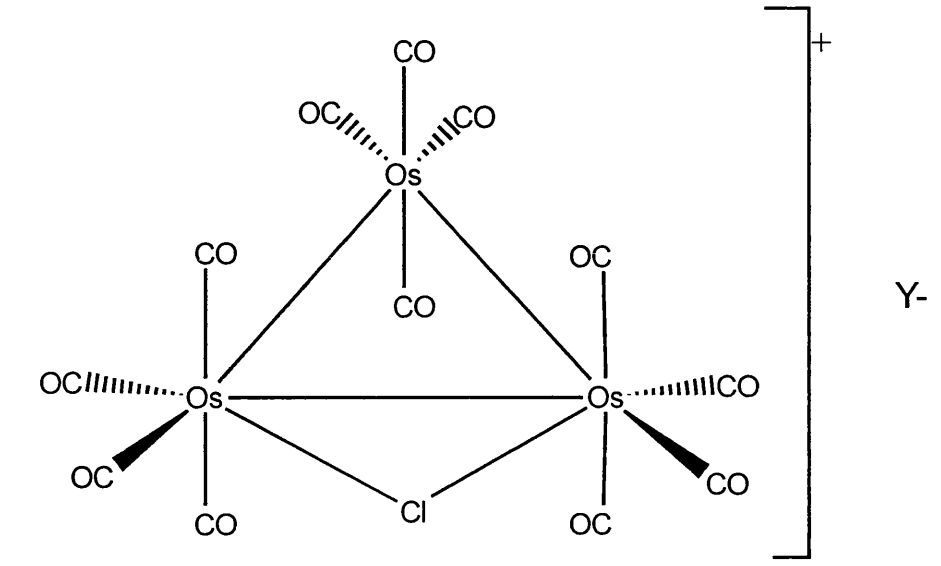

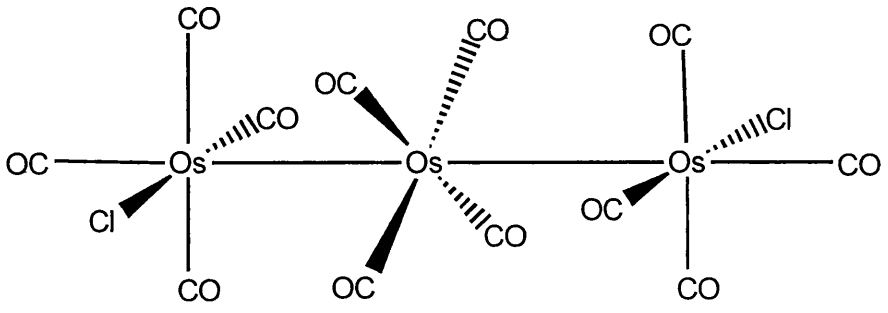

diequatorial

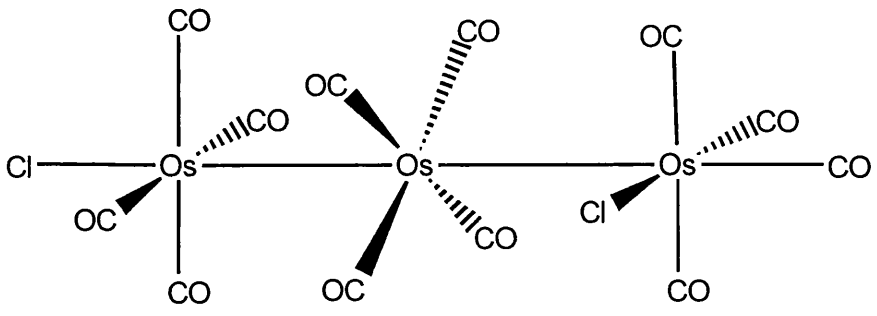

axial-equatorial

1.2.4 Reactions with electron donors

The carbonyl $[Os_3(CO)_{12}]$ is readily hydrogenated by bubbling hydrogen through a refluxing octane solution for 2 hours to form $[Os_3(\mu\text{-}H)_2(CO)_{10}]$ with the loss of two CO ligands. The cluster $[Os_3(\mu\text{-}H)_2(CO)_{10}]$ has been characterised by X-ray and neutron diffraction studies and it is found that the two hydrides bridge the same edge of the cluster (Figure 1.7). The unbridged Os-Os bonds are similar in length to those in $[Os_3(CO)_{12}]$,[45] while the hydride-bridged Os-Os bond is 2.681(1) Å and significantly shorter. Explanation of the shortness of the bridged bond in $[Os_3(\mu\text{-}H)_2(CO)_{10}]$ has been in terms of electron unsaturation or a simple consequence of having two small atoms bridging the osmium atoms. Electron counting indicates a 46-electron count compared with the 48-electron count for $[Os_3(CO)_{12}]$.[40] This deficiency has been explained in terms of an Os-Os double bond[40] or multi-centre delocalised bonds.[41,45]

Extensive NMR studies have been carried out on $[Os_3(\mu\text{-}H)_2(CO)_{10}]$ to evaluate CO exchange (^{13}C saturation transfer) and the ^{17}O quadrupolar coupling constant has been evaluated at 1.59 MHz together with ^{17}O spin-lattice measurements. ^{13}C spin lattice relaxation rates are strongly field dependent and indicate strong shielding anisotropy.[50,50]

The reactions of unsaturated materials such as acetylene with $[Os_3(\mu\text{-}H)_2(CO)_{10}]$ are well characterised. Clusters related to $[Os_3(\mu\text{-}H)_2(CO)_{10}]$ may also be formed by treating $[Os_3(CO)_{10}(L)_2]$ with H_2 with the elimination of CO.

Figure 1.7 X-ray structure of $[Os_3(\mu\text{-}H)_2(CO)_{10}]$ redrawn from reference 45.

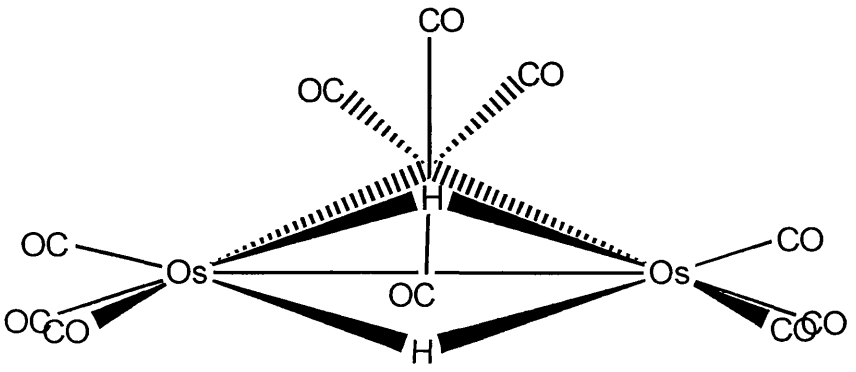

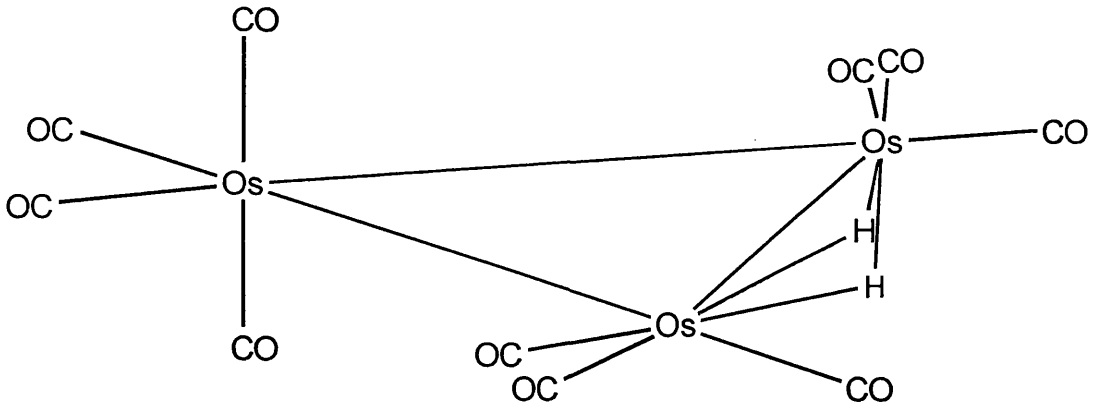

In our work we have demonstrated that $[Os_3(\mu\text{-}H)_2(CO)_{10}]$ reacts with diphosphine (L) ligands to form compounds, formally unsaturated, of the form $[Os_3(\mu\text{-}H)_2(CO)_8L]$, previously prepared by hydrogenation of $[Os_3(CO)_{10}L]$.[42,43] In fact it had been suggested that these compounds could not be prepared by the reaction of $[Os_3(\mu\text{-}H)_2(CO)_{10}]$ and bidentate phosphine ligands.[43] Hydrogenation of 1,2-diphos, compounds $[Os_3(CO)_{10}(diphos)]$ where diphos = $Ph_2P(CH_2)_nPPh_2$ [dppm (n = 1), dppe (n = 2), dppp (n = 3) and dppb (n = 4)], shows differences in reactivity towards H_2. Where diphos is dppm, dppe or dppp the corresponding clusters $[Os_3(\mu\text{-}H)_2(CO)_8(diphos)]$ are obtained in good yield, but the dppb analogue has not been reported. The symmetry of the dppm, dppe, dppp analogues is evidenced by the ^{31}P NMR spectra and by the X-ray structure in the case of dppm.[44] It is evident from the X-ray structure of the dppm complex, and its similarity with that of $[Os_3(\mu\text{-}H)_2(CO)_{10}]$ [45] that the short Os-Os distances are 2.6757(9)Å and 2.681(1)Å respectively. It is presumed that the bridging hydrides are well outside the Os_3 plane, thus removing any steric reason why the dppm and the two hydrides cannot occupy the same side of the metal triangle. This is in contrast to the protonation of $[Os_3(CO)_{10}(dppm)]$ which results in $[Os_3(\mu\text{-}H)(CO)_{10}(dppm)]^+$ in which the dppm and the hydride bridge different edges of the cluster.

1.2.5 CO or MeCN displacement leading to oxidative addition or displacement

CO and MeCN ligands may be displaced from the metal centres in clusters and thereby provide the starting clusters of choice for highly specific reactions or for reactions with highly substituted materials.

Both of the compounds 1,2-$[Os_3(CO)_{10}(MeCN)_2]$ and 1,2-$[Ru_3(CO)_{10}(MeCN)_2]$ are readily prepared and stored. *Axial* positions are adopted by the MeCN ligands[46] and in the *bis*-substituted compound the ligands are *anti* to each other. Both $[Os_3(CO)_{11}(MeCN)]$ and $[Ru_3(CO)_{11}(MeCN)]$ are also readily prepared and stored. Reactions of the MeCN derivatives generally take place at moderately low temperatures. Alternatively the $[M_3(CO)_{(12-x)}(MeCN)_x]$ intermediates may be prepared *in situ* by treating $[M_3(CO)_{12}]$ with Me_3NO in mixed CH_2Cl_2/MeOH/MeCN solution, the degree of substitution being controlled by the amount of Me_3NO added.[47] The MeCN derivatives may be viewed as intermediates as the MeCN is readily displaced if a better ligand is present.

1.3 Fluxional behaviour and NMR

Fluxionality is a major feature of triosmium and triruthenium chemistry and of the parent carbonyl complexes in particular. Studies have centred on CO mobility (studies by ^{13}CO NMR) and have established two major mechanisms for CO site exchange, *turnstile* and *merry-go-round.* The term *turnstile* is applied to the synchronous exchange one *axial* carbonyl with the two *equatorial* carbonyl ligands, with no transfer of CO between metal centres. The term merry-go-round is applied to the exchange of CO around two or more metal centres, in an ordered

circulation pattern which requires bridging CO transients.[48] By contrast with the turnstile mechanism there is transfer of CO between metal centres. The overall scrambling mechanism, in the respective parent dodecacarbonyls, remains unclear although it probably involves combined and geared turnstile/merry-go-round mechanisms. However, it is widely accepted that the resulting exchange is entirely delocalised over all CO groups and metal atoms in the molecule.[49] There are variants to this general scheme if bridging carbonyls are involved because bridge-terminal CO exchange can occur. Fluxional behaviour may be constrained by substituents as in the case of $[Os_3(\mu\text{-}H)_2(CO)_{10}]$.[50] The ^{13}CO VTNMR spectra for clusters containing bidentate ligands may enable the distinction to be drawn between bridging and chelating forms since different restrictions are placed on CO motions. In general the lack of any observed temperature effects on $J_{Os\text{-}P}$ or $J_{Os\text{-}H}$ couplings, viewed by observing the ^{187}Os satellites in either ^{31}P or ^{1}H experiments, indicate that there is no ligand migration between the metal centres.[51] However there are instances of hydride mobility in some of the larger cluster systems investigated.[51] In sharp contrast, the diaxially substituted cluster $[Os_3(CO)_{10}(Ph_2P\text{-}2\text{-}pyridyl)]$ undergoes pyridine migration between the two Os atoms while the phosphine is locked in place at the third this is observed by exchange of substituents R(a) and R(b) in Figure 1.8.[52]

Figure 1.8 Possible structures of $[Os_3(CO)_{10}(Ph_2P\text{-}2\text{-}pyridyl)]$ reproduced from reference 52. Whilst all the possibilities are shown the structure with a cross through them are not observed.

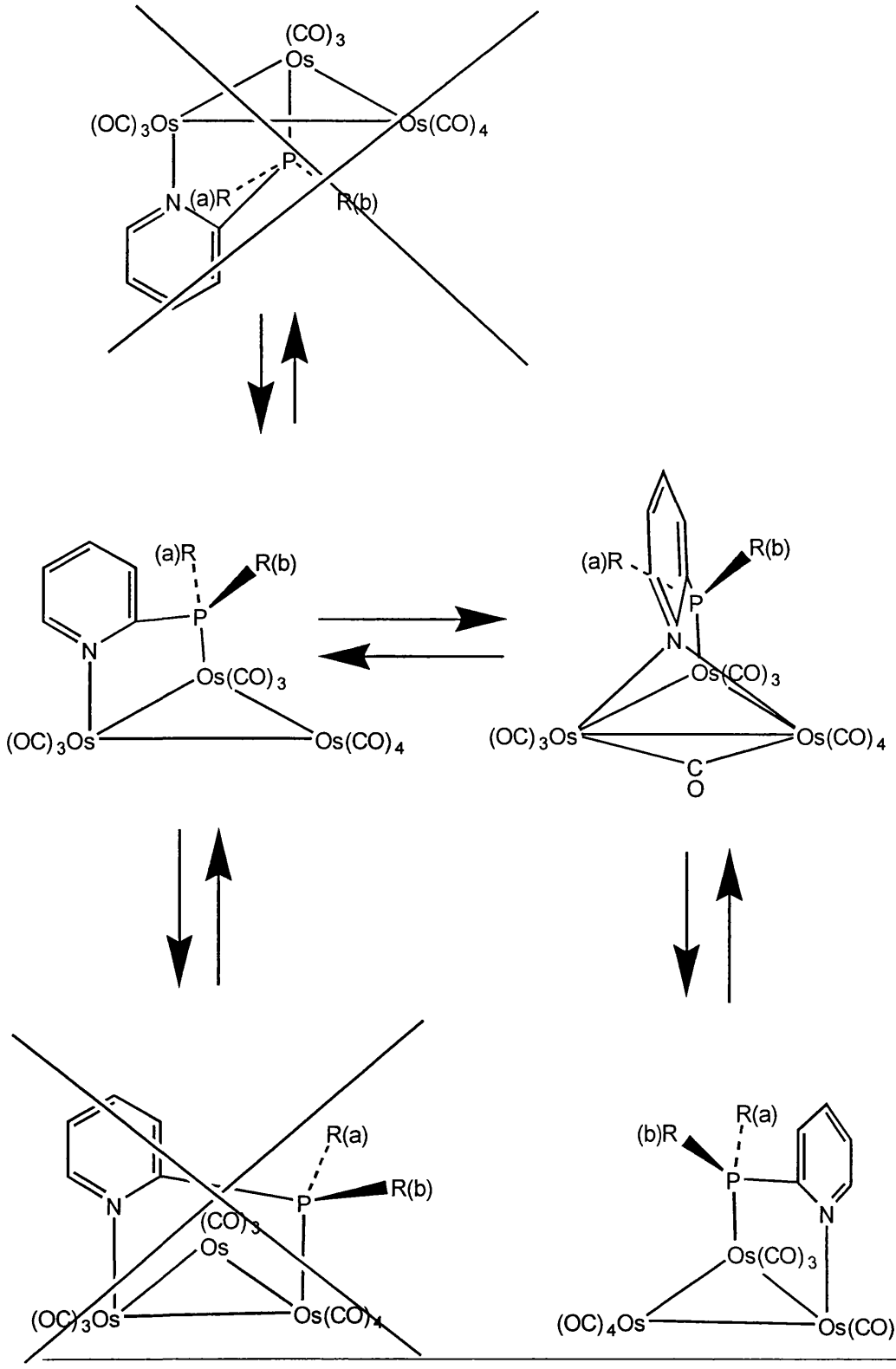

Neither osmium or ruthenium offer a readily tractable nucleus for direct observation NMR spectra. Apart from other considerations the low resonant frequency of ^{187}Os, ^{99}Ru and ^{101}Ru put them out of the tuning range of all but the newest broad-band probes. ^{189}Os is quite sensitive (twice the sensitivity of ^{13}C) but the lines are so broad as to afford no coupling information.[53] Low frequency (and therefore low γ) nuclei present special problems of low inherent sensitivity. There is considerable benefit to be gained in inverse detection by HMQC,[54] as the sensitivity enhancement is proportional to $[\gamma_a/\gamma_b]^{5/2}$ (where $\gamma_a = \gamma$ of the detection nucleus and $\gamma_b = \gamma$ for the second nucleus[55]) where the γ_a nucleus is either ^{1}H, ^{19}F or ^{31}P.

There is very little literature on ruthenium NMR with much of it over fifteen years old.[57] There have been observations of both ^{99}Ru and ^{101}Ru including observations for $[Ru_3(CO)_{12}]$ but seemingly not for any other clusters.[56]

Direct detection ^{189}Os NMR has been carried out, as part of this work, on the standard OsO_4 in CCl_4 yielding a linewidth of ~1 kHz (see Figure 1.9). In our work signals from $[Os_3(\mu\text{-}H)_2(CO)_8(tolBINAP)]$ have been observed with a linewidth of ~20 kHz, in solution. Given these linewidths, detection is made considerably more difficult than the inherent sensitivity would suggest. The only direct detection ^{187}Os experiments, in the literature, carried out have been on molten OsO_4.[57] There have though been a number of developments that allow the observation of ^{187}Os by indirect means, which are more full discussed in Chapter 7.

Samples enriched in ^{187}Os have been used for determination of $J_{C\text{-}Os}$ couplings in $[Os_3(CO)_{12}]$ (99.8% ^{187}Os and 60% ^{13}C).[58] These couplings are as 90 and 115 Hz respectively for the *axial* and *equatorial* sites at 25 °C. At 150 °C a 1:3:3:1 quadruplet is observed with $J_{C\text{-}Os}$ 33 Hz. These values for the first time showed that the exchange process is intramolecular and involves CO migration over all the metal sites. In our work we have determined $^{1}J_{C\text{-}Os}$ couplings from natural abundance samples in the 100 mg range under standard $^{13}C\{^{1}H\}$ observation conditions, in a timescale of two hours at 500 MHz.[44]

Whilst stereochemistry, fluxionality and isomerisation are major areas of study in cluster chemistry, these phenomena are usually understood in terms of localised effects such as localised rotations or terminal-bridge conversions. In an attempt to unify these descriptions, the structures metal clusters have been describes in term of the ligand polyhedral model (LPM).[59] The LPM model makes use of evidence from ^{13}C solution NMR[60] (molecular motion in solution), ^{13}C MAS NMR[61] (molecular motion in solids) and X-ray evidence to develop a global scheme.[62]

The LPM breaks carbonyl structures into their components: 'an outer carbonyl polyhedron' and 'an inner metal polyhedron.' The manner in which one is arranged relative to the other governs the number of bridging and terminal carbonyl groups present. The LPM theory may also be applied to fluxional systems and it rationalises fluxional behaviour, in the solid state, in terms of the relative motions of inner and outer polyhedron.

Figure 1.9 Direct detection spectrum of ^{189}Os. Solution of OsO_4 in CCl_4 acquired in one minute demonstrating both the detection sensitivity of the nucleus and its broad linewidth; indicating a fast T_2 relaxation process. The scale is in Hz.[44]

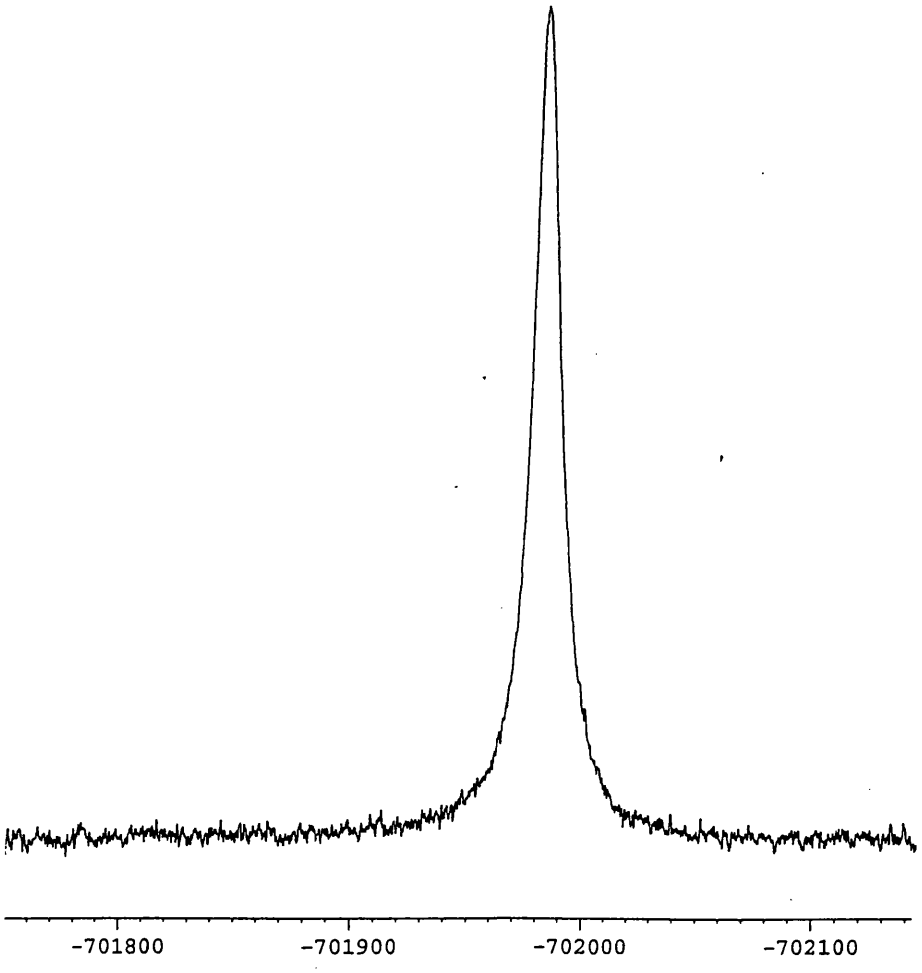

The LPM theory interprets fluxional behaviour, relevant to solution studies, in terms of ligand polyhedral rearrangements.[63] However, other than the elegance of a unified approach it is not clear that LPM offers any particular advantages, over considering localised systems, for M_3 clusters.

Different fluxional processes may be distinguished on the basis of the observable times scales of the different spectroscopic methods. Coalescence phenomena are routinely observed in ^{13}C CO and ^{31}P NMR of M_3 clusters and are used as a tool for the investigation of fluxional behaviour. Vibrational spectra offer a picosecond 'snapshot' and may be observed in terms of band shape changes, with most relevance to the observation of proton transfer in organic systems.[64] NMR spectra are observed over 10^{-4}-10^{-9} s and so the molecules are probed over a relatively long time-scale,[55] so it is possible to observe time averaged coalescence spectra. X-ray diffraction on the other hand has a theoretical time-scale of 10^{-8} s. However this figure is rather a misleading one as the collection of data is usually over a period of hours and at the very least the collection of a single diffraction is going to take of the order of 10^2 s. This is the equivalent of 10^{21} summed 'snapshots' of the situation: a summed average of all the vibrational, rotational fluxional and diffusion processes. It is sometimes difficult to distinguish a static disorder in a crystal from one in which different atom configurations are in dynamic equilibrium.

Chapter 2 Reactions of 2,2'-bis(diphenylphosphino)-1-1'binaphthyl with $[Ru_3(CO)_{12}]$

Table of contents:

2.1 Introduction

Asymmetric hydrogenation has long been studied and often takes the form of the addition of hydrogen to a carbon-carbon double bond in the presence of a transition metal catalyst containing a resolved chiral ligand.[65] The details of this approach are, however, beyond the scope of this work. In general the metal centre involved is almost always either rhodium(I) or ruthenium(II) and the ligands are often chelating diphosphines. The chelating ligands are either resolved chiral ligands or inherently enantiomerially pure materials such as DIOP or CHIRAPHOS (see Figure 2.1) which are prepared from (+)-tartaric acid, which is cheap and readily available.[66] The search for suitable diphosphines has occupied a considerable amount of synthetic effort with a few (BINAP, see Figure 2.1) having been shown to have good generality. One of the reasons BINAP is so effective is the presence of bulky phenyl substituents, which project the chiral conformation by some considerable distance into the coordination sphere by steric crowding. With this in mind it is conceivable that steric induction is possible across a metal cluster triangle. In view of this background BINAP was chosen as the ligand for this study.

BINAP, 2,2'-bis(diphenylphosphino)-1-1'binaphthyl, is a well known chiral auxiliary that has found many catalytic industrial applications with rhodium and ruthenium metal centres.[66,67,68] There are over 350 references to BINAP in the literature. The majority of known BINAP compounds are with either ruthenium or rhodium metal centres. Reported BINAP systems are, however, almost

Figure 2.1 Some examples of chiral ligands

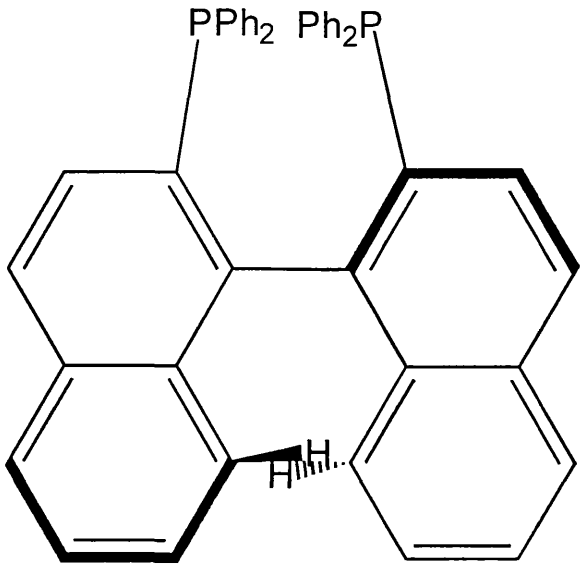

(R)-(+)-2,2'-Bis(diphenylphosphino)-1,1'-binaphthyl '(R)-BINAP'

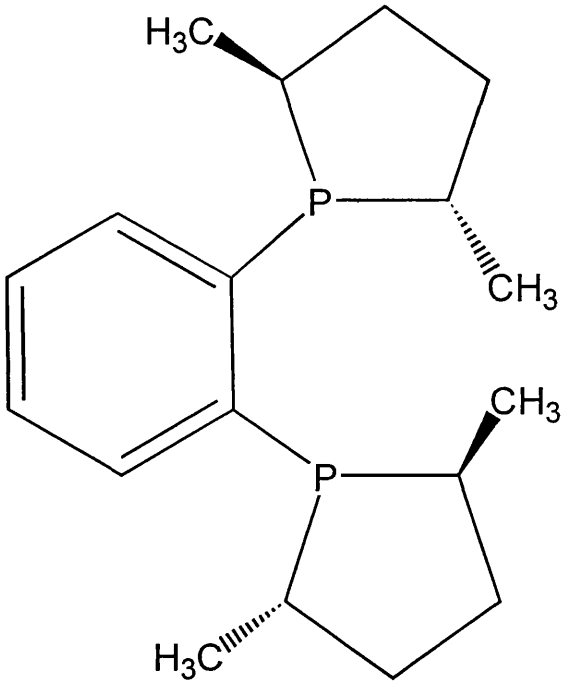

(-)-1,2-Bis(2R,5R)-2,5-dimethyl-phosphanolano)benzene '(R,R)-Me-DUPHOS'

exclusively mononuclear and as a result solely involve chelating BINAP. All previous crystallographic studies having been confined to chelating BINAP. Proctor[66] classed the main catalytic uses of BINAP as allylic rearrangement, hydrogenation of alkenes, hydrogenation of allylic alcohols, and the reduction of ketones. The most commercially significant reaction is the production of enantiomerically pure menthol on a tonnage scale by the Takasago process.

There are only two reports of BINAP clusters one in our work and the other by Nordlander.[14,69] The first reported instance of BINAP bound in a compound with more than one metal centre is $[Ru_3(\mu_3\text{-}Cl)_2(\mu\text{-}Cl)_3\{BINAP\}_3]BF_4$, however this is not an authentic cluster as the X-ray structure shows that it has three octahedral Ru(II) atoms linked by chloride bridges and the BINAP is chelating.[70] It has been shown that BINAP can co-ordinate with metals with a distorted square-planar geometry in $[Rh(nbd)(BINAP)]ClO_4$.[71] $[Ru(acac)_2\{(S)\text{-}BINAP\}]$, used to catalyse the asymmetric hydrogenation of 2-(6'-methoxy-2'-naphthyl)acrylic acid to yield (S)-naproxen in high optical purity, adopts an octahedral geometry.[72] BINAP has also been shown to adopt a pseudo square planar geometry in $[Rh\{(S)\text{-}Cy\text{-}BINAP\}(COD)]ClO_4$.[73] Prior to this work the only authentic BINAP metal cluster appears to have been $[Ru_4(\mu\text{-}H)_4(CO)_{10}\{(S)\text{-}BINAP\}]$, formed as a product of direct substitution of $[Ru_4(\mu\text{-}H)_4(CO)_{12}]$.[74] The complex $[Ru_4(\mu\text{-}H)_4(CO)_{10}\{(S)\text{-}BINAP\}]$ contains a chelating BINAP ligand and in this context has no significant structural differences to known mononuclear ruthenium complexes. In the work described in this chapter the first example of a bridging BINAP ruthenium compound is presented.[11]

Figure 2.2 The basic Heck reaction via the elimination of X (where X = halogen, for example).

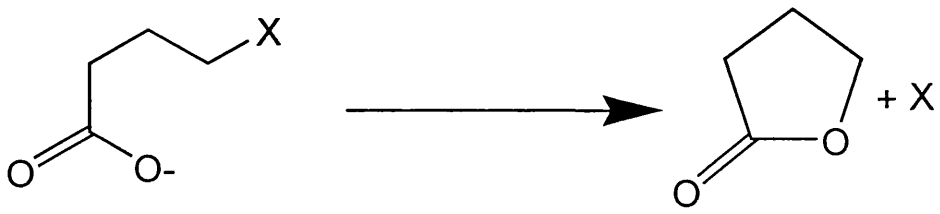

A Heck type reaction using a palladium BINAP complex to promote a highly stereo selective ring closure.[75] Where R = H, ee values of up to 84% have been obtained.

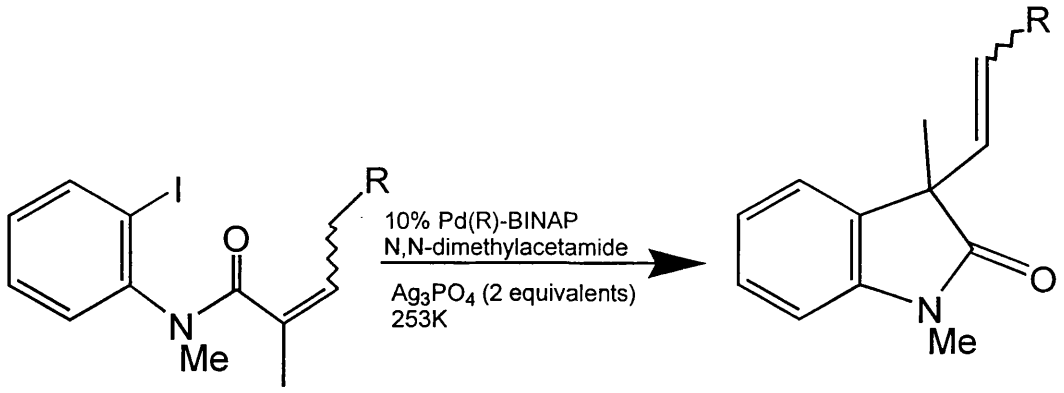

2.2 Objectives of the work described in this chapter

Our objectives for the work described in the present chapter were as follows:

a) To synthesise new triruthenium clusters of the form $[Ru_3(CO)_x(BINAP)]$ (where x = 11, 10, 9).

b) To investigate the mechanisms of fluxionality in the systems by means of ^{13}C and ^{31}P NMR.

c) To compare these results with those of the ruthenium compounds prepared in the following chapter and other know model compounds in the series $[Os_3(CO)_{10}\{Ph_2P(CH_2)_nPPh_2\}]$ (where n = 1 – 4), $[Os_3(CO)_{11}\{Ph_2P(CH_2)_nPPh_2\}]$ (where n = 1 – 4) and $[Os_3(CO)_{10}\{Ph_2P(CH_2)_nPPh_2\}_2]$ (where n = 1 – 4).

d) To investigate the possibility of chiral induction across the cluster by either further substitution or the exchange of labile substituents.

2.3 Thermal reaction of BINAP with $[Ru_3(CO)_{12}]$

Direct thermal reaction of $[Ru_3(CO)_{12}]$ with (R)-BINAP is slow but in refluxing octane over a period of 45 minutes a complex of apparent formula $[Ru_3(CO)_9(BINAP)]$ was formed as an orange solid in 38% yield along with small amounts of two uncharacterised products, one mauve and one yellow, which are not $[Ru_3(CO)_x(BINAP)]$ (x = 10 or 11) based on IR evidence. A double doublet signal at δ -16.49 in the ^1H NMR spectrum of $[Ru_3(CO)_9(BINAP)]$ established that it is a hydrido cluster with non-equivalent ^{31}P couplings. The formula $[Ru_3(\mu\text{-}H)(CO)_9\{\mu_3\text{-}(BINAP\text{-}H)\}]$ is consistent with IR and NMR and mass spectrometry data. This is the first example of an orthometallated BINAP complex with metallation occurring at one of the phenyl groups to give a μ_3-ligand. The orange solid did not produce crystals of suitable quality for single crystal X-ray study. This result is in marked contrast to those achieved for similar reactions with the series dppm, dppe, dppp and dppb which generate the corresponding $[Ru_3(CO)_{10}L]$ complexes which, on further loss of CO, orthometallate at temperatures greater than 100 ° C. This may possibly be explained in terms of the greater flexibility of the BINAP molecule allowing movement around the naphthyl-naphthyl linkage and the rapid conversion of $[Ru_3(CO)_{10}(BINAP)]$ into the observed product.

2.3.1 Spectroscopic characterisation of $[Ru_3(\mu\text{-}H)(CO)_9(\mu\text{-}BINAP\text{-}H)]$

The double doublet signal at δ -16.49 in the ^1H NMR spectrum established that $[Ru_3(\mu\text{-}H)(CO)_9(\mu\text{-}BINAP\text{-}H)]$ is a hydrido cluster. Successive decoupling (see

Figure 2.4) of the two ^{31}P NMR signals at δ 26.92 and 42.16 established that the hydride signal was a double doublet as a result of coupling to two non-equivalent ^{31}P nuclei. The $^{13}C\{^{1}H\}$ NMR spectrum is extremely complex showing over 20 signals (doublets, triplets and multiplets) and confirmed that the BINAP ligand had lost C_2 symmetry (as does the ^{31}P NMR spectrum), which is consistent with orthometallation. On the basis of this and mass spectrometric evidence, it is proposed that this material is the cluster $[Ru_3(\mu\text{-}H)\{\mu_3\text{-}(C_6H_4)PPhC_{20}H_{12}PPh_2\}(CO)_9]$. There is no evidence of either inter or intramolecular CO exchange as the ^{13}C (CO) spectrum is identical throughout the temperature range –65 °C to +60 °C.

2.3.2 Attempted carbonylation of the cluster $[Ru_3(\mu\text{-}H)(CO)_9(\mu\text{-BINAP-H})]$

Attempts to carbonylate $[Ru_3(\mu\text{-}H)(CO)_9(\mu\text{-BINAP-H})]$ to give $[Ru_3(CO)_{10}(BINAP)]$ (presumed to be an intermediate in the formation of the orthometallated hydride species) by passing CO through refluxing octane or decane solutions both at reflux and room temperature were unsuccessful. The only product was the mauve uncharacterised compound from the original preparation (identical IR spectra).

2.4 Reaction of (R)-BINAP with $[Ru_3(CO)_{12}]$ in the presence of $Me_3NO{\bullet}2H_2O$

Many phosphine substituted derivatives of $[Ru_3(CO)_{12}]$ have been simply prepared by reaction in the presence of Me_3NO and therefore we applied this method. The cluster $[Ru_3(CO)_{12}]$ was treated with (R)-BINAP in the presence of

trimethylamine-*N*-oxide dihydrate ($Me_3NO•2H_2O$) in the mixed solvent system: methanol, acetonitrile and dichloromethane under reflux for 1 hour. In addition to some very minor uncharacterised products, the major product, obtained in 80% yield as orange-brown crystals, was shown to be the quite unexpected product $[Ru_3(\mu\text{-}OH)_2(CO)_8\{\mu\text{-}(R)\text{-}BINAP\}]$. The crystals were coated with a sticky film, which could not be washed off, probably accounting for the C and H analytical data being rather higher than calculated. However FAB mass spectra are consistent with the formulation given.

Single crystals were grown by slow diffusion of ethanol into a dichloromethane solution and the structure determined is shown in Figure 2.7 and selected bond lengths and angles in Table 2.2. There is considerable doubt about the origins of the hydroxy ligands in $[Ru_3(\mu\text{-}OH)_2(CO)_8$ (BINAP)]. Oxide or hydroxide ligands have been found in osmium and ruthenium clusters and are normally derived, sometimes adventitiously, from water or dioxygen.[76,77] In this case there is the alternative that the hydroxide ligands are derived from trimethylamine-*N*-oxide. However we have been unable to carry out labelling experiments to confirm this. It is remarkable that no $[Ru_3(CO)_{10}$(BINAP)] at all is formed and that the yield of $[Ru_3(\mu\text{-}OH)_2(CO)_8$(BINAP)] is 80%, given that no such product has been established previously in spite of the considerable use that has been made of the $[Ru_3(CO)_{12}]$/tertiary phosphine/Me_3NO system in the preparation of disubstituted derivatives of the trinuclear osmium and ruthenium carbonyls.[78,79]

Figure 2.4 $[Ru_3(\mu\text{-H})(CO)_9(\mu\text{-BINAP-H})]$. Top $^1H\{^{31}P\}$ with CPD (composite pulse decoupling) of both signals ^{31}P A + B using the GARP scheme. CW (continuous wave) selective decoupling of the two ^{31}P NMR signals (A + B). The $^{31}P\{^1H\}$ spectrum is shown at the bottom.

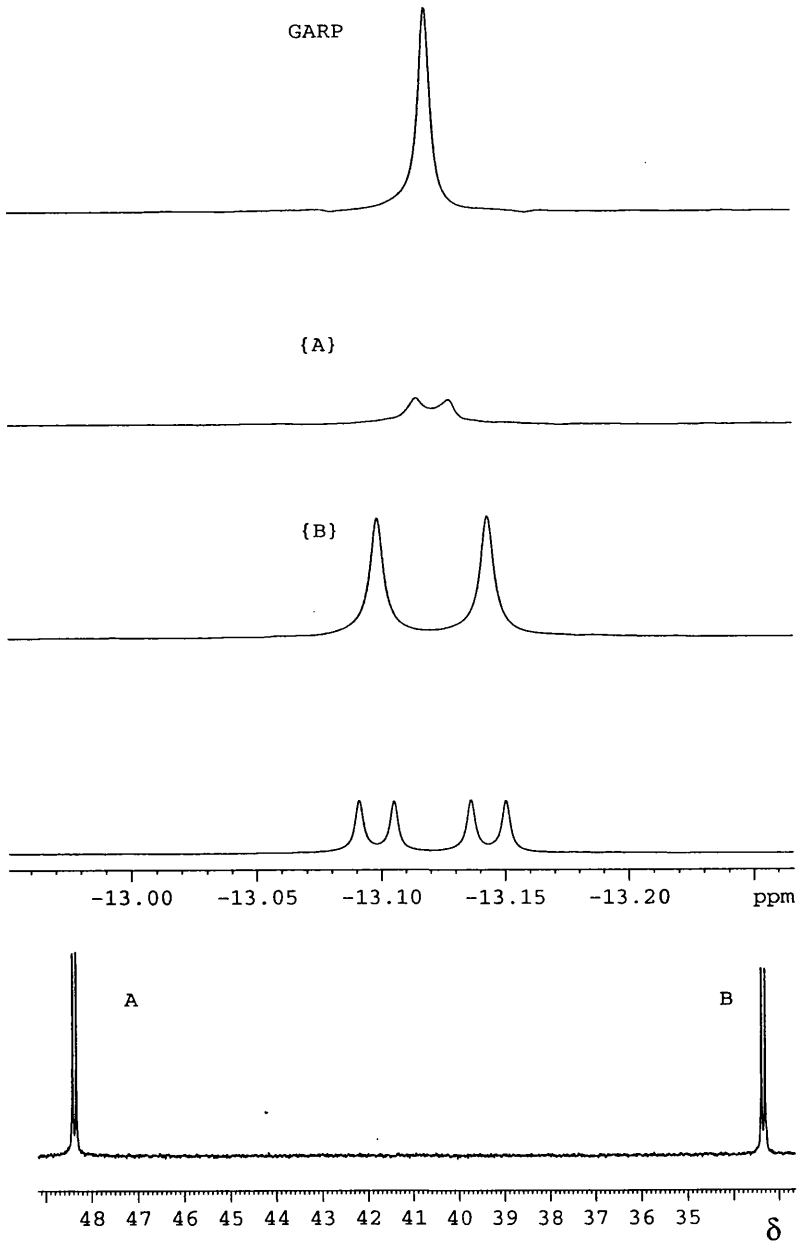

The only possibly related report is the formation of $[Os_3(\mu\text{-}OH)(\mu\text{-}MeOCO)\{\eta^1\text{-}(Me_2N)_2CS\}(CO)_9]$ (10%) in the system $[Os_3(CO)_{12}]$/tetramethylthiourea/$Me_3NO.2H_2O$ reacting in methanol/benzene but even here the major product (50%) is the substituted derivative $[Os_3(CO)_{11}\{\eta^1\text{-}(Me_2N)_2CS\}]$.

2.4.1 Spectroscopic characterisation of $[Ru_3(\mu\text{-}OH)_2(CO)_8(BINAP)]$

The ^1H NMR spectrum showed the expected spectrum in the phenyl and naphthyl region consistent with C_2 symmetry, although some of the signals were extremely broad at room temperature (signals X and Y in Figure 2.5). A high-field triplet at δ -1.48 (2H), showing equal coupling to both ^{31}P nuclei (J = 4.0 Hz), is not in the correct shift range for hydride ligand. However, μ-hydroxy ^1H NMR signals have been reported at δ -1.08 for $[Os_3(\mu\text{-}OH)(\mu\text{-}MeOCO)\{\mu\text{-}SC(NMe_2)_2\}(CO)_9]$,[80] at δ -1.61 for $[Os_3(\mu\text{-}H)(\mu\text{-}OH)(CO)_9(PMe_2Ph)]$,[81] at δ 0.54 for $[Os_3(\mu\text{-}H)(\mu\text{-}OH)(CO)_9(PEt_3)]$,[82] at δ 0.44 for $[Os_3(\mu\text{-}H)(\mu\text{-}OH)(CO)_8(dppm)]$,[42] at δ 0.20 for $[Os_3(\mu\text{-}H)(\mu\text{-}OH)(CO)_{10}]$,[83] and at δ -1.63, -1.30 and -1.48 for various PPh_3-substituted derivatives of this compound. Therefore it seems likely that the product is a dihydroxy complex. The $^{31}P\{^1H\}$ NMR singlet is also consistent with C_2 symmetry as for BINAP itself. The fluxionality of $[Ru_3(\mu\text{-}OH)_2(CO)_8(BINAP)]$ is demonstrated in Figure 2.5 which shows variable-temperature ^1H NMR spectra of the cluster. The OH ^1H NMR signal is essentially temperature-independent and the ^{13}C NMR spectra for the CO ligands and the $^{31}P\{^1H\}$ NMR spectra likewise (see Figure 2.4).

2.4.2 Crystal structure of $[Ru_3(\mu\text{-}OH)_2(CO)_8(BINAP)]$ and (R)-BINAP

To examine the consequences, and indeed to confirm the presence of, the hydroxy bridge a single-crystal X-ray structure of $[Ru_3(\mu\text{-}OH)_2(CO)_8(BINAP)]$ was carried out by Professor A. J. Deeming. Selected bond lengths and angles are to be found in Table 2.2. For comparative purposes the single-crystal X-ray structure of (R)-BINAP was also carried out.

The two similar molecules of $[Ru_3(\mu\text{-}OH)_2(CO)_8(BINAP)]$ were detected, A and B, in the unit cell ($Z = 8$) contain isosceles triangles of ruthenium atoms with the unique longer non-bonded Ru....Ru edge bridged by (R)-BINAP and two OH ligands. The unbridged Ru-Ru distances are 2.814(3) and 2.820(2) Å (molecule A) and 2.810(3) and 2.812(2) Å (molecule B), while the Ru....Ru distances are 3.023(2) Å (molecule A) and 3.030(2) Å (molecule B). The cluster $[Ru_3(\mu\text{-}OH)_2(CO)_8(BINAP)]$ is a 50-electron species and, as expected, has only two Ru-Ru bonds. It is believed that the Ru....Ru distance is as short as observed to accommodate the two OH bridges. Indeed the distance is similar to those in related triruthenium clusters with double alkoxy-bridges for which Ru....Ru distances are the range 3.002 to 3.072 Å.[84] Therefore the Ru....Ru distance in $[Ru_3(\mu\text{-}OH)_2(CO)_8(BINAP)]$ is probably controlled by the OH bridges and the favoured Ru-O distances and may therefore not be optimal for bridging BINAP.

In addition to these changes on coordination, there are significant differences in the conformation of the PPh_2 groups and in the approach of Ph to naphthyl groups on going from free BINAP to μ-BINAP in the cluster. In free BINAP the Ph groups are distant from the naphthyl groups but the process of rotating about Ph_2P-naphthyl

bonds to achieve coordination results in one phenyl of each PPh_2 aligning in a parallel graphitic type manner to the naphthyl group to which the PPh_2 is not bonded directly. This alignment is found in chelating BINAP complexes but also in μ-BINAP as may be seen in the space-filling picture of $[Ru_3(\mu\text{-}OH)_2(CO)_8(BINAP)]$ (Figure 2.7b). We believe that this alignment has a marked effect on the barrier to rotation of two of the four phenyl groups, the two that are aligned parallel to the naphthalene rings.

Because the structure of BINAP has not been reported, it was determined for comparison with the known structures of chelating BINAP and the unique structure of bridging BINAP that we have observed. A projection of the molecular structure of (R)-BINAP are shown in Figure 2.8, selected bond lengths and angles are in Table 2.3. The dihedral angle between the two naphthyl groups in free BINAP is 88.3 °, compared with 78.1 ° in $[Ru_3(\mu\text{-}OH)_2(CO)_8(BINAP)]$ and the values typically found for chelating BINAP in the range 65 to 77 °. In contrast to coordinated BINAP, there is freedom to rotate about the naphthyl-PPh_2 bonds in the free BINAP and the observed conformation reduces the lone pair-lone pair repulsions and is therefore not pre-organised to coordinate either as a chelating or bridging ligand. The orientation of the phosphorus lone pairs was assessed by placing a ghost H-atom on each phosphorus in an idealised position with all HPC angles equal. The torsional angle HP(1)P(2)H was calculated to be 165.8 °. The corresponding angle in $[Ru_3(\mu\text{-}OH)_2(CO)_8(BINAP)]$ is the torsional angle Ru(1)P(1)P(2)Ru(2) which is 1.9 °, which is close to zero as expected. There needs to be an approximately 90 ° rotation about each naphthyl-PPh_2 bond of free BINAP to set up the correct conformation for coordination.

The other major difference between free, chelating and bridging BINAP is the P(1).....P(2) distance which is 4.218 Å in free (R)-BINAP and 4.719 Å in $[Ru_3(\mu\text{-}OH)_2(CO)_8(BINAP)]$. Typically this distance is lower in chelating than in free BINAP, for example, the P....P distance in $[PdCl_2(BINAP)]$ is 3.249 Å. This shortening on chelation results from the need to attain normal metal-phosphorus distances within the chelate ring, while the lengthening on bridging results from the requirement to redirect the phosphorus lone pairs towards the metal centres (see Figure 2.9). The Ph groups in chelating BINAP (Figure 2.9b) are clearly either *equatorial* or *axial*, providing the mechanism for transmission of asymmetry from the binaphthyl group towards the other ligands at the metal centre. This is an essential feature for achieving high enantiomer excesses in asymmetric catalysis. Similar effects are apparent in μ-BINAP (Figure 2.9c) although the *equatorial* Ph groups are drawn away from adjacent ligands in this case. The difference between chelating and μ-BINAP results directly from the angle between the P-M vectors being about 90 ° in Figure 2.9b but only 41.5 ° in Figure 2.9c.

2.4.3 Carbon-13 CO enrichment of $[Ru_3(CO)_{12}]$

Ruthenium carbonyl was finely powdered and placed in an ampoule with pure n-heptane and the dead volume of the ampoule was calculated to be sufficient to admit sufficient CO gas to allow a 10% enrichment. All dissolved gas was removed with a 'freeze-pump-thaw' cycle repeated three times. ^{13}CO (98% Aldrich) was then admitted to the ampoule which was then sealed. On heating to 100 ° C in an oven all the $[Ru_3(CO)_{12}]$ dissolved to form an orange. The ampoule

was left in the oven for three days. A 10% enrichment, estimated by NMR, was achieved.

2.4.4 Carbonyl NMR studies assisted by ^{13}CO enrichment

The $^{13}C\{^1H\}$ NMR spectrum of a ^{13}CO-enriched sample of $[Ru_3(CO)_8(\mu\text{-}OH)_2(BINAP)]$ contains the expected four signals associated with C_2 symmetry: δ 206.5 (s), 205.9 (s), 205.4 (s) and 198.6 (d, J_{PC} = 4.0 Hz), the doublet being best assigned to the carbonyls in Figure 2.7 which are *trans* to the ^{31}P nuclei across the bonding Ru-Ru edges. This spectrum does not change noticeably between -65 and 40 °C indicating that the observed coalescence in the ^1H spectrum is not the result of fluxionality in the $M_3(CO)_{10}$ framework.

Figure 2.5 Variable-temperature ^1H NMR data for, $[Ru_3(\mu\text{-}OH)_2(CO)_8\{\mu\text{-}(R)\text{-}BINAP\}]$. The spectrum ($CDCl_3$, 400 MHz) is marked to show the *ortho* (A and C) *meta* (B and D) and *para* (E) sites of the phenyl ligands. The freely rotating phenyl signals appear between δ 7.2-7.4.

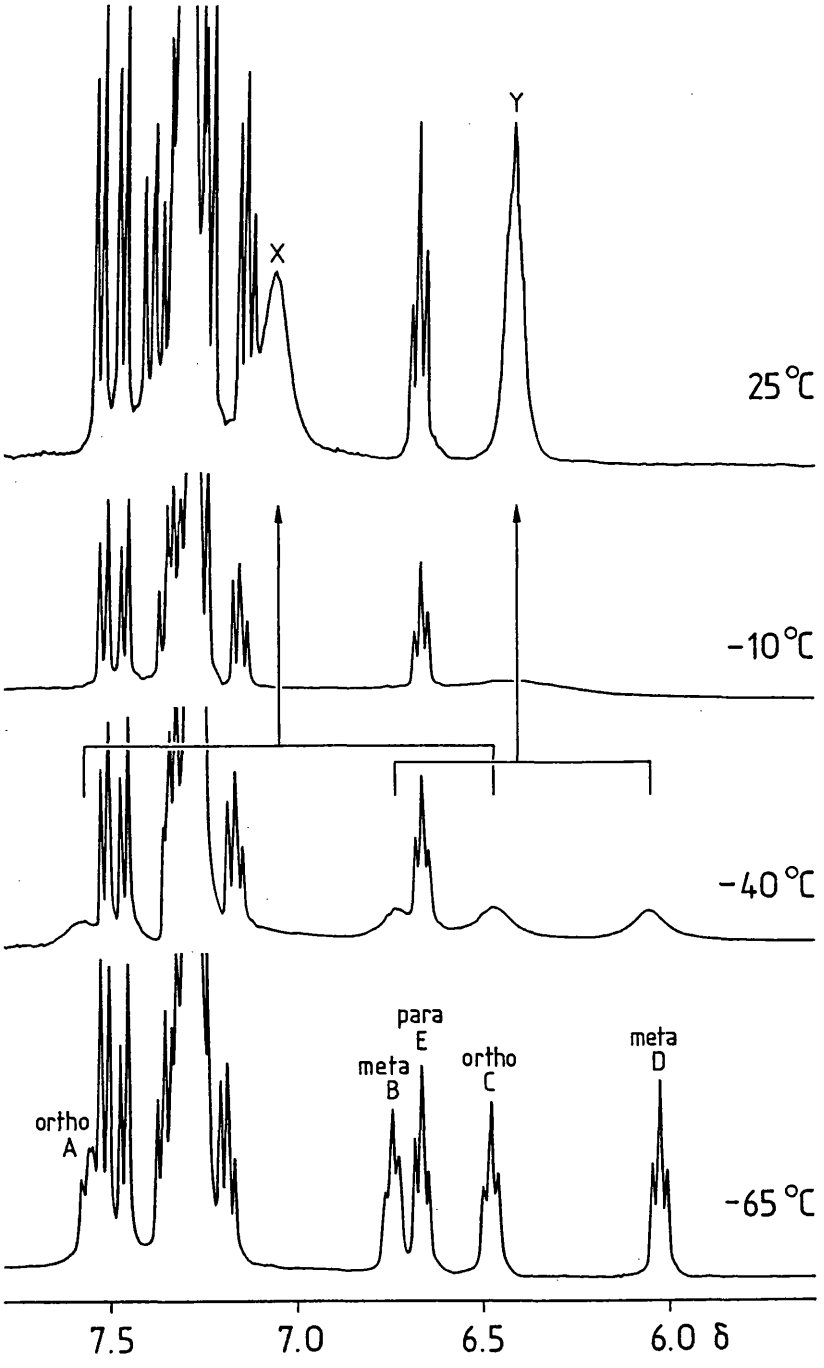

Figure 2.6 $[Ru_3(\mu\text{-}OH)_2(CO)_8\{\mu\text{-}(R)\text{-}BINAP\}]$, ^1H 400 MHz COSY NMR, –65 ° C The phenyl correlations are marked.

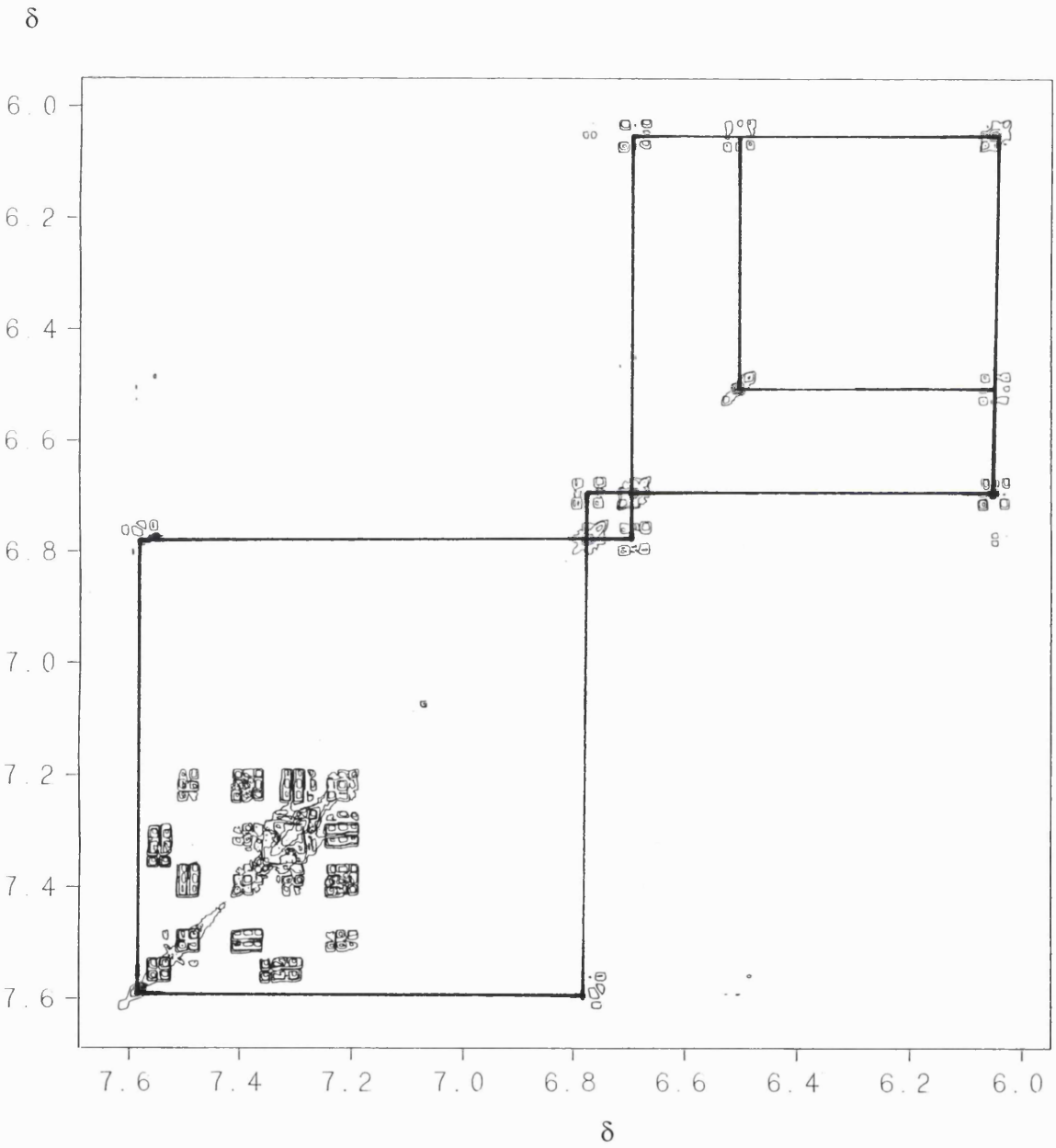

Figure 2.7a/b. Top Crystal structure of $[Ru_3(\mu\text{-}OH)_2(CO)_8\{\mu\text{-}(R)\text{-}BINAP\}]$. Showing the crystallographic labelling scheme. Thermal ellipsoids are shown at 30% probability. Note the absence of the Ru(1)….Ru(2) bond implied by the increased Ru…..Ru distance from 2.810(3) to 3.030(2)Å.

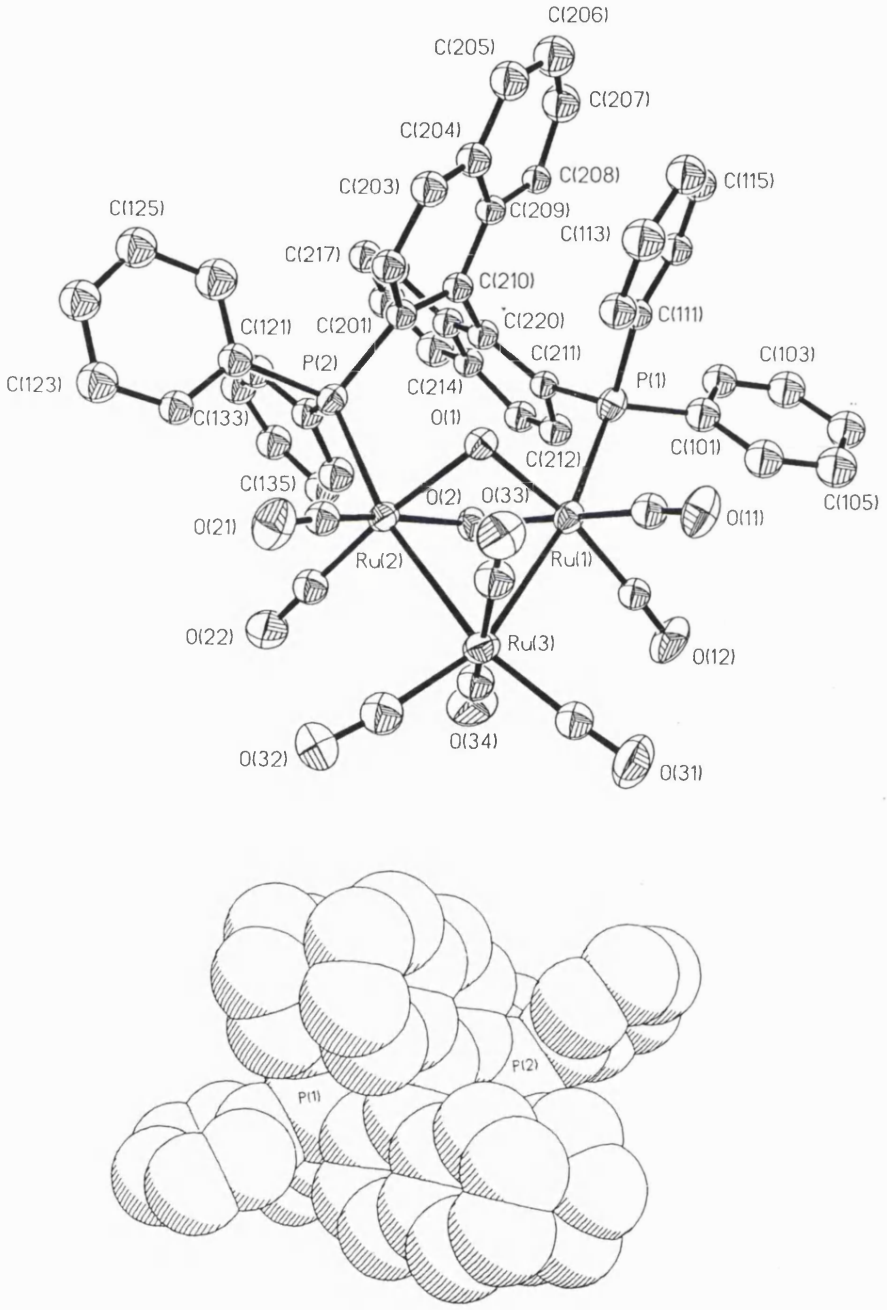

Figure 2.8. Crystal structure of [(R)-BINAP] showing the P....P distance as 4.218 (2) Å in contrast to $[Ru_3(\mu\text{-}H)(CO)_8\{(R)\text{-}BINAP\}]$ at 4.719 (3) Å.

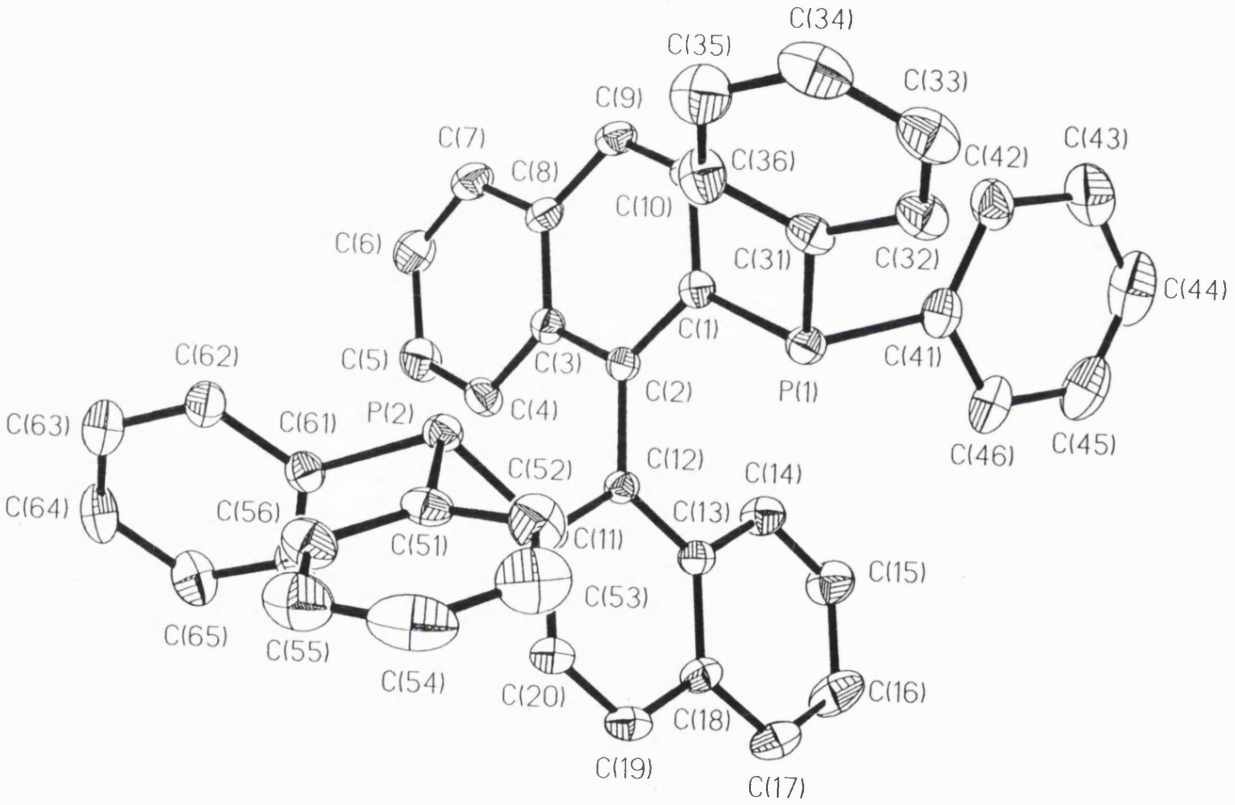

Table 2.1 Selected crystal data for $[Ru_3(OH)_2(CO)_8\{(R)\text{-BINAP}\}]$ and (R)-BINAP

crystal size (mm)	0.35 x 0.25 x 0.18	0.46 x 0.43 x 0.40
formula	$C_{52}H_{34}O_{10}P_2Ru_3$	$C_{44}H_{32}P_2$
Fw	1183.94	622.64
colour	red	colourless
crystal system	orthorhombic	monoclinic
space group	$P2_12_12_1$	$P2_1$
Temp (K)	293(2)	293(2)
a (Å)	17.982(5)	9.151(3)
b (Å)	23.775(4)	18.783(5)
c (Å)	24.262(9)	10.036(4)
β (deg)	90	103.11(3)
V (Å^3)	10372(5)	1680.0(9)
Z	8	2
d_{calc} (g cm^{-3})	1.516	1.231
μ(Mo Kα) (mm^{-1})	0.978	0.160
F(000)	4704	652
2θ range (degrees)	5 to 45	5 to 50
no. reflections measured	7289	3205
no. independent reflections	7288	3016
wR2 (all data)	0.2218	0.1320,
R1 [$I>2\sigma(I)$]	0.0690	0.0492
goodness-of-fit on F^2	1.049	1.073
Data/parameters	7284/687	3012/414
Absolute structure parameter		0.0(2) 0.05(9)
Largest differential peak/hole eÅ^{-3}	1.344, -0.800	0.225, -0.254

Figure 2.9 Contrasting modes of BINAP (a) free (b) chelating (c) bridging. The P...P distances are marked in each case.

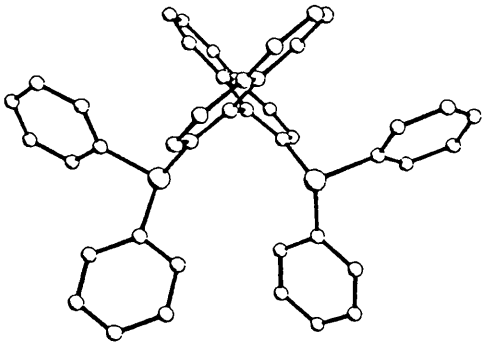

(a) 4.218 Å

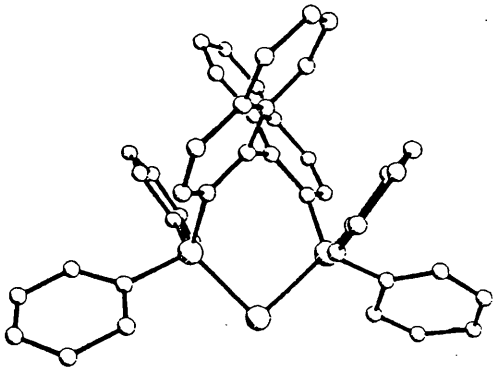

(b) 3.249 Å

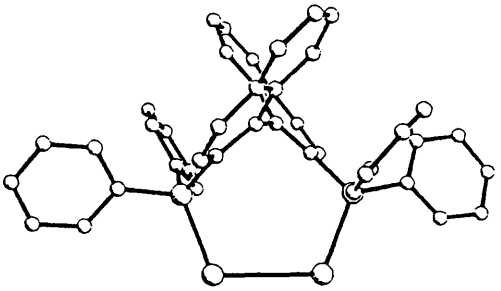

(c) 4.719 Å

Table 2.2

Selected Bond Lengths (Å) and Angles (deg) for $[Ru_3(\mu\text{-}OH)_2(CO)_8(BINAP)]$

Molecule A		Molecule B	
Ru(1)-O(2)	2.102(13)	Ru(4)-O(4)	2.112(12)
Ru(1)-O(1)	2.111(13)	Ru(4)-O(3)	2.118(13)
Ru(1)-P(1)	2.391(6)	Ru(4)-P(3)	2.400(6)
Ru(1)-Ru(3)	2.814(3)	Ru(4)-Ru(6)	2.810(3)
Ru(1)-Ru(2)	3.023(2)	Ru(4)-Ru(5)	3.030(2)
Ru(2)-O(1)	2.102(13)	Ru(5)-O(3)	2.111(14)
Ru(2)-O(2)	2.133(14)	Ru(5)-O(4)	2.124(13)
Ru(2)-P(2)	2.394(6)	Ru(5)-P(4)	2.403(6)
Ru(2)-Ru(3)	2.820(2)	Ru(5)-Ru(6)	2.812(2)
P(1)-C(101)	1.79(2)	P(3)-C(311)	1.83(2)
P(1)-C(211)	1.84(2)	P(3)-C(301)	1.86(2)
P(1)-C(111)	1.82(2)	P(3)-C(401)	1.86(2)
P(2)-C(131)	1.81(2)	P(4)-C(331)	1.83(2)
P(2)-C(121)	1.82(2)	P(4)-C(411)	1.84(2)
P(2)-C(201)	1.85(2)	P(4)-C(321)	1.86(2)
O(2)-Ru(1)-O(1)	79.1(5)	O(4)-Ru(4)-O(3)	79.5(5)
O(2)-Ru(1)-P(1)	87.7(4)	O(4)-Ru(4)-P(3)	90.2(4)
O(1)-Ru(1)-P(1)	89.7(4)	O(3)-Ru(4)-P(3)	88.7(4)
Ru(3)-Ru(1)-Ru(2)	57.65(6)	Ru(6)-Ru(4)-Ru(5)	57.43(6)
O(1)-Ru(2)-O(2)	78.6(5)	O(3)-Ru(5)-O(4)	79.4(5)
O(1)-Ru(2)-P(2)	88.3(4)	O(3)-Ru(5)-P(4)	89.1(4)
O(2)-Ru(2)-P(2)	90.2(4)	O(4)-Ru(5)-P(4)	88.6(4)
Ru(3)-Ru(2)-Ru(1)	57.44(6)	Ru(6)-Ru(5)-Ru(4)	57.34(6)
Ru(1)-Ru(3)-Ru(2)	64.91(6)	Ru(4)-Ru(6)-Ru(5)	65.23(6)
Ru(2)-O(1)-Ru(1)	91.7(5)	Ru(5)-O(3)-Ru(4)	91.5(5)
Ru(1)-O(2)-Ru(2)	91.1(5)	Ru(4)-O(4)-Ru(5)	91.3(5)

Table 2.3

Selected Bond Lengths (Å) and Angles (deg) for (R)-BINAP.

P(1)-C(31)	1.819(5)	P(2)-C(11)	1.843(5)
P(1)-C(1)	1.830(5)	C(1)-C(2)	1.375(7)
P(1)-C(41)	1.843(6)	C(2)-C(12)	1.499(6)
P(2)-C(61)	1.823(6)	C(11)-C(12)	1.380(7)
P(2)-C(51)	1.839(5)		
C(31)-P(1)-C(1)	103.5(2)	C(51)-P(2)-C(11)	100.6(2)
C(31)-P(1)-C(41)	103.3(3)	C(2)-C(1)-P(1)	118.7(4)
C(1)-P(1)-C(41)	101.4(2)	C(10)-C(1)-P(1)	122.1(4)
C(61)-P(2)-C(51)	102.3(3)	C(12)-C(11)-P(2)	118.7(4)
C(61)-P(2)-C(11)	102.1(2)	C(20)-C(11)-P(2)	121.7(4)

2.4.5 Dynamic ^{1}H NMR behaviour in the phenyl region, assignment of phenyl signals by COSY at low temperature

Fluxionality of $[Ru_3(\mu\text{-}OH)_2(CO)_8(BINAP)]$ is apparent in the variable-temperature ^{1}H NMR spectra of the cluster (Figure 2.5). The OH signal is essentially temperature-independent. Analysis of a COSY ^{1}H NMR spectrum (Figure 2.6) showed that the exchange is occurring between protons giving signals A and C to give X and between B and D to give Y and that the coupling is entirely consistent with two equivalent Ph groups giving rise to signals A to E (see Figure 2.5 for the labelling scheme), that is these two phenyl groups have non-equivalent *ortho* and *meta* positions as a result of restricted rotation at low temperature. Exchange is between non-equivalent 2 and 6 positions and between 3 and 5 positions as a result of restricted rotation about two of the four Ph-P bonds. This can be rationalised by unrestricted rotation of two Ph groups and restricted rotation of the two Ph groups aligned with the naphthyl groups. We are assuming that it is the phenyls that lie parallel to the naphthyl groups that experience the greatest barrier to rotation as it is easy to see the cause of the rotational barrier. To our knowledge restricted phenyl rotation of this kind has not been reported for chelating BINAP.

2.5 Conclusions

a) A new cluster $[Ru_3(\mu\text{-}OH)_2(CO)_8(BINAP)]$ of C_2 symmetry may be prepared in good yield by treatment of the parent cluster $[Ru_3(CO)_{12}]$ with BINAP in the presence of $Me_3NO{\bullet}2H_2O$. This cluster presents the novel phenomenon of bridging dihydroxy groups between the two metal centres that also carry the bridging BINAP ligand.

b) A new cluster $[Ru_3(\mu\text{-}H)(CO)_9(BINAP\text{-}H)]$ may be prepared by thermal treatment of the parent cluster $[Ru_3(CO)_{12}]$ with the ligand BINAP in refluxing octane. This material is the first example of metallated BINAP. There is consequential loss of C_2 symmetry and suppression of CO fluxional processes expected for the unobserved precursor $[Ru_3(CO)_{10}(BINAP)]$.

c) Products analogous to the expected $[M_3(CO)_{10}L]$ type cluster have not been generated by the above reactions nor could we generate them by reversal of the orthometallation process by treatement of $[Ru_3(\mu\text{-}H)(CO)_9(BINAP\text{-}H)]$ with CO.

d) These unusual products and the inability to produce the expected decacarbonyl cluster $[Ru_3(CO)_{10}(BINAP)]$ are in marked contrast to the results described in the following chapter where the expected triosmium $[Os_3(CO)_{11}(BINAP)]$ and $[Os_3(CO)_{10}(BINAP)]$ clusters are described.

2.6 Experimental

The parent carbonyl compound $[Ru_3(CO)_{12}]$ was obtained from Strem and (R)-BINAP was obtained from Aldrich. All solvents were purified prior to use by standard methods.

2.6.1 Reaction of $[Ru_3(CO)_{12}]$ with (R)-BINAP in the presence of $Me_3NO{\bullet}2H_2O$.

Solid samples of ruthenium carbonyl (0.050 g) and (R)-BINAP (0.070 g) were finely ground together and added to a solution of trimethylamine-*N*-oxide (0.050 g) in methanol (1 cm^3) and acetonitrile (5 cm^3). Dichloromethane (35 cm^3) was added and the mixture refluxed under nitrogen for 1 hour. The resulting solution was passed through a short column of silica to remove any excess of the amine oxide and the solvent was removed under reduced pressure. The residual solid was separated by TLC on silica (Merck 5715 pre-prepared plates) eluting with a dichloromethane-hexane mixture (3:7 v/v). The main orange-brown band was extracted with dichloromethane to yield $[Ru_3(\mu\text{-}OH)_2(CO)_8\{\mu\text{-}(R)\text{-}BINAP\}]$ as an orange-brown solid (80%). The parent molecular ion centred at 1184 (calculated 1184) and the successive loss of five CO ligands were observed in the FAB MS. Analysis: Calculated for $C_{52}H_{34}O_8P_2Ru_3$: C, 54.22; H, 2.98%. Found: C, 55.59; H, 4.72%. Crystals for single crystal X-ray structure were obtained by slow evaporation of a solution in 2-ethoxyethanol. $\nu(CO)/cm^{-1}$ (hexane): 2066(m), 2028(m), 2017(vs), 1986(w), 1972(w), 1937(s), 1911(vs); $\delta(^{31}P)$ ($CDCl_3$ 20 °C) 40.22 (s); $\delta(^1H)$ ($CDCl_3$ 20 °C) exchanging Ph signals (broad above -65 °C), δ 6.03

(t, *meta*), 6.48 (t, *ortho*), 6.67 (t, *para*), 6.76 (t, *meta*), 7.56 (dd, *ortho*); other signals: δ 7.35 - 7.48 (overlapping m), 7.47 (d), 7.52 (d), -1.48 (t, OH, J_{PH} 4.0 Hz); δ($^{13}C\{^1H\}$) ($CDCl_3$ 20 °C) d 206.5 (s), 205.9 (s), 205.4 (s), 198.6 (d, J = 35.3 Hz) Ph and naphthyl signals: δ 143.6 to 126.6.

2.6.2 Direct thermal reaction of $[Ru_3(CO)_{12}]$ with (R)-BINAP

A mixture of ruthenium carbonyl (0.030 g) and (R)-BINAP (0.030 g) in octane (15 cm^3) was heated under nitrogen under reflux for 45 min. The cooled solution was filtered through a short silica column and the solvent was removed under reduced pressure (10^{-3} mm Hg) to give a brown residue. This was dissolved in CH_2Cl_2 and loaded on to TLC plates (SiO_2) and eluted with a dichloromethane/hexane mixture (3:7 by volume) to give three bands. Two gave small amounts of uncharacterised material: a mauve residue (0.004 g) and a yellow residue (0.001 g), while the main orange-brown band gave an orange solid (0.023 g, 38%) characterised as $[Ru_3(\mu\text{-}H)(\mu_3\text{-BINAP-H})(CO)_9]$. Analysis. Calculated for $C_{53}H_{32}O_9P_2Ru_3$: C, 54.04; H, 2.74%. Found: C, 54.81; H, 3.22%. The highest mass peaks observed in the FAB MS correspond to the loss of 2CO from $[Ru_3(\mu\text{-}H)(CO)_9(\mu_3\text{-BINAP-H})]$. ν(CO)/$cm^{-1}$ (hexane): 2065(vs), 2027(vs), 2014(vs), 1985(s), 1970(s), 1962(m), 1948(m); δ(^{31}P) δ 42.1 (dd, J_{PP} = 40, J_{HP} = 43 Hz), 26.8 (dd, J_{PP} = 40, J_{HP} = 14 Hz), (coupling between hydride ligand and ^{31}P was observed), δ(^1H) 8.26 (m), 7.69 (d), 7.55-7.49 (m), 7.40(dd), 7.30-7.20 (m), 7.09 (dd), 7.05 (t), 6.90 (t), 6.84 (m), 6.82 (m), 6.78 (d), 6.66 (dd), 6.53 (d), 6.40 (dd), 6.37 (m), 6.33 (d), 6.28 (t), 6.19 (t), -16.49 (dd, J_{PH} = 14.0, 42.5 Hz, Ru*H*Ru); δ$^{13}C\{^1H\}$ CO signals, δ 202.9 (s), 202.8 (s), 202.7 (s), 198.2 (s), other signals at

168.7 (d), 150.1 (d), 144.0 (s) and about 40 signals (doublets and singlets, δ 123 to 138).

2.6.3 Carbon-13 CO enrichment of $[Ru_3(CO)_{12}]$ and preparation of derivatives

$[Ru_3(CO)_{12}]$ (1g) was placed in a 220 cm^3 Carius tube containing 80 cm^3 of heptane. The solution was frozen in liquid nitrogen and pumped for five minutes at 10^{-1} Torr. The freeze-pump-thaw cycle was repeated three times. The ^{13}CO (99% ^{13}CO) was supplied by the Aldrich Chemical Co. in a steel cylinder at atmospheric pressure. The ^{13}CO was admitted to the Carius tube via a two-way oblique tap. The Carius tube was then flame sealed and placed in an oven at 55°C for three days. Enrichment was determined by NMR against a standard. 10 cm^3 of $CDCl_3$ was doped with a small amount of n-octane (chosen as it was non volatile). 30 mg of $[Ru_3(CO)_{12}]$ with natural isotopic abundances were dissolved in 1 cm^3 of this stock solution at 40 °C and, an identical sample was prepared using the ^{13}CO enriched material. The intensities of the carbonyl peaks were integrated against the octane signal. The enrichment was determined as the percentage increase in integral. This sample was used to synthesise ^{13}CO-enriched $[Ru_3(\mu\text{-}OH)_2(CO)_8\{\mu\text{-}(R)\text{-}BINAP\}]$ by the method given in Section 1.6.1.

2.6.4 Crystal structure determination for $[Ru_3(\mu\text{-}OH)_2(CO)_8(BINAP)]$ and (R)-BINAP

Single crystals of $[Ru_3(\mu\text{-}OH)_2(CO)_8(BINAP)]$ were obtained by overlaying a saturated CH_2Cl_2 solution with 2-ethoxyethanol and allowing solvent diffusion to occur at room temperature. Single crystals of (R)-BINAP were obtained by slow evaporation of an ethanolic solution. Crystals of each were mounted on glass fibres on a Nicolet R3m/v diffractometer. Data were collected at 293(2) K using graphite-monochromated Mo-K_α radiation (λ = 0.71073 Å). Three standard reflections were measured every 97 reflections and showed very small variations in intensity. Intensities were corrected for Lorentz and polarisation effects and empirical absorption corrections were applied for $[Ru_3(\mu\text{-}OH)_2(CO)_8(BINAP)]$ but not for (R)-BINAP, based upon Ψ-scans. The structures were solved by direct methods in space group and the structures were refined by full-matrix least-squares refinement of $|F^2|$, using SHELXTL-PLUS. H-atoms were included in calculated positions using a riding model with C-H distance of 0.96 Å and fixed isotropic thermal parameters of 0.08 $Å^2$. All other atoms were refined anisotropically except the carbon atoms in $[Ru_3(CO)_8(\mu\text{-}OH)_2(BINAP)]$. There are two independent molecules in the unit cell. The data were collected by Professor A. J. Deeming and the structure determined by Dr. D. M. Speel and Professor A. J. Deeming at UCL.

Chapter 3. Reactions of $[Os_3(CO)_{12}]$ with (R)-2,2'-bis(diphenylphosphino)-1,1'-binaphthyl [BINAP]

3.1 Introduction

Earlier in this work (Chapter 2) the characterisation of the first example of BINAP bridging an M-M bond in an M_3 cluster was described.[44] The reactions of simple diphosphines ligands with $[Os_3(CO)_{12}]$ have been thoroughly and systematically studied. However, given the unprecedented nature of the cluster $[Ru_3(\mu\text{-}OH)_2(CO)_8\{R\text{-}BINAP\}]$, a comparative study was justified. As the reactions of $[Os_3(CO)_{10}(MeCN)_2]$ or $[Os_3(CO)_{12}]$ with diphosphine ligands are usually very similar to those of $[Ru_3(CO)_{10}(MeCN)_2]$ or $[Ru_3(CO)_{12}]$, we were interested to compare these two parallel systems. In later parts of this work tolBINAP (the 4-tolyl analogue of BINAP) has been shown to bridge two metal centres (see Chapter 4) in a product formed from reaction of BINAP with $[Os_3(\mu\text{-}H)_2(CO)_{10}]$.

The reactions of $[Os_3(CO)_{12}]$ with bidentate diphosphine ligands such as dppp and dppe are well known and the dppe products characterised by single crystal X-ray were obtained from a mixture of the bridging and chelating isomers of $[Os_3(CO)_{10}\{dppe\}]$.[85,86] It is also established that dppm only forms the bridging isomer 1,2-$[Os_3(CO)_{10}\{dppm\}]$ because of the steric limitations of the five membered ring.[90] 1,2-$[Os_3(CO)_{10}\{dppm\}]$ is formed by the direct reaction of $[Os_3(CO)_{12}]$ with dppm in the presence of Me_3NO and was characterised by an X-ray study.[85,87] However initially characterisation was on the basis of the observed fluxionality in the ^{13}C NMR spectra.[88] More highly substituted triruthenium clusters have been reported including $[Ru_3(CO)_6\{dppe\}_3]$[89] but such

reports are rarer for triosmium clusters on account of its lower reactivity as assessed by reaction rates with PPh_3.[90,91]

Rather than using $[Os_3(CO)_{12}]$ directly, it has been more usual to synthesis these compounds by the reaction of, the mixed butadiene adducts 1,1- and 1,2-$[Os_3(C_4H_6)(CO)_{10}]$[92] or more recently 1,2-$[Os_3(CO)_{10}(MeCN)_2]$.[93] The main reason that these milder and therefore more direct reactions are preferred over thermal reactions of the parent carbonyl is the better yield of the simple substituted clusters and a reduction or elimination in the amount of the orthometallated materials and higher nuclearity clusters produced. It has been shown that orthometallation is a reversible process for dppm.[28] Dppm reacts with $[Os_3(CO)_{12}]$ by thermolysis to form amongst other clusters $[Os_3(\mu\text{-}H)(CO)_8\{\mu\text{-}Ph_2PCH_2P(Ph)C_6H_4]$ which can then be converted to 1,2-$[Os_3(CO)_{10}\{dppm\}]$ by refluxing in a solution saturated with CO.

Just prior to the publication of our work we were made aware[14] that Ebbe Nordlander and his group at the University of Lund had been following a similar line of work.[69] However the recent publication of the Lund group does not contain a crystal structure for $[Os_3(\mu\text{-}H)(CO)_8(R\text{-}BINAP\text{-}H)]$, nor do they report the ^{13}C data which confirms that $[Os_3(CO)_{10}(R\text{-}BINAP)]$ is chelating, nor the ^{31}P fluxional behaviour for $[Os_3(CO)_{11}(R\text{-}BINAP)]$. More recently a single crystal X-ray structure has been determined, by Monari, confirming the 1,1 structure established by our earlier NMR studies on $[Os_3(CO)_{10}(BINAP)]$.[94] However, reassuringly the results of the Lund group do serve to confirm the fundamental conclusions of this work.

3.2 Objectives of the work described in this chapter

The aims and objectives of the work carried out in this chapter were:-

a) To incorporate a chelating chiral diphosphine at one metal centre or a bridging chiral diphosphine at two metal centres in trinuclear clusters.
b) To examine the reactivity at the remaining metal atoms to appraise the consequences of including a chiral ligand.
c) To explore the reactivity of any orthometallated materials towards carbon monoxide and hydrogen under a variety of conditions with the aim of reversing orthometallation reactions.
d) To establish whether chiral selectivity can be transmitted across a cluster.
e) To explore and contrast BINAP triosmium clusters with the BINAP triruthenium clusters described in Chapter 2.

3.3 Thermal reactions

3.3.1 Thermal reactions of $[Os_3(CO)_{12}]$ with BINAP

Treatment of $[Os_3(CO)_{12}]$ with (R)-BINAP in refluxing hydrocarbon solvent (heptane or octane) gave three isolable products, which are air and thermally stable and can be separated on silica. Similar products, but in different yields, were obtained when the mixture was purged with CO gas during the reaction or when (R)-BINAP is treated with $[Os_3(CO)_{10}(MeCN)_2]$ in THF. The FAB mass spectra of the products in a 3-nitrobenzyl alcohol matrix are consistent with the formulae $[Os_3(CO)_x\{(R)\text{-BINAP}\}]$ **1** (x = 11), **2** (x = 10) and **3** (x = 8). Clusters 1 and 2 are simple substituted compounds while 3 is an orthometallated derivative.

Carbonylation of $[Os_3(\mu\text{-H})(CO)_8\{(R)\text{-BINAP-H}\}]$ was attempted by refluxing a solution under an atmosphere of CO, by reaction with CO under pressure in an autoclave, and by refluxing with the solution being purged with CO. None of these methods yielded the desired cluster 1,2-$[Os_3(CO)_{10}\{R\text{-BINAP}\}]$ or indeed the other possible isomer 1,1-$[Os_3(CO)_{10}\{R\text{-BINAP}\}]$. As will become clearer, 1,1-$[Os_3(CO)_{10}\{R\text{-BINAP}\}]$ is the likely product from this reaction in view of the established structure for the orthometallated product.

3.3.2 Crystal structure of $[Os_3(\mu\text{-H})(CO)_8(\mu_3\text{-BINAP-H})]$

As has been commented on before, there are relatively few X-ray structures of BINAP derivatives in the literature. This is quite probably because of poor

packing characteristics associated with BINAP complexes leading to relatively poor crystals that are at the boundaries of what is acceptable for data collection on a non area detector diffractometer. However a single-crystal structure determination for $[Os_3(\mu\text{-}H)(CO)_8(\mu_3\text{-}BINAP\text{-}H)]$ has established the arrangement of the orthometallated BINAP ligand at the triosmium unit. Generally poor crystals were obtained from a mixed methanol-dichloromethane solution and an adequate but not ideal crystal was selected for study. The molecular structure is shown in Figure 3.1 and selected bond lengths and angles are in Table 2. Unlike the assumed precursor cluster $[Os_3(CO)_{10}(R\text{-}BINAP)]$, which has 1,1-di*equatorial* BINAP coordination (see later), the orthometallated cluster $[Os_3(\mu\text{-}H)(CO)_8(\mu_3\text{-}BINAP\text{-}H)]$ has 1,1-*axial-equatorial* coordination of the BINAP at Os(2) as well as a bridging coordination of the orthometallated phenyl group across metal atoms Os(1) and Os(3). Figure 3.1 shows that the mode of μ_3-bridging in this ligand system requires the BINAP to have *axial-equatorial* coordination in order for a phenyl group to approach the other osmium atoms. Thus Os(2) is bonded to P(1) and P(2) and orthometallation has occurred at Os(3) which carries the σ-Os(3)-C(101) bond, while Os(1) has an η^2-contact to C(101) and C(106) of the orthometallated phenyl ring. The geometry of the η^1,η^2-phenyl is unexceptional with the σ-Os(3)-C(101) bond being significantly shorter than the Os-C distances in the η^2-contact. The hydride ligand was not located but CO ligand positions indicate that it is bridging atoms Os(2) and Os(3), which are connected by the longest Os-Os contact [3.061(2) Å] compared with Os(1)-Os(2) [2.885(2) Å] and Os(1)-Os(3) [2.799(2) Å]. On this basis the hydride must lie close to the intersection of the C(22)-Os(2) and C(33)-Os(3) vectors, slightly above the Os_3 plane. The orthometallated ligand is a 7-electron donor making the

cluster a 48-electron species. Although we would expect there to be three Os-Os bonds, the Os(2)-Os(3) distance of 3.061(2) Å would normally be considered too long for a bonding interaction. However, this long bond is the result of there being a bridging hydride across it.

The previously reported cluster $[Ru_3(\mu\text{-H})(CO)_9\{\mu_3\text{-(R)-BINAP-H}\}]$[11] has significantly different spectroscopic characteristics from those of $[Os_3(\mu\text{-H})(CO)_8\{\mu_3\text{-(R)-BINAP-H}\}]$ and, with the extra CO ligand, it is probable that it has a phenyl group without any η^2-contact. No suitable crystals of $[Ru_3(\mu\text{-H})(CO)_9\{\mu_3\text{-(R)-BINAP-H}\}]$ for XRD work were formed and therefore this cannot be confirmed. There is no basis for establishing the mode of attachment of the orthometallated phenyl group from spectroscopic data although it should be possible to detect the phenyl-H group in the NMR spectra. As far as we have been able to determine from COSY and selective decoupling experiments the phenyl-H signals are overlapped by the naphthyl signals and therefore we have not been able to analyse these spectra successfully.

Figure 3.1 Crystal structure of $[Os_3(\mu\text{-H})(CO)_8\{\mu_3\text{-BINAP-H}\}]$. The hydride presumed to bridge Os2 and Os3 is not shown as it was not directly detected.

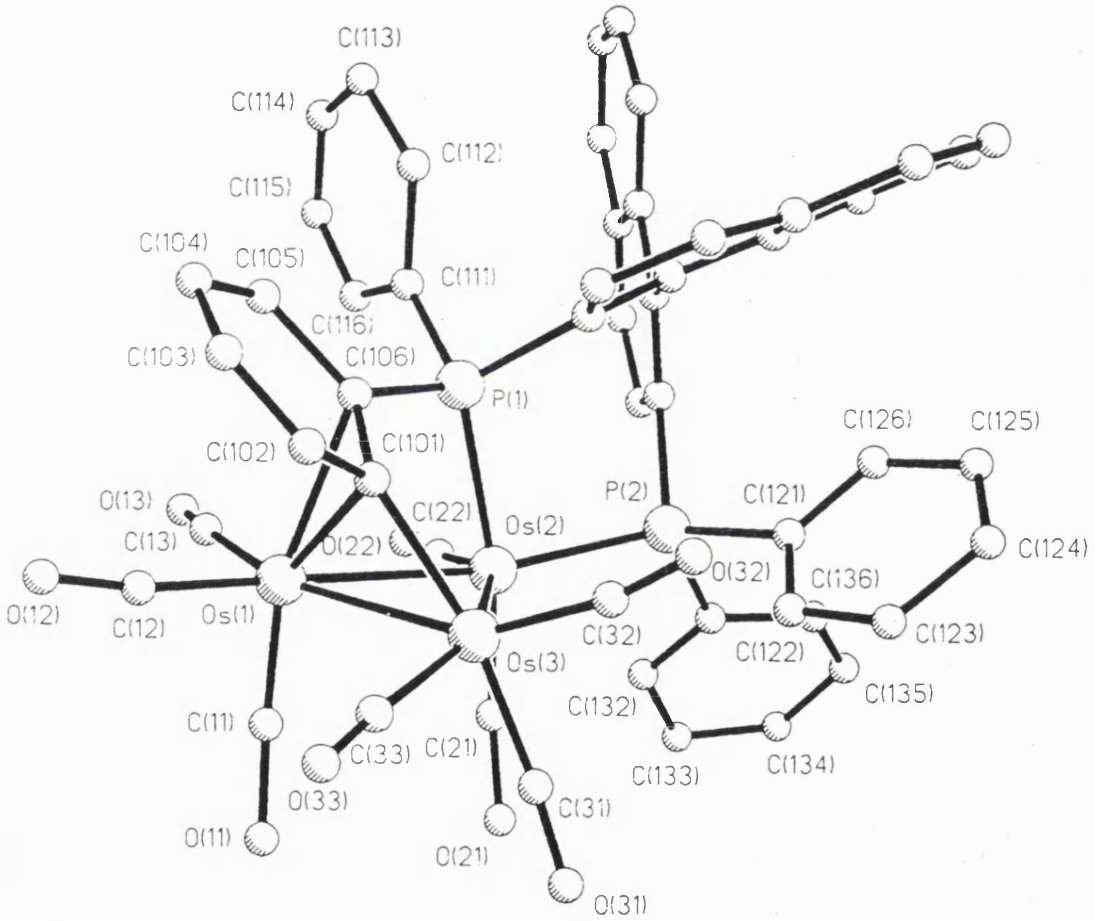

3.3.3 Spectroscopic characterisation of $[Os_3(\mu\text{-}H)(CO)_8(\mu_3\text{-}BINAP\text{-}H)]$

In light of the crystal structure (discussed in the previous section) it may be readily envisaged that the cluster $[Os_3(CO)_{10}(R\text{-}BINAP)]$ should undergo loss of one or two CO ligands followed by rapid internal oxidative addition to yield orthometallated species. Indeed there is direct evidence for this from our monitoring of the $^{31}P\{^1H\}$ NMR spectra of $[Os_3(CO)_{11}(BINAP)]$ in toluene d_8 during its thermolysis in an NMR tube (see Section 3.8.1). The major product from the reaction of $[Os_3(CO)_{12}]$ with BINAP in refluxing heptane or octane was initially assigned the stoichiometry $[Os_3(\mu\text{-}H)(CO)_8\{\mu_3\text{-}(R)\text{-}BINAP\text{-}H\}]$ purely on the basis of its spectroscopic data, principally the mass spectrum. It is not surprising that a cluster with apparent formula $[Os_3(CO)_8\{BINAP\}]$, which would be unsaturated, has undergone internal oxidative addition. The ^1H and $^{13}C\text{-}\{^1H\}$ NMR spectra are extremely complex but the double doublet signal in the hydride region of the ^1H NMR spectrum at δ -16.86 ($J_{P\text{-}H}$ = 8.3 and 17.3 Hz) is consistent with an orthometallation product. The different couplings of the two ^{31}P nuclei indicate that the phosphorus nuclei are non equivalent. An examination of the aromatic region shows that signals cover a considerably wider shift range than that of the parent BINAP molecule or that previously reported for $[Ru_3(OH)_2(CO)_8(R\text{-}BINAP)]$ indicating that the cluster has lost C_2 symmetry and pointing towards the possibility of metallation at a phenyl group. The $^{31}P\text{-}\{^1H\}$ NMR spectrum (^1H-decoupled in the aromatic but not the hydride region) shows a double doublet for each of the non-equivalent phosphorus nuclei. This confirms the loss of C_2 symmetry. Each phosphorus atom is coupled to the hydride as well as to each other.

3.3.4 Attempted carbonylation of $[Os_3(\mu\text{-}H)(CO)_8(\mu_3\text{-}BINAP\text{-}H)]$

As, at this stage, we were most interested in obtaining the cluster $[Os(CO)_{10}(BINAP)]$ (with either the phosphines bridging one edge of the M_3 triangle or chelating to one metal centre) in high yield for subsequent work. Attempts were made to carbonylate the orthometallated cluster $[Os_3(\mu\text{-}H)(CO)_8(\mu_3\text{-}BINAP\text{-}H)]$ to reverse the orthometallation reaction. Given the low yield of 1,1-$[Os(CO)_{10}(BINAP)]$ obtained from the direct reaction of $[Os_3(CO)_{10}(MeCN)_2]$ with BINAP or the thermal reaction of $[Os_3(CO)_{12}]$ with BINAP, it was hoped that the carbonylation might provide a higher yield route to 1,1-$[Os(CO)_{10}(BINAP)]$ or less likely 1,2-$[Os(CO)_{10}(BINAP)]$. The cluster $[Os_3(\mu\text{-}H)(CO)_8(\mu_3\text{-}BINAP\text{-}H)]$ has the BINAP coordinated as a bridge between three metal centres over one face of the cluster. However the two phosphorus atoms are chelating at one Os atom so that the reversal of the orthometallation by the addition of CO could have provided a route to 1,1-$[Os_3(CO)_{10}(BINAP)]$. No change in the IR or ^1H NMR spectra was observed on attempted carbonylation either at ambient temperature in dichloromethane or in refluxing octane. It is possible that carbonylation under higher pressure might be more satisfactory.

3.4 Reaction of $[Os_3(MeCN)_2(CO)_{10}]$ and BINAP

A solution of the cluster $[Os_3(MeCN)_2(CO)_{10}]$ and an equimolar quantity of (R)-BINAP in dry THF was refluxed for 30 min. The products isolated by TLC on silica were $[Os_3(CO)_{10}(BINAP)]$ (80%) and very minor quantities of $[Os_3(CO)_{11}(BINAP)]$ and $[Os_3(\mu\text{-}H)(CO)_8(BINAP\text{-}H)]$ which were only characterised by their IR spectra.

Figure 3.2 Variable temperature $^{13}C\{^1H\}$ $[Os_3(CO)_{10}(BINAP)]$ in, $CDCl_3$ solution recorded at 9.4 T. The inset shows the ^{31}P coupled triplet ($J_{P\text{-}C}$ = 7.9 Hz), $CDCl_3$ recorded at 7.05 T.

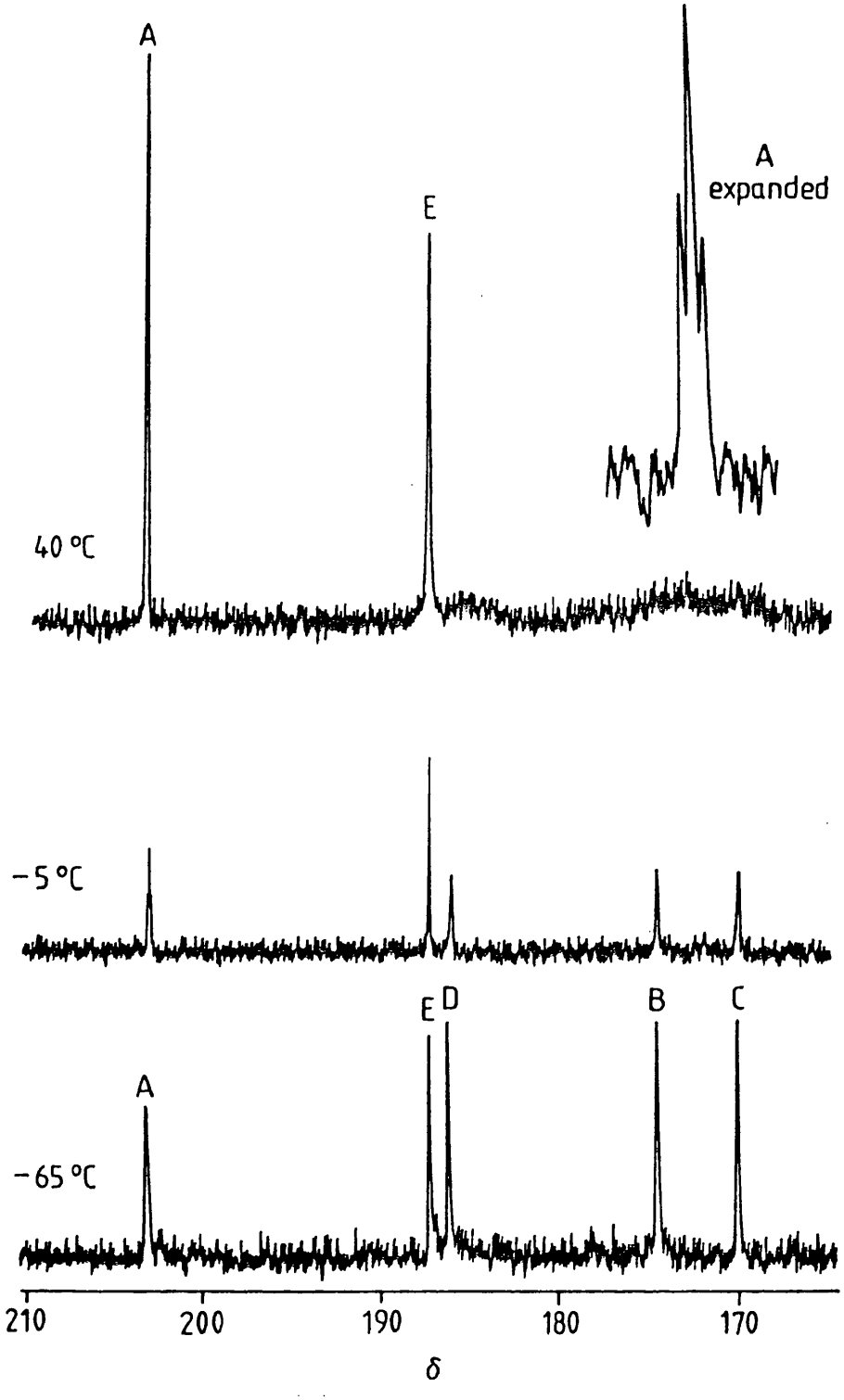

3.4.5 Spectroscopic characterisation and fluxional behaviour of $[Os_3(CO)_{10}(BINAP)]$

The ^{13}C-$\{^1H\}$ NMR spectra of this compound clearly indicate that BINAP is chelating and the cluster is without doubt the 1,1-isomer, as was later confirmed by an X-ray study.[94] It is predicted that there will be five different CO ligand environments in ratio 2:2:2:2:2 for both 1,1- and 1,2-isomers of $[Os_3(CO)_{10}(BINAP)]$ (Figure 3.3). Five signals are indeed observed at -65 °C at δ 203.0, 187.2, 186.1, 174.4 and 169.9 (Figure 3.2). The observation of a 1:2:1 triplet for the signal at δ 203.0 (J_{PC} = 7.9 Hz) (more clearly resolved at intermediate temperatures above –65 °C) can only be reconciled with the 1,1-structure, with this signal assigned to the carbonyl ligands **A** (Figure 3.3). For comparison, the 1,1-isomer of $[Os_3(CO)_{10}(PMe_2Ph)_2]$ gives a 1:2:1 triplet at δ 202.1 (J_{PC} = 9.5 Hz) for the corresponding *axial* carbonyl ligands of the $Os(CO)_2(PMe_2Ph)_2$ group. This assignment of structure for $[Os_3(CO)_{10}(BINAP)]$ is confirmed by the pattern of NMR coalescences at higher temperatures. Three of the five CO signals (those at δ 186.1, 174.4 and 169.9) broaden on raising the temperature to -5 °C and are close to coalescence at 40 °C. The signals at δ 203.0 and 187.2 remain sharp over this temperature range. A process involving a merry-go-round exchange at the $Os_2(CO)_8$ unit with intermediates containing bridging CO will exchange the CO ligands **B**, **C** and **D** while leaving the CO ligands **A** and **E** unaffected as observed. Figure 3.3 shows this process for cluster $[Os_3(CO)_{10}(BINAP)]$ which it is believed, is the only one to fit the observed behaviour. The BINAP ligand prevents a merry-go-round process occurring on any other edge of the cluster. We did not measure the spectrum above 40 °C

3.4.5 Spectroscopic characterisation and fluxional behaviour of $[Os_3(CO)_{10}(BINAP)]$

The ^{13}C-$\{^1H\}$ NMR spectra of this compound clearly indicate that BINAP is chelating and the cluster is without doubt the 1,1-isomer, as was later confirmed by an X-ray study.[94] It is predicted that there will be five different CO ligand environments in ratio 2:2:2:2:2 for both 1,1- and 1,2-isomers of $[Os_3(CO)_{10}(BINAP)]$. Five signals are indeed observed at -65 °C at δ 203.0, 187.2, 186.1, 174.4 and 169.9 (Figure 3.2). The observation of a 1:2:1 triplet for the signal at δ 203.0 (J_{PC} = 7.9 Hz) (more clearly resolved at intermediate temperatures above –65 °C) can only be reconciled with the 1,1-structure, with this signal assigned to the carbonyl ligands **A**. For comparison, the 1,1-isomer of $[Os_3(CO)_{10}(PMe_2Ph)_2]$ gives a 1:2:1 triplet at δ 202.1 (J_{PC} = 9.5 Hz) for the corresponding *axial* carbonyl ligands of the $Os(CO)_2(PMe_2Ph)_2$ group. This assignment of structure for $[Os_3(CO)_{10}(BINAP)]$ is confirmed by the pattern of NMR coalescences at higher temperatures. Three of the five CO signals (those at δ 186.1, 174.4 and 169.9) broaden on raising the temperature to -5 °C and are close to coalescence at 40 °C. The signals at δ 203.0 and 187.2 remain sharp over this temperature range. A process involving a merry-go-round exchange at the $Os_2(CO)_8$ unit with intermediates containing bridging CO will exchange the CO ligands **B**, **C** and **D** while leaving the CO ligands **A** and **E** unaffected as observed. This process which it is believed, is the only one to fit the observed behaviour for the cluster $[Os_3(CO)_{10}(BINAP)]$. The BINAP ligand prevents a merry-go-round process occurring on any other edge of the cluster. We did not measure the spectrum above 40 °C because of the risk of thermal decarbonylation to give the

cluster $[Os_3(\mu\text{-}H)(CO)_8(\mu_3\text{-}BINAP\text{-}H)]$ which we have shown to occur at higher temperatures. On the basis of this comparative evidence, there is no way to interpret the NMR behaviour of the cluster in terms of the alternative isomer, that is 1,2-$[Os_3(CO)_{10}\{(R)\text{-}BINAP\}]$. The overriding piece of evidence is the coupling of the two *axial* CO ligands at the $Os(CO)_2\{BINAP\}$ sub-unit to both ^{31}P nuclei equally.

3.4.6 Protonation of $[Os_3(CO)_{10}(BINAP)]$

The cluster $[Os_3(CO)_{10}(BINAP)]$, in a solution of CD_2Cl_2, was treated with a sixteen fold excess of trifluroacetic acid in a 5mm NMR tube. The reaction was monitored by ^1H NMR, with particular attention paid to the negative chemical shift region (δ 0 to –30). No change in the ^1H NMR spectrum was observed over six hours and no evidence for hydride formation was observed. This is surprising in view of related clusters under similar conditions.

3.4.7 Hydrogenation of $[Os_3(CO)_{10}(BINAP)]$

The cluster $[Os_3(CO)_{10}(BINAP)]$ in a refluxing solution of heptane was treated with a continuous stream of hydrogen bubbling through the solution. The reaction was monitored by ^1H NMR spectroscopy, with particular attention paid again to the negative chemical shift region (δ 0 to –30). The results of the reaction are not consistently reproducible, although on occasion a hydride signal consistent with 1,1-$[Os_3(\mu\text{-}H)_2(CO)_8(BINAP)]$ has been observed. However there is no evidence for facile or complete hydrogenation to this product but minor traces of the orthometallated species were observed.

3.5 Reaction of $[Os_3(CO)_{11}(MeCN)]$ with BINAP

As expected, the main cluster formed from the reaction contains monodentate BINAP. We believe this to be $[Os_3(CO)_{11}(\eta^1\text{-BINAP})]$. The ^1H NMR spectrum is complex, consistent with an unsymmetrical BINAP ligand, and the $^{31}P\text{-}\{^1H\}$ NMR spectrum shows two moderately broad singlets at δ -14.1 and 8.2 at room temperature. Free BINAP gives a signal at δ -14.5 while $[Os_3(CO)_{11}\{BINAP\}]$ shows two signals, one at δ 8.2 representing the coordinated phosphorus and one at δ -14.1 representing free phosphorus. It is reasonable to suppose that one $^{31}P\{^1H\}$ singlet at δ 8.2 shown by this cluster corresponds to coordinated phosphorus atoms.

3.5.1 Study of fluxional behaviour of $[Os_3(CO)_{11}(BINAP)]$ by ^{31}P NMR and its spectroscopic characterisation

Variable-temperature NMR spectra of the cluster were recorded to explore possible nonrigidity. Indeed, there are clear changes in the $^{31}P\text{-}\{^1H\}$ NMR spectrum in $CDCl_3$ with changes in temperature (Figure 3.4). The two sharp singlets for free and coordinated ^{31}P nuclei at 27 °C broaden considerably at -20 °C and resolve at -65 °C into four sharp singlets at δ -10.8 and 5.4 (major isomer **A**) and at δ -17.9 and 8.7 (minor isomer **B**). We considered initially that these isomers might have different sites of attachment of BINAP at the $Os_3(CO)_{11}$ unit, but the IR spectrum in solution is closely similar to those of other tertiary phosphine compounds of the type $[Os_3(CO)_{11}L]$ in which the ligand L is known to be *equatorial*. There is no precedent for *axial* tertiary phosphine coordination in such compounds. The simplicity of the spectrum is only consistent with *equatorial* coordination for both isomers **A** and **B** present in solution. Hence we

conclude that the isomers both have *equatorial* coordination but with different conformational arrangements within the η^1-BINAP ligand which do not affect the ν(CO) IR spectrum. Note that the largest chemical shift difference between the isomers is for the free PPh_2 group (Signals at δ -10.8 and –17.9 Figure 3.4). Rotation about the Ph_2P-naphthalene bonds leads to the lone-pair pointing inwards or outwards from the centre of the ligand. In free BINAP in the solid both lone-pairs point inwards and in η^1-BINAP in the solid one points inwards but the coordinated one, of necessity, points outwards. We believe therefore that isomers **A** and **B** have the conformations in-out and out-out (approximate lone-pair directions) respectively and that rotation about the Ph_2P-naphthalene bond for the uncoordinated PPh_2 group is rapid at room temperature. At -65 °C this rotation is slow leading to the observed spectra (Figure 3.4). Figure 3.6 represents our proposed structures for isomers **A** and **B**. As described in the previous chapter the ^{31}P-$\{^1H\}$ NMR spectra of free BINAP has been explored, over a range of temperatures, down to -100°C (at 600 MHz) with no analogous fluxional effects being visible.

Figure 3.3 Fluxional carbonyl "merry-go-round" mechanism for $[Os_3(CO)_{10}BINAP]$

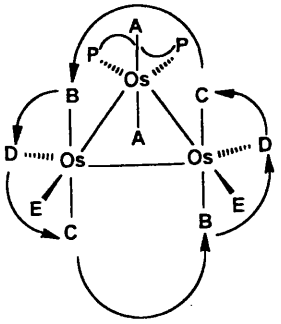

Figure 3.4 $^{31}P\{^{1}H\}$ variable temperature NMR of $[Os_3(CO)_{11}(BINAP)]$ in $CDCl_3$ solution at 9.4 T. Coordinated signals are to downfield and the free signals are to the upfield. The signal marked * is that of free BINAP.

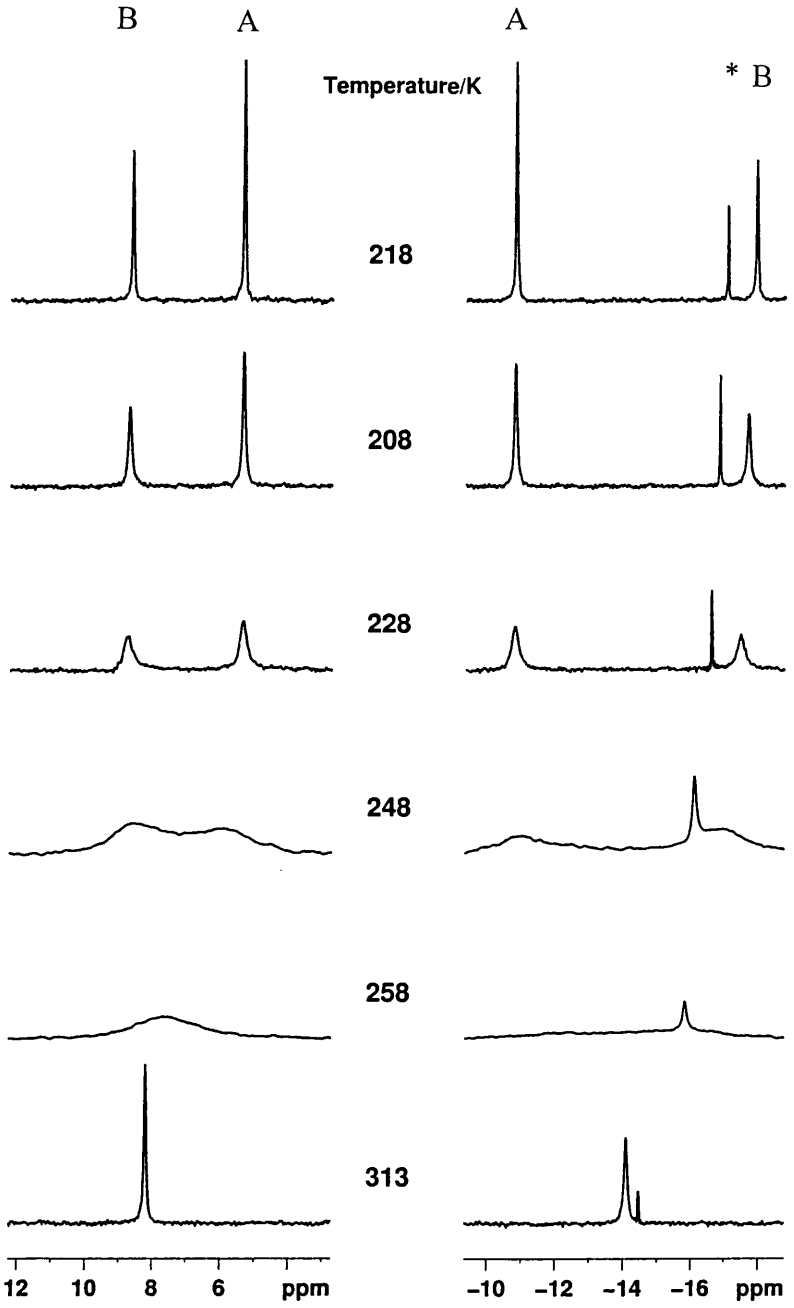

Figure 3.5 Single crystal X-ray structure of $[Os_3(CO)_{11}(BINAP)]$, showing the unprecedented *equatorial* η^1-coordination of the ligand to the metal triangle. Note the potential flexibility of the BINAP and its overall bulk with respect to the cluster.

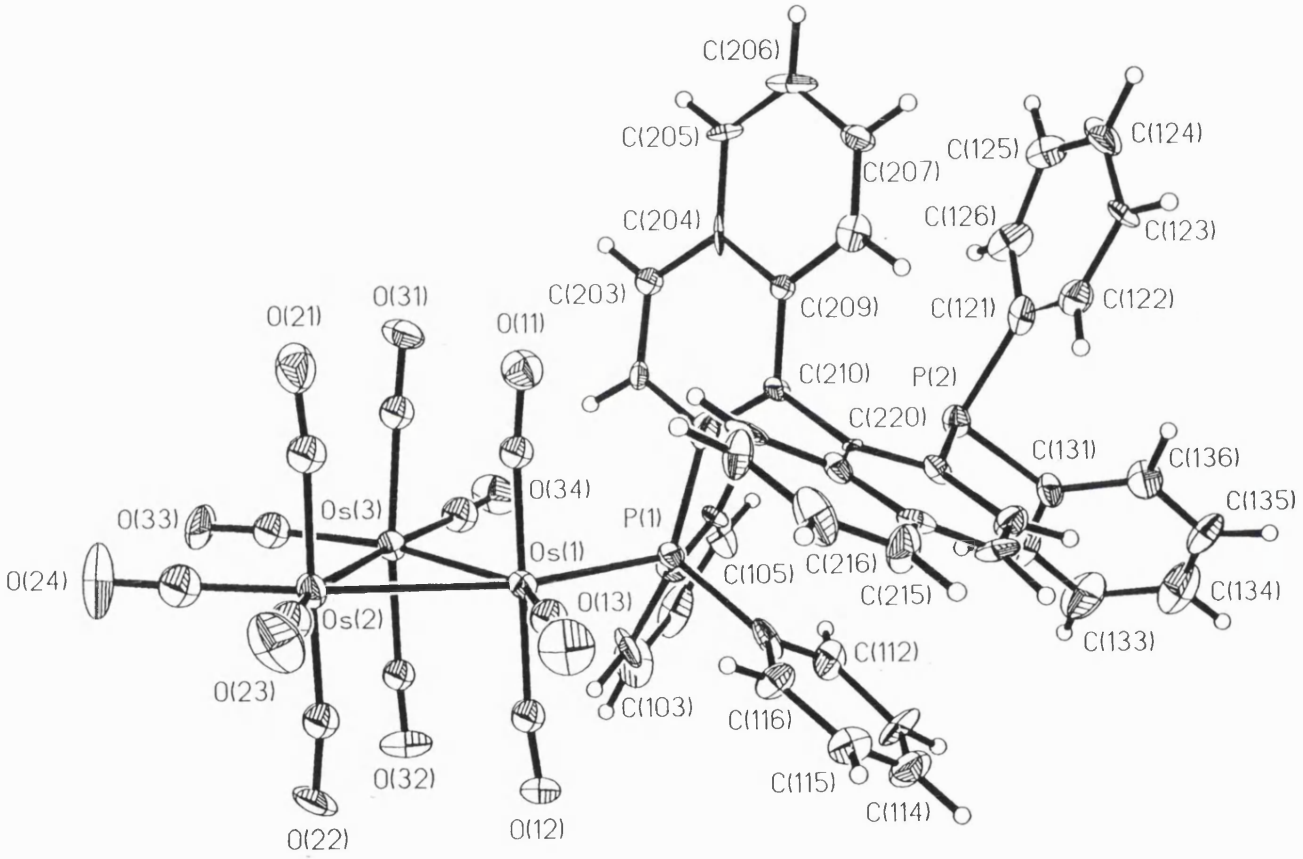

3.5.2 Crystal structure of $[Os_3(CO)_{11}(BINAP)]$

Monodentate BINAP has not previously been observed so the single-crystal X-ray structure has been determined of the cluster, obtained as yellow crystals of $[Os_3(CO)_{11}(BINAP)]\bullet 0.5CH_2Cl_2$ by evaporation of a dichloromethane-hexane mixture. Generally we have found that clusters containing BINAP are difficult to crystallise in a suitable form for single-crystal studies and the two structures reported in this chapter are for crystals that are of less than ideal quality. In addition there was the problem that $[Os_3(CO)_{11}(BINAP)]\cdot 0.5CH_2Cl_2$ formed thin plates which made the structure determination much more difficult. The molecular structure is shown in Figure 3.5 and selected bond lengths and angles are in Table 1. The structure has the monodentate BINAP ligand in an *equatorial* site as we predicted from NMR data. There is no evidence in the many crystal structures determined for clusters of the type $[M_3(CO)_{11}L]$ (M = Ru or Os, L = tertiary phosphine or arsine) for coordination in any but an *equatorial* position.[8] *Axial* sites are crowded as a result of interactions between *axial* ligands and, although *axial* substitution is probably favoured electronically, it is only observed with small or rod-shaped ligands. Relative to the structure of (R)-BINAP[11] in the crystal, there has been a rotation about one naphthyl-PPh_2 bond to allow coordination to Os(1). In free (R)-BINAP the two lone-pairs are directed inwards and the uncoordinated PPh_2 group in $[Os_3(CO)_{11}(BINAP)]$ has a similar conformation to that of the PPh_2 groups in the crystal structure of the free ligand.

Figure 3.6 Two arrangements of $[Os_3(CO)_{11}(BINAP)]$ **A** and **B** showing the interactions of the phosphines to give the ^{31}P NMR behaviour observed.

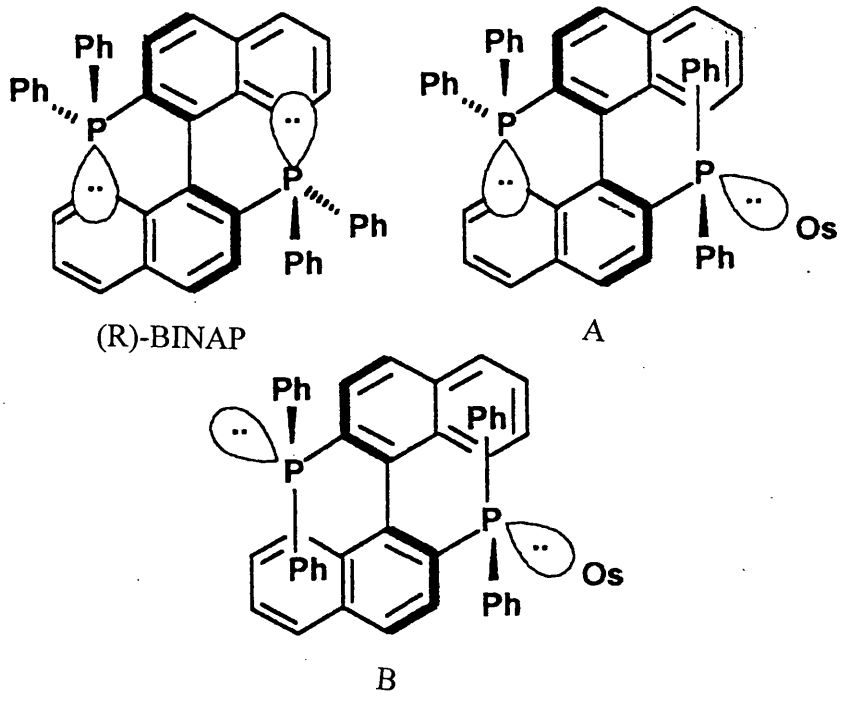

(R)-BINAP A

B

3.6 Reaction of $[Os_3(CO)_{11}(MeCN)]$ and BINAP

A solution of two mole equivalents of the cluster $[Os_3(MeCN)(CO)_{11}]$ and one mole equivalent of (R)-BINAP in dry THF was refluxed. The products isolated by TLC on silica were $[Os_3(CO)_{10}(BINAP)]$ (5%), $[Os_3(CO)_{11}(BINAP)]$ (70%), $[\{Os_3(CO)_{11}\}_2(BINAP)]$ (15%) and $[Os_3(\mu\text{-}H)(CO)_8(BINAP\text{-}H)]$ (5%) which were initially characterised by comparison of their IR spectra to those known for the series $[Os_3(CO)_{10/11}(diphosphine)_{1/2}]$ where diphosphine is dppe or dppp[95] and on the basis of FAB mass spectra. Despite numerous attempts it has not proved possible to grow single crystals of $[\{Os_3(CO)_{11}\}_2(BINAP)]$ suitable for an X-ray study.

3.6.10 Spectroscopic characterisation of $[\{Os_3(CO)_{11}\}_2(BINAP)]$

The reaction of $[Os_3(CO)_{11}(BINAP)]$ with $[Os_3(CO)_{11}(MeCN)]$ yields, as expected, the cluster containing the ligand BINAP bridging two $Os_3(CO)_{11}$ cluster units. The ^1H NMR spectrum is simpler than that of $[Os_3(CO)_{11}(BINAP)]$ and therefore consistent with a more symmetrical BINAP ligand than that found in $[Os_3(CO)_{11}(BINAP)]$. The $^{31}P\{^1H\}$ NMR spectrum shows one singlet at δ 7.4 at room temperature. Free BINAP gives a signal at δ -17.0 ($CDCl_3$ 20 °C) and $[Os_3(CO)_{11}(BINAP)]$ shows two signals one at (δ -14.1) representing the coordinated phosphorus and one at (δ 8.2) representing free phosphorus. It is reasonable to suppose that the $^{31}P\{^1H\}$ singlet (δ 7.4) shown by this cluster corresponds to two equivalent coordinated phosphorus atoms consistent with a BINAP bridge between two clusters.

3.7 Conclusions

The trinuclear cluster $[Os_3(CO)_{11}\{(R)\text{-BINAP}\}]$ containing monodentate (R)-BINAP is formed by thermal treatment of $[Os_3(CO)_{12}]$ with 2,2'-bis(diphenylphosphino)-1,1'-binaphthyl, (R)-BINAP. This complex decarbonylates thermally to give the cluster $[Os_3(CO)_{10}\{(R)\text{-BINAP}\}]$, which was shown spectroscopically to contain chelating BINAP. On further thermal decarbonylation orthometallation at a phenyl group takes place to give $[Os_3(\mu\text{-H})(CO)_8\{\mu_3\text{-(R)-BINAP-H}\}]$. There is no evidence for restricted rotation about P-Ph bonds within the PPh_2 groups as we have previously observed for $[Ru_3(\mu\text{-OH})_2(CO)_8\{\mu\text{-(R)-BINAP}\}]$.[11] This restricted rotation is an effect of crowding and therefore appears to be a distinct property of μ-coordination across a metal-metal bonded pair of metal atoms rather than chelation of BINAP. However, both clusters $[Os_3(CO)_{11}(BINAP)]$ and $[Os_3(CO)_{10}(BINAP)]$ are fluxional, but as a result of different processes. The cluster $[Os_3(CO)_{11}(BINAP)]$ exists as two interconverting isomers (^{31}P NMR evidence) which indicate different conformations within the monodentate (R)-BINAP ligand. These observations are consistent with restricted rotations about the Ph_2P-naphthyl bonds. The decacarbonyl cluster $[Os_3(CO)_{10}(BINAP)]$ has C_2 symmetry and shows ^{13}C NMR coalescences consistent with a dynamic merry-go-round motion at the two $Os(CO)_4$ units but not at the $Os(CO)_2$(BINAP) unit. Single crystal X-ray structures of clusters $[Os_3(CO)_{11}(BINAP)]$ and $[Os_3(\mu\text{-H})(CO)_8(BINAP\text{-H})]$ confirm these two new modes of BINAP coordination. In our work, it has proved impossible to obtain suitable single

crystals for XRD to establish whether BINAP is chelating or bridging in $[Os_3(CO)_{10}(BINAP)]$, however others have achieved a satisfactory X-ray structure, showing that it is indeed chelating BINAP.[94] However a comparison of the ν(CO) IR spectra of $[Os_3(CO)_{10}(BINAP)]$ with those of related complexes of the type $[Os_3(CO)_{10}(diphosphine)]$ which are know to contain either chelating or bridging diphosphines has been carried out.[95] Isomers are formed in some cases. For example 1,1- and 1,2-isomers of $[Os_3(CO)_{10}(Ph_2PCH_2CH_2PPh_2)]$ have been characterised.[95] The IR spectrum of $[Os_3(CO)_{10}(BINAP)]$ did not correspond unambiguously with the spectra of either of the isomeric forms of $[Os_3(CO)_{10}(Ph_2P(CH_2)_nPPh_2)]$ (where n = 1-4), although the match was closer for the 1,1-isomers than the 1,2-isomers.[95]

3.8 Experimental

Direct thermal reaction of $[Os_3(CO)_{12}]$ with BINAP in heptane

A solution of BINAP (0.040 g) and $[Os_3(CO)_{12}]$ (0.060 g) in heptane (25 cm^3) was refluxed under nitrogen for 3.5 h. The solution became darker after 1.5 h and faint orange after 3.5 h. The solution was cooled to 5 °C for one hour to allow the excess of $[Os_3(CO)_{12}]$ to crystallise. After filtration through a thin layer of silica, the solvent was removed from the filtrate under reduced pressure. The residual solid was separated by preparative TLC (2 mm, Merck 1045), eluting with a dichloromethane/hexane mixture (3:7 by volume). Three bands yielded yellow $[Os_3(CO)_{11}(BINAP)]$ (10%), orange $[Os_3(CO)_{10}(BINAP)]$ (15%) and yellow $[Os_3(\mu\text{-}H)(CO)_8(BINAP\text{-}H)]$ (14%) respectively.

$[Os_3(CO)_{11}BINAP]$: IR (cyclohexane) , ν(CO)/cm^{-1}: 2066vs, 2030vs, 2009s, 1992vw, 1976vs, 1961s, 1942w; ^1H NMR ($CDCl_3$, 20°C): δ 6.15 (t), 6.45 (d), 6.5 to 7.8 (overlapping multiplets), 8.40 (dt); ^{31}P-{^1H} NMR ($CDCl_3$, 20°C): δ -16.5 (s) and 5.5 (s) at room temperature and δ 5.4 (s), -10.8 (s) (isomer A), 8.7 (s), -17.9 (s) (isomer B) at -65 °C; FABMS : observed centre of isotopic envelope 1504, calculated for parent molecular ion 1500.

$[Os_3(CO)_{10}BINAP]$: IR (cyclohexane), ν(CO)/cm^{-1}: 2095 m, 2049 s, 2015 s, 2010 vs, 1999m, 1988 m, 1971w, 1904 w. ^1H NMR ($CDCl_3$, 20°C): δ 6.40 (d), 6.85 (d), 6.92 (td), 7.0 to 7.3 (overlapping m), 7.35 (td), 7.45 (dd), 7.84 (d), 7.89 (d). ^{13}C-{^1H} NMR (100 MHz, $CDCl_3$, 20°C): δ 203.0, 187.2, 186.1, 174.4, 169.9 (CO-signals), 141 to 125 (aryl signals, many overlapping). ^{31}P-{^1H} NMR ($CDCl_3$, 20°C) δ -5.8 (s). FABMS: Observed centre of isotopic envelope 1473, calculated for parent molecular ion 1472.

$[Os_3(\mu\text{-}H)(CO)_8(BINAP\text{-}H)]$: IR (cyclohexane) ν(CO)/cm^{-1}: 2108 m, 2055 s, 2037 s, 2020 vs, 2000 m, 1992 s, 1979 s, 1963 w, 1958 w. ^1H NMR ($CDCl_3$, 20°C): δ 8.46 (d), 7.7 to 7.2 (overlapping m), 7.10 (dt), 6.93 (m), 6.8 to 6.6 (overlapping m), 6.40 (d), 6.19 (dd), -16.93 (dd, J_{PH} = 8.3, 17.3 Hz). ^{13}C-{^1H} NMR ($CDCl_3$ 20°C): δ 184.7, 183.8, 178.8, 178.1 (CO-signals), 151 to 122 (complex aryl signals). ^{31}P-{^1H} NMR ($CDCl_3$, 20°C): δ 4.18 and 2.13. FABMS: Observed centre of isotopic envelope 1417, calculated for parent molecular ion 1417. (Found: C, 45.35; H, 2.7; P, 4.0. $C_{52}H_{32}O_8Os_3P_2$ requires C, 44.1; H, 2.3; P, 4.35%).

Direct thermal reaction of $[Os_3(CO)_{12}]$ with BINAP in octane

A solution of BINAP (0.040 g) and $[Os_3(CO)_{12}]$ (0.060 g) in octane (25 cm^3) was refluxed under nitrogen for 3.5 h. The solution became darker after 1.5 h and faint orange after 3.5 h. The solution was cooled to 5 °C for one hour to allow the excess of $[Os_3(CO)_{12}]$ to crystallise. After filtration through a thin layer of silica, the solvent was removed from the filtrate under reduced pressure. The residual solid was separated by preparative TLC (2 mm, Merck 1045), eluting with a dichloromethane/hexane mixture (3:7 by volume), yielding three bands yellow $[Os_3(CO)_{11}(BINAP)]$ (12%), orange $[Os_3(CO)_{10}(BINAP)]$ (24%) and yellow $[Os_3(\mu\text{-}H)(CO)_8(BINAP\text{-}H)]$ (36%) respectively.

Reaction of $[Os_3(MeCN)_2(CO)_{10}]$ and BINAP

A solution of the cluster $[Os_3(MeCN)_2(CO)_{10}]$ (0.1g) and an equimolar quantity of (R)-BINAP in dry THF (25 cm^3) was refluxed for 30 min. The products isolated by TLC on silica were $[Os_3(CO)_{10}(BINAP)]$ (80%) and very minor quantities of $[Os_3(CO)_{11}(BINAP)]$ and $[Os_3(\mu\text{-}H)(CO)_8(BINAP\text{-}H)]$ which were only characterised by their IR spectra.

Reaction of $[Os_3(MeCN)_2(CO)_{11}]$ and BINAP

A solution of the cluster $[Os_3(MeCN)_2(CO)_{11}]$ (0.1g) and an equimolar quantity of (R)-BINAP in dry THF (25 cm^3) was refluxed for 45 min. The products isolated by TLC on silica were $[Os_3(CO)_{11}(BINAP)]$ (80%) and very minor quantity of $[Os_3(CO)_{10}(BINAP)]$ which was only characterised by its IR spectrum.

Synthesis of [{$Os_3(CO)_{11}$}$_2$(BINAP)] from [$Os_3(CO)_{11}$(MeCN)] and BINAP

A solution of two mole equivalents of the cluster [Os_3(MeCN)$(CO)_{11}$] (0.12 g) and one mole equivalent of (R)-BINAP (0.040g) in dry THF (25 cm^3) was refluxed and monitored by IR. The solution changed from the very pale yellow of the acetonitrile adduct, to the slightly deeper yellow of the phosphine adduct in a few minutes. The solvent was removed under reduced pressure. The residual solid was separated by preparative TLC on silica (2mm, Merck 1045), eluting with dichloromethane/hexane mixture (3:7 by volume). Four bands were recovered [$Os_3(CO)_{10}$(BINAP)] (5%), [$Os_3(CO)_{11}$(BINAP)] (50%), [{$Os_3(CO)_{11}$}$_2$(BINAP)] (15%) and [Os_3(μ-H)$(CO)_8$(BINAP-H)] (5%).

3.8.1 Direct thermal reaction of [$Os_3(CO)_{12}$] with BINAP in decane with CO saturation

A solution of BINAP (0.040 g) and [$Os_3(CO)_{12}$] (0.060 g) in decane (25 cm^3) was refluxed for 45 minutes, with CO gas being passed through the solution. The solution was cooled to 5 °C for one hour to allow the excess of [$Os_3(CO)_{12}$] to crystallise. After filtration through a thin layer of silica, the solvent was removed from the filtrate under reduced pressure. The residual solid was separated by preparative TLC (2 mm, Merck 1045), eluting with a dichloromethane/hexane mixture (3:7 by volume). Three bands were recovered corresponding to [$Os_3(CO)_{10}$(BINAP)] 5% and [Os_3(μ-H)$(CO)_8$(BINAP-H)] 40% as well as an uncharacterised band assumed to be a higher nuclearity cluster.

3.8.2 Thermolysis of $[Os_3(CO)_{11}(BINAP)]$ 1

A solution of the cluster $[Os_3(CO)_{11}(BINAP)]$ (0.010 g) in 1.1 cm^3 of toluene-d_8 in a 10 mm NMR tube was heated at 105 °C and ^{31}P spectra were observed over 5.5 hours. Conversion to clusters $[Os_3(CO)_{10}(BINAP)]$ and $[Os_3(\mu\text{-}H)(CO)_8(BINAP\text{-}H)]$ was observed. Given the poor mixing experienced in NMR tubes[54,55] the results may be considered indicative of the reactions occurring but the quantitative data extracted is likely to be poor and this is therefore not presented.

3.8.2 X-ray structure determinations.

Yellow crystals of $[Os_3(CO)_{11}(BINAP)]\bullet 1/2CH_2Cl_2$ and $[Os_3(\mu\text{-}H)(CO)_8(BINAP\text{-}H)]$ were grown from hexane/dichloromethane mixtures. X-ray data were collected at room temperature using a Nicolet R3v/m diffractometer with crystals mounted in air. Details of the crystal structure determinations are given in Table 3. Structures were solved by direct methods using SHELXTL PLUS and refined using SHELXL93. All non-H atoms of $[Os_3(CO)_{11}(BINAP)]$ $1/2CH_2Cl_2$ except for CH_2Cl_2 were refined anisotropically and the positions of the dichloromethane C and Cl atoms were fixed in the final cycles of refinement. Only the Os, P and O atoms of the cluster $[Os_3(\mu\text{-}H)(CO)_8(BINAP\text{-}H)]$ were refined anisotropically. H-atoms in both crystals were included in idealised positions, riding upon their respective carbon atoms, with C-H distance fixed at 0.96 Å and isotropic thermal parameters at 0.08 $Å^3$. Professor A. J. Deeming at UCL carried out the structure determination.

Table 1 Selected bond lengths (Å) and angles (°) for the cluster $[Os_3(CO)_{11}\{(R)\text{-BINAP}\}]$

Os(1)-Os(2)	2.989(2)	P(1)-C(111)	1.83(3)
Os(2)-Os(3)	2.880(2)	P(1)-C(201)	1.88(2)
Os(1)-Os(3)	2.915(2)	P(2)-C(121)	1.83(2)
Os(1)-P(1)	2.405(6)	P(2)-C(131)	1.84(2)
P(1)-C(101)	1.80(3)	P(2)-C(211)	1.80(2)
Os(1)-Os(3)-Os(2)	60.00(4)	Os(1)-P(1)-C(201)	110.8(7)
Os(2)-Os(1)-Os(3)	59.40(4)	C(101)-P(1)-C(111)	99.4(12)
Os(1)-Os(2)-Os(3)	60.60(4)	C(101)-P(1)-C(201)	100.0(12)
Os(3)-Os(1)-P(1)	102.8(2)	C(111)-P(1)-C(201)	113.3(12)
Os(2)-Os(1)-P(1)	161.9(2)	C(121)-P(2)-C(131)	100.7(12)
Os(1)-P(1)-C(101)	117.2(8)	C(121)-P(2)-C(211)	102.2(14)
Os(1)-P(1)-C(111)	114.9(8)	C(131)-P(2)-C(211)	102.7(11)

Table 2 Selected bond lengths (Å) and angles (°) for the cluster $[Os_3(\mu\text{-}H)(CO)_8\{(R)\text{-}BINAP\text{-}H\}]$

Os(1)-Os(2)	2.885(2)	Os(1)-C(106)	2.45(3)
Os(2)-Os(3)	3.061(2)	P(1)-C(111)	1.80(5)
Os(1)-Os(3)	2.799(2)	P(1)-C(201)	1.84(4)
Os(2)-P(1)	2.399(9)	P(1)-C(106)	1.86(4)
Os(2)-P(2)	2.380(10)	P(2)-C(121)	1.83(4)
Os(1)-C(101)	2.35(3)	P(2)-C(131)	1.86(4)
Os(3)-C(101)	2.113)	P(2)-C(211)	1.87(3)
P(1)-Os(2)-P(2)	93.5(4)	Os(2)-P(2)-C(121)	119.0(14)
Os(1)-Os(2)-P(1)	74.4(30	Os(2)-P(2)-C(131)	115.0(12)
Os(3)-Os(2)-P(1)	84.5(2)	Os(2)-P(2)-C(211)	107.3(11)
Os(2)-P(1)-C(201)	112.4(4)	P(1)-C(106)-C(101)	119(3)
Os(2)-P(1)-C(111)	124(2)	P(1)-C(106)-C(105)	118(3)
Os(2)-P(1)-C(106)	105.0(12)		

Table 3 Crystal data and structure solution and refinement parameters for clusters $[Os_3(CO)_{11}(BINAP)]$ $1/2CH_2Cl_2$ and $[Os_3(\mu\text{-}H)(CO)_8(BINAP\text{-}H)]$

	$[Os_3(CO)_{11}(BINAP)]$ $1/2CH_2Cl_2$	$[Os_3(\mu\text{-}H)(CO)_8(\mu_3\text{-}BINAP\text{-}H)]$
Formula	$C_{55.5}H_{33}ClO_{11}Os_3P_2$	$C_{52}H_{32}O_8Os_3P_2$
M	1543.81	1417.32
Description	yellow plate	yellow block
Crystal size/mm	0.27 × 0.15 × 0.04	0.60 × 0.34 × 0.27
Crystal system	monoclinic	orthorhombic
Space group	$P2_1$	$P2_12_12_1$
a/Å	15.610(4)	10.661(4)
b/Å	10.957(2)	21.26(2)
c/Å	16.186(4)	24.21(2)
β/°	108.97(2)	90
U/Å^3	2618.0(11)	5489(6)
Z	2	4
D_c/g cm^{-3}	1.958	1.715
μ(Mo-Kα)/cm^{-1}	74.34	70.32
F(000)	1458	2664
No. orientation reflections, 2θ range/°	28, 13-23	25, 16-28
Scan mode	ω-2θ	ω
2θ range/°	5-50	5-50
hkl range	0,0,-18 to 18,13,18	0,0,0 to 12,25,28
Total data	4958	5266
Unique data	4773	5266
Parameters in refinement	571	321
R (all data)[b]	0.0783	0.1131
[$I>2\sigma(I)$]	0.0595	0.0891
Goodness of fit	1.068	1.075
Maximum peak, hole in final difference Fourier map/eÅ^{-3}	1.37, -1.38	3.93, -2.10

a. Both structures: Direct methods structure solution, graphite-monochromated Mo-Kα radiation (λ = 0.71073 Å), three standard reflections every 97, no decay, data corrected for absorption empirically by Ψ-scan method, maximum and minimum transmission 0.986 and 0.501 for **1** and 0.930 and 0.728 for **3**, full-matrix least-squares refinement on F^2. b. $R = \Sigma||F_o|-|F_c||/\Sigma|F_o|$.

Chapter 4 Reactions of the cluster $[Os_3(\mu\text{-}H)_2(CO)_{10}]$ with tolBINAP and comparison with other diphosphines in the series $Ph_2P(CH_2)_nPPh_2$ (n = 1 to 4)

Table of contents:

4.1 Introduction: triosmium dihydride systems, unsaturation and reactivity

Numerous examples exist of monohydrido complexes containing diphosphines which are formed by either protonation or hydrogenation. Somewhat rarer are references to dihydrido clusters of the type $[Os_3(\mu\text{-}H)_2(CO)_8(diphosphine)]$ containing diphosphines. These have been prepared previously by hydrogenation of clusters of the type $[Os_3(CO)_{10}L]$ (where L = diphosphine).[42,105]

There are very few examples of terminal hydride ligands in clusters and these are rarer than their bridging counterparts. One example of a terminal hydride cluster has the form $[Os_3H_2(CO)_{10}L]$ (L = PR_3, CO, etc.) which has one terminal and one bridging hydride. This group of clusters is formed on the reaction of $[Os_3(\mu\text{-}H)_2(CO)_{10}]$ with a 2-electron donating ligand L such as, where L is CO, PR_3 or RCN.[96,97]

The cluster $[Os_3(CO)_{12}]$ is readily hydrogenated by bubbling hydrogen through a refluxing solution in octane for 2 hours at 130 °C to form $[Os_3(\mu\text{-}H)_2(CO)_{10}]$ with the loss of two CO ligands.[113] The cluster $[Os_3(\mu\text{-}H)_2(CO)_{10}]$ has been characterised by X-ray and neutron diffraction studies and it is found that the two hydride ligands bridge the same edge of the cluster.[98] The unbridged Os-Os bonds [2.815(1) Å] are similar in length to those in $[Os_3(CO)_{12}]$ [2.881(1) Å].[99] However, the hydride bridged Os-Os bond is [2.681(1) Å], which is significantly shorter. Explanation of the shortness of the bridged bond in $[Os_3(\mu\text{-}H)_2(CO)_{10}]$

has been in terms of electronic unsaturation, or a simple consequence of having two small atoms bridging the osmium atoms. The cluster is a 46-electron species and shows a 2 electron deficiency as against a closed shell configuration with three Os-Os single bonds.[40] This deficiency has been explained in terms of an Os-Os double bond,[40] or multi-centre delocalised bonds.[100] Certainly the compound behaves as if it is unsaturated and readily reacts with donor molecules to form adducts.[101]

The reactions of unsaturated hydrocarbons such as acetylene with $[Os_3(\mu\text{-}H)_2(CO)_{10}]$ are well characterised and explored elsewhere in this work. The activity of $[Os_3(\mu\text{-}H)_2(CO)_{10}]$ in catalysing alkene double bond shifts has been explored,[102] as well as the ability to insert alkynes into Os-H bonds.[103] It had been hoped that the compounds synthesised as described in this chapter, particularly the chiral cluster $[Os_3(\mu\text{-}H)_2(CO)_8(tolBINAP)]$ would have exhibited some migration or exchange of the hydride ligands, mirroring these hydrogen transfer reactions and which could possibly lead to catalytic activity analogous to that of $[Os_3(\mu\text{-}H)_2(CO)_{10}]$.[102] The reactivity of the cluster $[Os_3(\mu\text{-}H)_2(CO)_{10}]$ largely depends on the addition of donor groups at the unsaturated cluster. The replacement of CO ligands by tertiary phosphine ligands should reduce the electrophilicity of the cluster and might therefore ultimately diminish the reactivity of the cluster if the nucleophilic addition at the cluster controls the reactivity. There is also the possibility of steric factors restricting the reactivity of the hydrides. The activation of the clusters under conditions of pressure has been poorly explored.[104]

We have now shown that $[Os_3(\mu\text{-}H)_2(CO)_{10}]$ reacts with diphosphine ligands (diphos) to form compounds, formally unsaturated, of the form $[Os_3(\mu\text{-}H)_2(CO)_8(diphos)]$, previously prepared in some cases by hydrogenation of 1,2-$[Os_3(CO)_{10}(diphos)]$.[42] The compounds $[Os_3(CO)_{10}(diphos)]$ with different diphosphine ligands, that is where diphos = $Ph_2P(CH_2)_nPPH_2$ [dppm (n = 1), dppe (n = 2), dppp (n = 3) and dppb (n = 4)], show differences in reactivity towards H_2. When diphos is dppm, dppe or dppp, the corresponding substituted clusters $[Os_3(\mu\text{-}H)_2(CO)_8(diphos)]$ are obtained in good yield. The dppb analogue has not been reported previously.[42] Our results contradict an earlier report, that $[Os_3(\mu\text{-}H)_2(CO)_8(dppm)]$ could not be made by the reaction of $[Os_3(\mu\text{-}H)_2(CO)_{10}]$ and dppm.[105]

Another report of the reaction between $[Os_3(\mu\text{-}H)_2(CO)_{10}]$ and dppm indicates that the cluster $[Os_3(\mu\text{-}H)_2(CO)_{10}(dppm)]$ was readily prepared by the dropwise addition of $[Os_3(\mu\text{-}H)_2(CO)_{10}]$ to a dppm solution in equimolar ratio.[106] The NMR of $[Os_3(\mu\text{-}H)_2(CO)_{10}(dppm)]$ showed two hydride signals at δ -10.45 and –19.92 assigned as the terminal and the bridging hydrides respectively at low temperature whilst at higher temperatures the hydrides exchange rapidly.[107] What however is very apparent is that the mechanism of the reaction between $[Os_3(\mu\text{-}H)_2(CO)_{10}]$ and phosphines is very complex. A number of studies have focused on the isomerisation that can occur when a monophosphine L inserts into $[Os_3(\mu\text{-}H)_2(CO)_{10}]$ forming $[Os_3(\mu\text{-}H)(H)(CO)_{10}L]$ with five of the eleven resulting isomers having been detected in low temperature experiments.[101,108] These results go some way to exposing the true complexity of the mechanism of

phosphine addition reactions. In many cases the structural assignments are based on T_1 measurements.[101]

It is presumed that the bridging hydrides are well outside the Os_3 plane, thus removing any steric reason why the dppm and the two hydrides cannot occupy the same side of the metal triangle. This is in contrast to the situation found for the protonation of $[Os_3(CO)_{10}(\mu\text{-dppm})]$ which results in $[Os_3(\mu\text{-H})(CO)_{10}(dppm)]^+$ in which the μ-H ligand was not found to bridge the same pair of metal atoms as the diphosphine. In this case the hydride needs to be close to the Os_3 plane and there is insufficient room within the five membered $Os_2(\mu\text{-dppm})$ ring, which also lies in the Os_3 plane, to accommodate the hydride. This is in spite of the bridged Os-Os edge being the most electron rich edge of the cluster. In the case of $[Os_3(\mu\text{-H})_2(CO)_8(dppm)]$ there is no such structural problem.

Figure 4.1 Some possible isomers of $[Os_3(\mu\text{-}H)(H)(CO)_{10}L]$

reproduced from reference 101

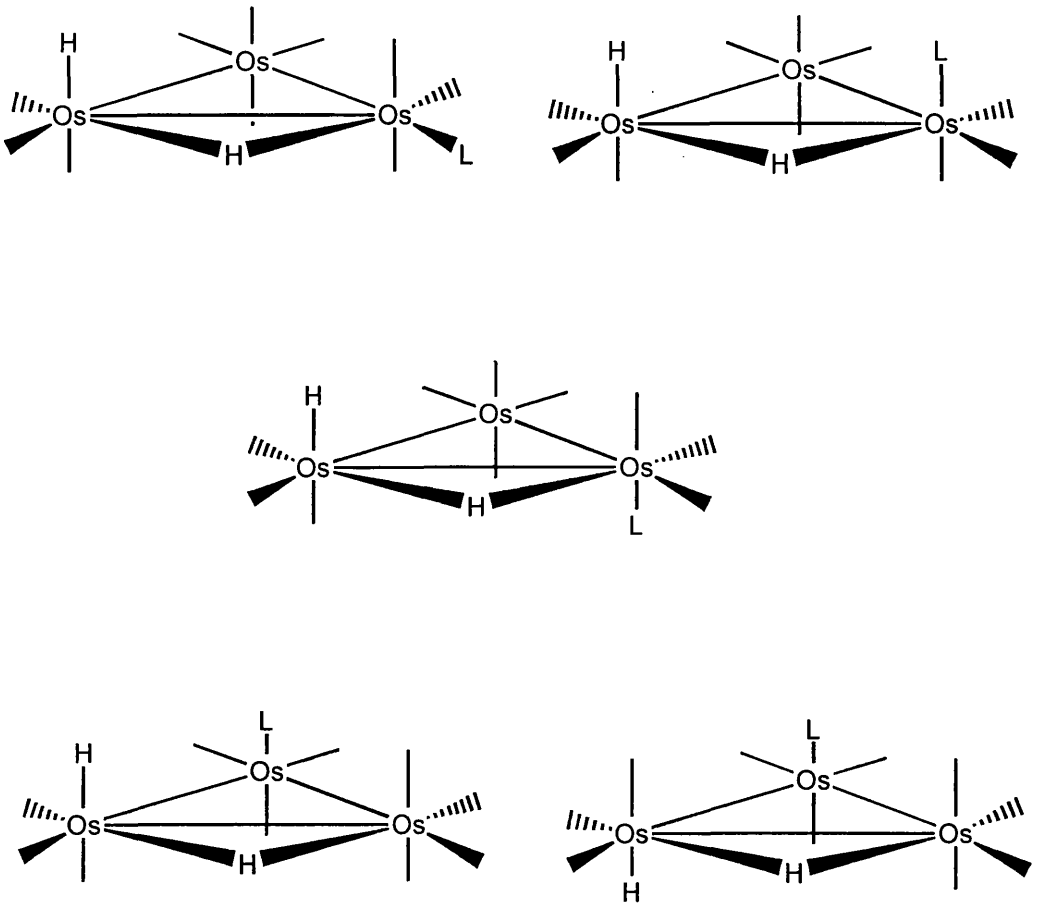

4.2 Objectives of the present work

The objectives for the work described in the present chapter were:-

a) To synthesise new triosmium clusters with bridging dihydride ligands, in particular to synthesis the cluster 1,2-$[Os_3(\mu\text{-}H)_2(CO)_8\{tolBINAP\}]$ and to compare these compounds with the known series of compounds.

b) To synthesise $[Os_3(\mu\text{-}H)_2(CO)_8(diphos)]$ where diphos = $Ph_2P(CH_2)_nP(Ph)_2$ (n= 1-4). To investigate the dynamic behaviour of these clusters by ^{13}C, ^{31}P and ^{1}H NMR spectroscopy and therefore the dynamics, if any, of intramolecular CO exchange

c) To assess the reactivity of the dihydride species synthesised towards CO to investigate the possibility of obtaining the $[Os_3H(\mu\text{-}H)(CO)_9(diphos)]$ from $[Os_3(\mu\text{-}H)_2(CO)_8(diphos)]$ by CO addition. Also to establish whether CO addition leads to H_2 displacement and the formation of the 1,2-isomer of $[Os_3(CO)_{10}(diphos)]$.

d) To assess the reactivity of the clusters towards acetylene and phosphine ligands etc.

e) To investigate the possibility of chiral induction across the cluster by further substitution.

4.3 Reaction of tolBINAP with $[Os_3(\mu\text{-}H)_2(CO)_{10}]$ to form $[Os_3(\mu\text{–}H)_2(CO)_8(tolBINAP)]$

Addition of an equimolar quantity of (R)-tolBINAP to a solution of $[Os_3(\mu\text{-}H)_2(CO)_{10}]$ in dry THF at room temperature over twenty four hours or at reflux over two hours gave the cluster $[Os_3(\mu\text{-}H)_2(CO)_8\{(R)\text{-}tolBINAP\}]$ in good yield. The ^1H NMR spectrum indicates a single isomer with a triplet signal for the hydride ligand [δ -9.21, and J_{PH} 12.5 Hz] (see Figure 4.1). The methyl groups appear as sharp singlets [δ 1.90 and 2.35] in the ^1H NMR spectrum. The phenyl rings appear as broad signals at room temperature between δ 5.7 and 7.0 sharpening at 0 °C at 500 MHz to show two triplets and two doublets, similar to the spectrum described for $[Ru_3(OH)_2(CO)_8\{R\text{-}BINAP\}]$[109] in Chapter 2. The naphthyl ring signals appear as an unresolved group of signals between δ 6.9 and 7.5. The $^{13}C\{^1H\text{-}^{31}P\}$ NMR spectrum for the CO ligands shows four singlets at δ 187.7, 184.8, 183.7 and 182.2. The $^{13}C\{^1H\}$ NMR spectrum for the CO ligands shows two singlets and two doublets [δ 187.7s, 184.8s, 183.7d (J_{PC} 3.75 Hz) and 182.2d (J_{PC} 4.5 Hz)]. The ^{31}P NMR spectrum shows a singlet [δ 28.2 (J_{OsP} 204 Hz)] down to –65 °C demonstrating the retention of C_2 symmetry. The $^1H\{^{31}P\}$ NMR spectrum also shows a sharp singlet in the hydride region which is also consistent with C_2 symmetry (see Figure 4.3).

4.4 Single crystal X-ray structure of $[Os_3(\mu\text{-}H)_2(CO)_8(tolBINAP)]$

The single crystal X-ray structure confirms the C_2 symmetry. The X-ray structure also highlights the shortening of the Os-Os bond length [2.6874(5) Å] across the bridged face of the cluster in the same way as that previously reported for $[Os_3(\mu\text{-}H)_2(CO)_{10}]$ with an Os-Os bond length of [2.681 (1)Å].[99] The hydride ligands were not detected directly but were placed by inference from the positions of the CO ligands. These structural data are also totally consistent with the observed ^{13}C NMR data. This cluster is formally unsaturated with 46 electrons and so, consistent with the X-ray evidence, the bridged edge of the cluster could be considered to have a double bond.

4.1.1 Fluxional behaviour of $[Os_3(\mu\text{-}H)_2(CO)_8(tolBINAP)]$ studied by ^1H NMR

The variable temperature ^1H NMR of $[Os_3(\mu\text{-}H)_2(CO)_8(tolBINAP)]$ (see Figure 4.2) shows considerable change in the aromatic region with temperature. The hydride ligand signal is temperature independent as are the $^{13}C\{^1H\}$ NMR signals of the CO ligands and the $^{31}P\{^1H\}$ NMR signals of phosphine ligands. With all the ligand NMR spectra except the ^1H NMR spectra showing temperature independence, it is safe to say that there is no mobility in the M_3 framework. Further confirmation of the static nature of the M_3 framework is given by the temperature independent nature of the ^1H-^{187}Os couplings and the ^{31}P-^{187}Os couplings. The $^{13}C\{^1H\}$ NMR spectrum contains the four expected CO signals,

two for the *axial* and *equatorial* CO ligands of the $Os(CO)_4$ group and two signals for the two sets of non-equivalent CO ligand *trans* to the hydride. These CO ligands give two sets of signals as a result of the C_2 symmetry imposed by the μ-tolBINAP ligand. The two non-equivalent CO ligand sets also show a coupling to the ^{31}P nucleus (J_{PC} 18.2 Hz and 15.0 Hz).

The low temperature COSY NMR spectrum has also been run for $[Os_3(\mu\text{-}H)_2(CO)_8(tolBINAP)]$. Given the similarity in the appearance of both the 1d and 2D spectra between this cluster and that of $[Ru_3(\mu\text{-}OH)_2(CO)_8\{(R)\text{-}BINAP\}]$ and the overall similarity in the geometry obtained from the X-ray structure it seems safe to interpret the fluxional behaviour observed in the ^1H NMR spectra for the phenyl groups in a similar way. Exchange is between the signals A and C coalescing to give X between B and D coalescing to give Y. This is simply explained in terms of restricted tolyl rotation about the CH_3-quaternary carbon axis of two of the four tolyl substituents. Exchange is between the non-equivalent 2 and 6 positions and between the non-equivalent 3 and 5 positions. Given that the para-tolyl form of the BINAP ligand was used for this work, whereas the straight phenyl form was used for the study of $[Ru_3(\mu\text{–}OH)_2(CO)_8\{(R)\text{–}BINAP\}]$, it is unsurprising that the CH_3 show no exchange. There are two sets of tolyl groups that are inequivalent regardless of any intramolecular dynamic processes. It is assumed that the phenyl or tolyl groups lying closest to the naphthyl planes are experiencing the greatest barrier to rotation. See Figure 4.3.

4.1.2 Attempted carbonylation of $[Os_3(\mu\text{-}H)_2(CO)_8(tolBINAP)]$

A solution of $[Os_3(\mu\text{-}H)_2(CO)_8(tolBINAP)]$ in hexane was refluxed with CO gas passing slowly through. After forty eight hours there was no change in the IR spectrum. The same experiment carried out at room temperature for eight hours also gave no change in the IR spectrum. This is in sharp contrast to the reaction of $[Os_3(\mu\text{-}H)_2(CO)_{10}]$ with CO which readily cleaves open one of the Os–H–Os bridges leaving a terminal hydride and a bridging hydride in the cluster $[Os_3(H)(\mu\text{–}H)(CO)_{11}]$.[110] Introduction of the tolBINAP ligand has suppressed this reactivity.

4.1.3 Attempted reaction of $[Os_3(\mu\text{–}H)_2(CO)_8(tolBINAP)]$ with acetylene

A solution of $[Os_3(\mu\text{–}H)_2(CO)_8(tolBINAP)]$ in hexane was saturated with acetylene and left to stand under acetylene. After forty eight hours no change was observed in the IR spectrum. This is in contrast to the reaction of $[Os_3(\mu\text{–}H)_2(CO)_{10}]$ with acetylene which proceeds readily to form $[Os_3(\mu\text{–}H)(CO)_{10}\{\mu\text{–}CH{=}CH_2\}]$.[111]

Figure 4.2 Variable temperature ^{1}H NMR, 500 MHz $CDCl_3$ $[Os_3(\mu\text{–}H)_2(CO)_8\{tolBINAP\}]$.

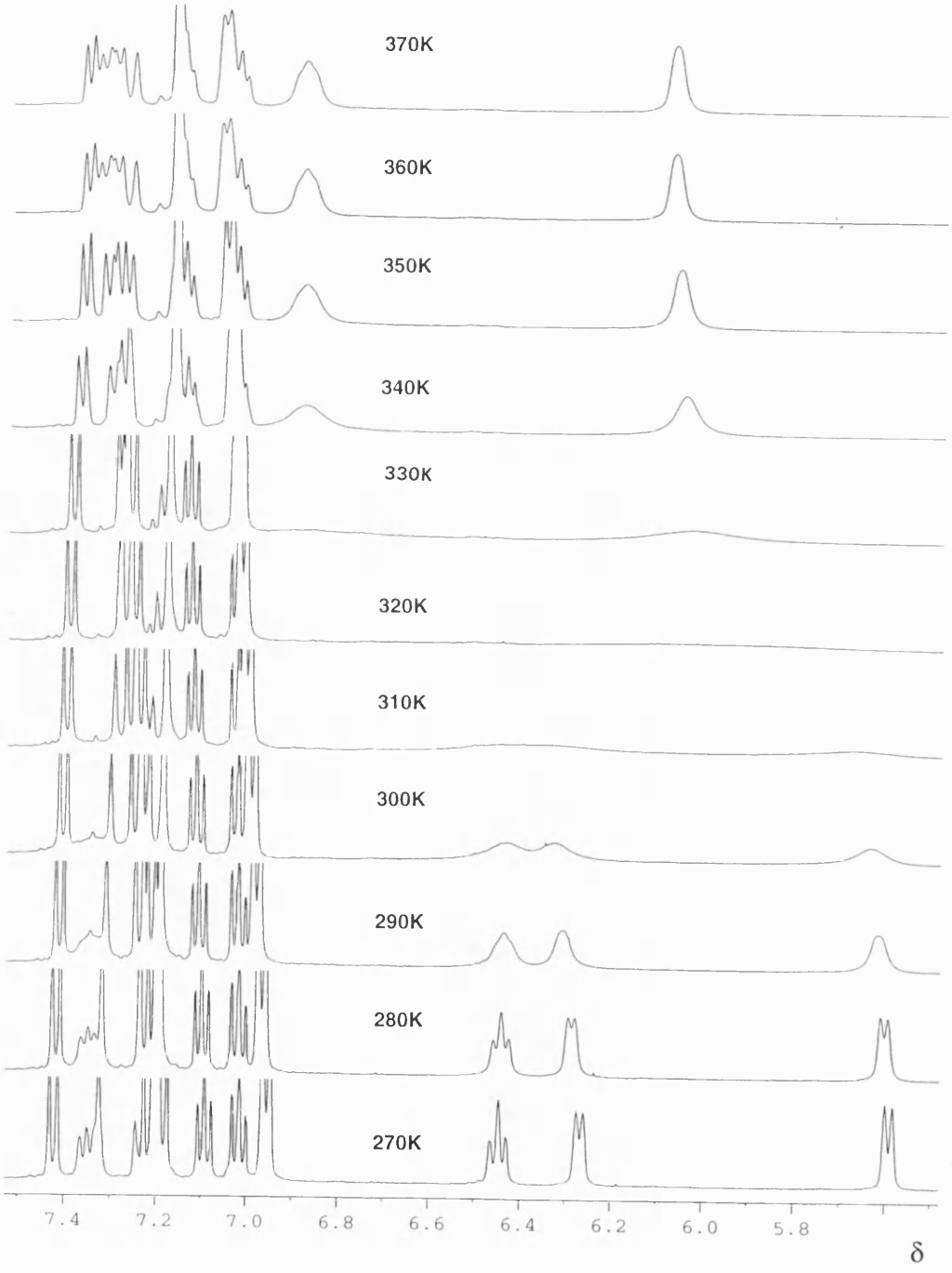

Figure 4.3 $[Os_3(\mu\text{–}H)_2(CO)_8\{tolBINAP\}]$

COSY ^1H NMR 500 MHz $CDCl_3$ at –65 ° C. Signals A and C are exchanging and coalesce to form signal X at higher temperatures. Signals B and D are exchanging and coalesce to form signal Y at higher temperatures. The spectrum was acquired using 256 increments and 2 (using pulsed field Z-gradients) transients per increment. Processed with a shifted QSINE window function and zero filled to 1K by 1K data points in both dimensions.

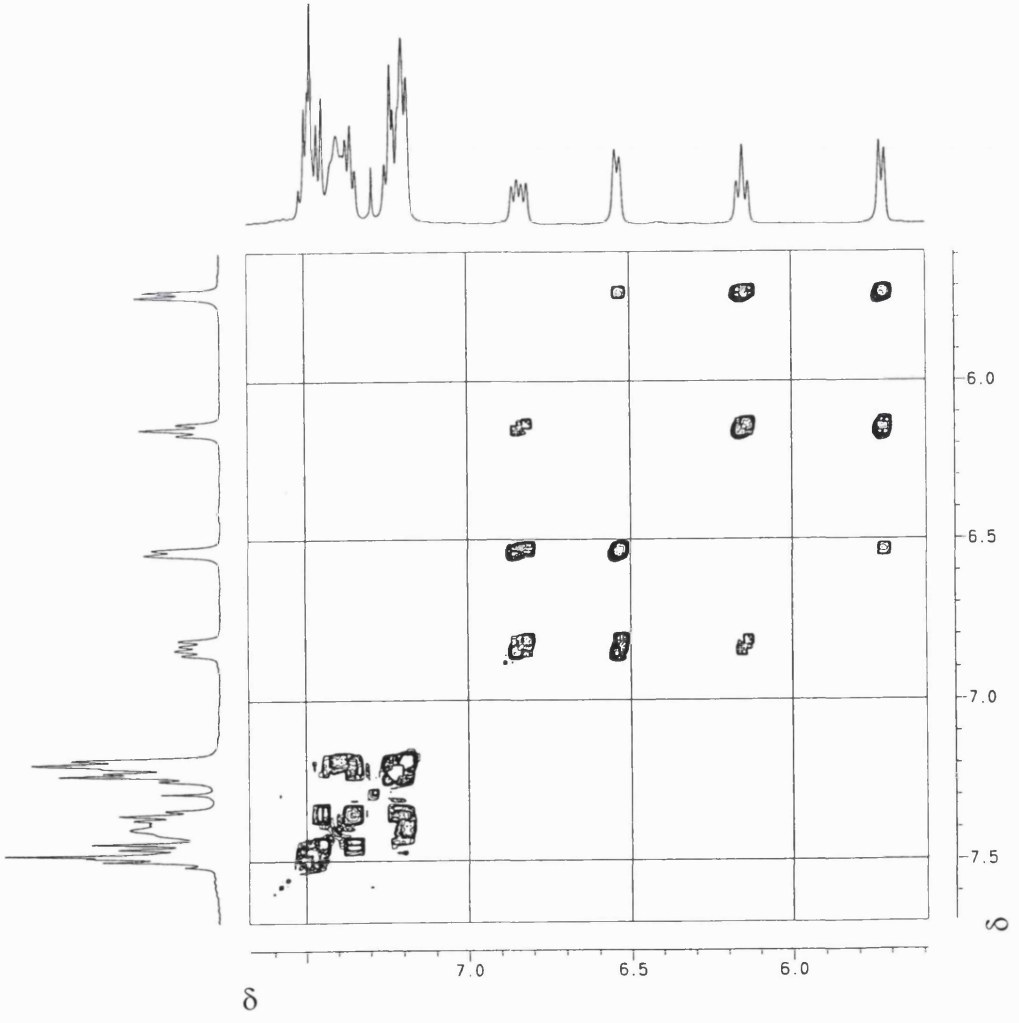

Figure 4.5 Crystal structure of $[Os_3(\mu\text{-}H)_2(CO)_8(tolBINAP)]$ with carbonyls omitted to show the metal triangle more clearly.

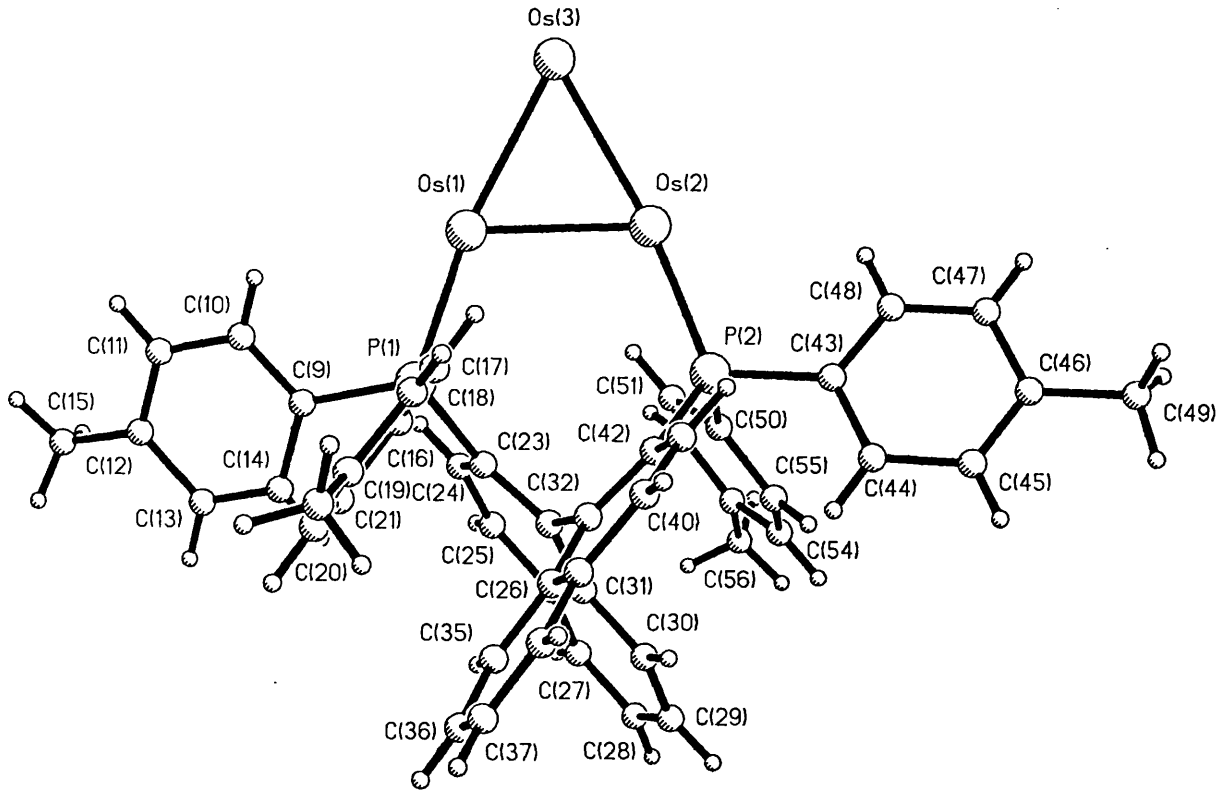

Figure 4.6 X-ray structure of $[Os_3(\mu\text{-}H)_2(CO)_8(dppm)]$

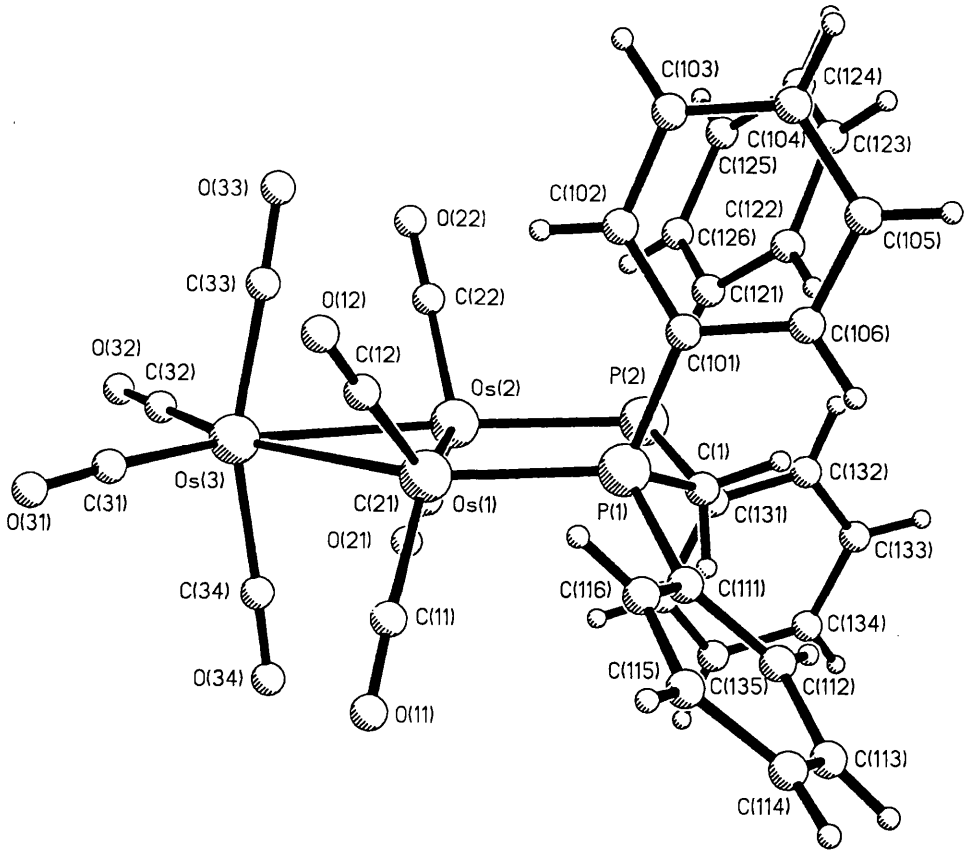

Table 1 Selected single crystal X-ray data for $[Os_3(\mu\text{-}H)(CO)_8\{tolBINAP\}]$ and $[Os_3(\mu\text{-}H)(CO)_8\{dppm\}]$

Parameter	$[Os_3(\mu\text{-}H)(CO)_8\{dppm\}]$	$[Os_3(\mu\text{-}H)(CO)_8\{tolBINAP\}]$
crystal size (mm)	0.35 x 0.25 x 0.18	0.45 x 0.35 x 0.25
formula	$C_{33}H_{24}O_8Os_3P_2$	C57H48O11Os3P2
Fw	1181.06	1541.49
colour	red	green
crystal system	monoclinic	orthorombic
space group	$P2_1/c$	$P2_12_12_1$
Temp (K)	293(2)	103(2)
a (Å)	10.024(2)	13.7322(3)
b (Å)	29.826(6)	19.4193(4)
c (Å)	120.93(2)	21.1105(5)
β (deg)	109.57(3)	90
V (Å^3)	3406.7(11)	5629.5(2)
Z	4	4
d_{calc} (g cm^{-3})	2.303	1.819
μ(Mo Kα) (mm^{-1})	0.71073	0.71070
F(000)	2176	2944
2θ range (degrees)	2.67 to 26.00	3.24 to 26.00
no. independent reflections	6110	10797
wR2 (all data)	0.0893	0.0502
R1 [$I>2\sigma(I)$]	0.0805	0.0490
goodness-of-fit on F^2	1.086	1.124
Data/parameters	6087/211	10797/659
peak/hole eÅ^{-3}	6.615, -4.795	6.868, -2.23

4.1.4 Reaction of $[Os_3(\mu\text{-}H)_2(CO)_8(tolBINAP)]$ with $P(OMe)_3$

Addition of a twofold excess of $P(OMe)_3$ to a solution of $[Os_3(\mu\text{-}H)_2(CO)_8(tolBINAP)]$ in hexane at room temperature yielded the cluster $[Os_3(\mu\text{–}H)_2(CO)_7(tolBINAP)\{P(OMe)_3\}]$ in good yield. The ^1H NMR indicates the expected loss of symmetry resulting in non-equivalent hydride ligands, giving rise to a pair of doublet of doublets with a small chemical shift difference [*ca.* δ 0.01]. The $^{31}P\{^1H\}$ spectrum shows two signals in the intensity ratio 1:2. Probably the ^{31}P nuclei of the tolBINAP ligand should be non-equivalent but, because of the low resolution of the spectrum we were able to obtain these are not resolved. We cannot determine the position of the $P(OMe)_3$ in this complex, however it is likely that the substitution is equatorial as all known phosphine clusters present equatorial substitution. In view of the lack of addition of CO to $[Os_3(\mu\text{–}H)_2(CO)_8(tolBINAP)]$, it is surprising that the reaction with $P(OMe)_3$ occurs so readily.

4.1.5 Reaction of $[Os_3(\mu\text{-}H)_2(CO)_8(tolBINAP)]$ with $[Ph_2P(CH_2)_nPPh_2]$

Addition of the diphosphines in the series $Ph_2P(CH_2)_nPPh_2$ (where n = 1 to 4) to solutions of $[Os_3(\mu\text{-}H)_2(CO)_8(R\text{-}tolBINAP)]$ in CH_2Cl_2 at ambient temperature, under reflux and on UV photolysis leads to no discernible change in the IR spectra over a period of days. This indicates that the third Os in the M_3 triangle is relatively unreactive and that only very good ligands such as $P(OMe)_3$ will react with it.

4.5 Synthesis of $[Os_3(\mu\text{-}H)_2(CO)_8\{\mu\text{-}Ph_2P(CH_2)_nPPh_2\}]$ (n = 1 to 4)

4.1.6 Synthesis and characterisation of the cluster $[Os_3(\mu\text{-}H)_2(CO)_8(\mu\text{-}dppm)]$

The cluster $[Os_3(\mu\text{-}H)_2(CO)_{10}]$ was treated with dppm in refluxing THF for one hour. One major product was isolated in 50 % yield as red crystals which was spectroscopically characterised as $[Os_3(\mu\text{-}H)_2(CO)_8(\mu\text{-}dppm)]$. The FAB mass spectra are consistent with the formulation given. The ^1H NMR showed the expected triplet at δ -10.31 and the IR spectrum matched the previously reported spectrum.[42]

4.1.7 Synthesis and characterisation of the cluster $[Os_3(\mu\text{-}H)_2(CO)_8(\mu\text{-}dppe)]$

Similarly the cluster $[Os_3(\mu\text{-}H)_2(CO)_{10}]$ was reacted with dppe in refluxing THF for one hour. One major product was isolated in 40 % yield as orange crystals which was spectroscopically characterised as $[Os_3(\mu\text{-}H)_2(CO)_8(\mu\text{-}dppe)]$.

4.1.8 Synthesis and characterisation of the cluster $[Os_3(\mu\text{–}H)_2(CO)_8(\mu\text{–}dppp)]$

Similarly the cluster $[Os_3(\mu\text{-}H)_2(CO)_{10}]$ was reacted with dppp in refluxing THF for one hour. One major product was isolated in 20 % yield as mauve crystals which was spectroscopically characterised as $[Os_3(\mu\text{–}H)_2(CO)_8(\mu\text{–}dppb)]$.

4.1.9 Synthesis and characterisation of the cluster $[Os_3(\mu\text{–}H)_2(CO)_8(\mu\text{–}dppb)]$

The cluster $[Os_3(\mu\text{–}H)_2(CO)_{10}]$ was reacted with dppb in refluxing THF for one hour. No major product was isolated. However, the ^1H NMR spectrum of the mixture obtained showed a minor hydride triplet consistent with $[Os_3(\mu\text{–}H)_2(CO)_8(\mu\text{–}dppb)]$ at δ - 10.03. No IR spectrum had been previously reported and the mixture we obtained could not be separated to give a pure product.

4.1.10 Attempted carbonylation of $[Os_3(\mu\text{–}H)_2(CO)_8\{\mu\text{–}Ph_2P(CH_2)_nPPh_2\}]$ where n = 1-4

The clusters $[Os_3(\mu\text{–}H)_2(CO)_8\{\mu\text{–}Ph_2P(CH_2)_nPPh_2\}]$ were reacted with CO at atmospheric pressure in refluxing THF for forty eight hours. No products were isolated. Neither FAB, APCI or electrospray mass spectra could be used to identify any new products. The ^1H NMR showed no change in the hydride region. There was no observable change in the IR spectra. Given that low temperatures favour systems with - ΔG and since $\Delta S^{\#}$ is in this case negative it is likely that low temperatures and high pressures will favour carbonylation.

4.1.11 Attempted reaction of $[Os_3(\mu\text{–}H)_2(CO)_8\{\mu\text{–}Ph_2P(CH_2)PPh_2\}]$ with acetylene where n = 1-4

The cluster $[Os_3(\mu\text{–}H)_2(CO)_8\{\mu\text{–}Ph_2P(CH_2)_nPPh_2\}]$ was reacted with acetylene in refluxing n-hexane for twenty four hours. No new products were isolated.

Neither FAB, APCI or electrospray mass spectra identified any new products. The ^{1}H NMR spectrum showed no change in the hydride region and there was no observable change in the IR spectra.

4.1.12 Crystal structure of $[Os_3(\mu\text{–}H)_2(CO)_8\{\mu\text{–}Ph_2P(CH_2)PPh_2\}]$ and comparison with the related tolBINAP cluster and $[Os_3(\mu\text{–}H)_2(CO)_{10}]$

The large red crystals grown, from hexane or $CHCl_2$ or $CDCl_3$ by slow evaporation, for this study were of less than ideal quality, although in appearance they were large and well formed all the crystals tried were twinned. A crystal of acceptable quality was found but even using a CD area diffractometer the residual (R) was still around 9% and the goodness of fit (GOOF) was 1.086 which is somewhat worse than that reported for the previous structure for which full data is not available.[105] The formal double bonded character of the Os–Os bond bridged by the diphosphine ligand is indicated by the short bond length of 2.6757(9) Å as compared to the two longer Os–Os non-bridged bond lengths of 2.8117(10) Å and 2.8008(8) Å the value of the bridged Os–Os bond is comparable to that found for the bridged bond in the cluster $[Os_3(\mu\text{–}H)_2(CO)_8(tolBINAP)]$ which is 2.6874(5) Å. These values are interestingly slightly different to those previously reported for this cluster with the short bond at 2.681(1) Å and the other bonds being at 2.820(1) Å and 2.812(1) Å respectively. The hydrides were not located directly but by inference from the positions of the carbonyls by the insertion of ghost atoms and refinement with these in position. We had originally planned to obtain structures of the dppe and dppp analogues to assess any changes in the bridged bond length with ring size. However although visually reasonable crystals were

easy to grow the crystals were in all cases so badly twinned as to preclude obtaining structures of the necessary quality.

4.6 Conclusions

a) A novel route to clusters of the from $[Os_3(\mu\text{-}H)_2(CO)_8(diphos)]$ has been demonstrated for several diphosphine ligands. These clusters had previously been prepared by the reaction of $[Os_3(CO)_{10}L_2]$ with hydrogen in a refluxing solvent.

b) The cluster $[Os_3(\mu\text{-}H)(CO)_{10}]$ reacts readily with a variety of diphosphine ligands L to form the clusters $[Os_3(\mu\text{-}H)(CO)_8L]$ in moderate to high yields by this simple one step synthesis.

c) The single crystal X-ray structures of the clusters $[Os_3(\mu\text{-}H)_2(CO)_8\{tolBINAP\}]$ and $[Os_3(\mu\text{-}H)_2(CO)_8\{dppm\}]$ both show a short Os-Os distance similar to that found for the parent dihydride $[Os_3(\mu\text{-}H)_2(CO)_{10}]$.

d) NMR and X-ray studies have confirmed that the clusters synthesised have retained their C_2 symmetry.

e) The dihydrido clusters prepared are highly air stable.

f) The dihydrido clusters have also shown themselves to be highly unreactive even towards such reagents as acetylene or carbon monoxide in marked contrast to the parent dihydride $[Os_3(\mu\text{-}H)_2(CO)_{10}]$ which readily reacts with these reagents.

g) The lack of reactivity may be attributed to the reduction in electrophilicity due to the presence of two two electron donating phosphine ligands and also possibly because of steric crowding around the $Os(\mu\text{-}H)_2Os$ bridged set of atoms.

4.7 Experimental

Synthesis of $Os_3(\mu\text{-}H)_2(CO)_{10}$

3 g of $Os_3(CO)_{12}$ prepared using a reported procedure were[112], ground to a fine powder and placed in a five-litre flask containing 2.5 litres of n-octane. The yellow suspension was purged vigorously with hydrogen to remove any dissolved oxygen and the mixture was brought to a vigorous reflux with hydrogen slowly passed through the yellow solution. After about 5 min at reflux, saturated with hydrogen, a purple tinge appeared in the solution and after two hours the reaction had gone to completion as detected by changes in the IR spectrum. The solvent was removed under reduced pressure and $Os_3(\mu\text{-}H)_2(CO)_{10}$ was obtained as a purple solid (90 % yield), which was characterised by IR and ^1H NMR spectra.[113]

The ligands dppm, dppe and 4-tolBINAPwere purchased from Aldrich and used without further purification. NMR spectra were acquired on a Bruker AC300 or AMX400 spectrometers and processed using XWIN-NMR and XWIN-PLOT and on a Varian VXR400 spectrometer. FAB mass spectra were acquired on a ZAB spectrometer (MNBA matrix). IR spectra were recorded on a Nicolet 280 FT-IR spectrometer. Solvents were dried and distilled by standard methods prior to use.

4.1.14 Preparation of $[Os_3(\mu\text{-}H)_2(CO)_8(\mu\text{-dppm})]$

A solution of 0.1 g of $[Os_3(\mu\text{-}H)_2(CO)_{10}]$ and 0.03 g of dppm in THF was refluxed for one hour under nitrogen. The solvent was removed under reduce pressure. The

solid was dissolved in CH_2Cl_2 and loaded onto a silica column (BDH silica) eluent CH_2Cl_2/n-hexane (3:7 by volume). One major product was isolated in 50% yield (65 mg) as red crystals which was spectroscopically characterised as $[Os_3(\mu\text{-}H)_2(CO)_8(\mu\text{-}dppm)]$. FABMS: observed centre of the isotopic envelope 1182, calculated for the parent molecular ion (^{192}Os) 1182.

4.1.15 Preparation of $[Os_3(\mu\text{-}H)_2(CO)_8(\mu\text{-}dppe)]$

A solution of 0.1 g of $[Os_3(\mu\text{-}H)_2(CO)_{10}]$ and 0.033 g dppe in THF was refluxed for one hour under nitrogen. The solvent was removed under reduce pressure. The solid was dissolved in CH_2Cl_2 loaded onto a silica column (BDH silica), eluent CH_2Cl_2/n-hexane (4:6 by volume). One major product was isolated in 40 % yield (53 mg) as orange crystals which was spectroscopically characterised as $[Os_3(\mu\text{-}H)_2(CO)_8(\mu\text{-}dppe)]$, by comparison with previously reported data.[42] FABMS: observed centre of the isotopic envelope 1196, calculated for the parent molecular ion (^{192}Os) 1196.

4.1.16 Preparation of $[Os_3(\mu\text{-}H)_2(CO)_8(\mu\text{-}dppp)]$

0.1 g of $[Os_3(\mu\text{-}H)_2(CO)_{10}]$ and 0.035 g of dppp in THF was refluxed in THF for one hour under nitrogen. The solvent was removed under reduce pressure. The solid was loaded onto a silica column (BDH silica), eluent DICHLOROMETHANE/n-hexane (4:6 by volume). One major product was isolated in 30 % yield (38 mg) as purple crystals which were spectroscopically characterised as $[Os_3(\mu\text{-}H)_2(CO)_8(\mu\text{-}dppp)]$.

FABMS: observed centre of the isotopic envelope 1210, calculated for the parent molecular ion (^{192}Os) 1210.

4.1.17 Attempted preparation of $[Os_3(\mu\text{-}H)_2(CO)_8(\mu\text{—dppb})]$

0.1g of $[Os_3(\mu\text{-}H)_2(CO)_{10}]$ and 0.037 g of dppb in THF was refluxed for one hour under nitrogen. The reaction was monitored by IR at hourly intervals, no products were isolated from TLC of the reaction mixture.

4.1.18 Preparation of $[Os_3(\mu\text{-}H)_2(CO)_8(\mu\text{-tolBINAP})]$

A solution of 0.1g of $[Os_3(\mu\text{-}H)_2(CO)_{10}]$ and 0.075g of tolBINAP in THF was refluxed for two hours under nitrogen. The solvent was removed under reduced pressure. The solid was dissolved in CH_2Cl_2 and loaded onto a silica column (BDH silica), eluent CH_2Cl_2/n-hexane (3:7 by volume). One major product was isolated in 50% yield (87 mg) as green crystals which was spectroscopically characterised as $[Os_3(\mu\text{-}H)_2(CO)_8(\mu\text{-tolBINAP})]$. Elemental analysis: found: C, 44.60; H, 2.82; P, 4.03. Expected C, 45.58; H, 2.87; P, 4.20. FABMS: observed centre of the isotopic envelope (^{192}Os) 1478, calculated for the parent molecular ion 1478.

Table 4.2 Selected bond lengths and angles for the single crystal X-ray structure of $[Os_3(\mu\text{-}H)(CO)_8\{tolBINAP\}]$

Os(1)-Os(2)	2.6875(5)	P(1)-C(23)	1.838(11)
Os(2)-Os(3)	2.8320(5)	P(1)-C(201)	1.836(11)
Os(1)-Os(3)	2.8206(5)	P(2)-C(121)	1.827(11)
Os(1)-P(1)	2.346(3)	P(2)-C(131)	1.836(11)
P(1)-C(9)	1.839(11)	P(2)-C(211)	1.849(11)
Os(1)-Os(3)-Os(2)	56.7773(13)	Os(1)-P(1)-C(16)	112.8(4)
Os(2)-Os(1)-Os(3)	61.827(13)	C(9)-P(1)-C(16)	100.5(5)
Os(1)-Os(2)-Os(3)	61.400(13)	C(9)-P(1)-C(23)	100.6(5)
Os(3)-Os(1)-P(1)	170.31(7)	C(9)-P(1)-C(16)	100.5(5)
Os(3)-Os(2)-P(2)	172.21(7)	C(50)-P(2)-C(42)	111.1(5)
Os(1)-P(1)-C(9)	114.9(4)	C(43)-P(2)-C(42)	1001.8(5)
Os(1)-P(1)-C(23)	115.7(3)	C(50)-P(2)-C(43)	99.1(11)

Table 4.3 Selected bond lengths and angles for the single crystal X-ray structure of $[Os_3(\mu\text{-}H)(CO)_8(\mu\text{-}dppm)]$

Os(1)-Os(2)	2.6757(9)	P(1)-C(101)	1.801(13)
Os(2)-Os(3)	2.8008(8)	P(1)-C(1)	1.820(13)
Os(1)-Os(3)	2.8117(10)	P(2)-C(121)	1.805(14)
Os(1)-P(1)	2.320(3)	P(2)-C(131)	1.857(13)
P(1)-C(111)	1.80(2)	P(2)-C(1)	1.846(13)
Os(1)-Os(3)-Os(2)	56.77(2)	Os(1)-P(1)-C(1)	110.5(4)
Os(2)-Os(1)-Os(3)	61.32(2)	C(1)-P(1)-C(101)	106.6(4)
Os(1)-Os(2)-Os(3)	61.73(3)	C(1)-P(1)-C(111)	104.0(6)
Os(3)-Os(1)-P(1)	155.73(7)	C(121)-P(2)-C(131)	103.1(6)
Os(3)-Os(2)-P(2)	157.52(9)	C(1)-P(2)-C(121)	107.5(5)
Os(1)-P(1)-C(111)	116.7(4)		
Os(1)-P(1)-C(101)	116.6(3)		

Table 4.4 Infrared data

Compound	ν/cm^{-1} (cyclohexane)
$[Os_3(\mu\text{-}H)_2(CO)_8(\mu\text{-tolBINAP})]$	2067s, 2028vw, 2009vs, 1989vs, 1963s, 1948m
$[Os_3(\mu\text{-}H)_2(CO)_8(\mu\text{-dppm})]$	2066s, 2004vs, 1982s, 1954, 1943m
$[Os_3(\mu\text{-}H)_2(CO)_8(\mu\text{-dppe})]$	2063s, 2007vs, 1981vs, 1949m
$[Os_3(\mu\text{-}H)_2(CO)_8(\mu\text{-dppp})]$	2066s, 2007vs, 1980vs, 1948s 1943m

Table 4.5 NMR Data

Compound	δ ^{31}P NMR (ref. H_3PO_4)	δ ^{13}C NMR, carbonyl region only
$[Os_3(\mu\text{-}H)_2(CO)_{10}]$	N/A	187.74, 184.78, 183.74, 183.69, 182.22, 182.16
$[Os_3(\mu\text{-}H)_2(CO)_8(\mu\text{-tolBINAP})]$	28.2	187.71, 184.78, 183.74, 182.17

Compound	δ ^{1}H NMR ($CDCl_3$)	$J^{187}_{Os\text{-}^{1}H}$	$J^{31}_{P\text{-}^{1}H}$
$[Os_3(\mu\text{-}H)_2(CO)_{10}]$	-11.4 (N.B. depends strongly on the solvents used)	46	N/A
$[Os_3(\mu\text{-}H)_2(CO)_8(\mu\text{-}tolBINAP)]$	-9.16(t) Os*H*, 3.75 & 3.79 (s) CH_3, 5.59(d), 6.25(d), 6.45(t) & 7.35(t) $C_6H_4CH_3$, 6.96-7.45 complex naphthyl	42	12.5
$[Os_3(\mu\text{-}H)_2(CO)_8(\mu\text{-}dppm)]$	4.15(t) CH_2, 7.4 (m) C_6H_5, -10.31(t) Os*H*	Not measured	10.1
$[Os_3(\mu\text{-}H)_2(CO)_8(\mu\text{-}dppe)]$	7.26(m) CH_2, 7.45 (m) C_6H_5, -10.76(t) Os*H*	Not measured	9.6
$[Os_3(\mu\text{-}H)_2(CO)_8(\mu\text{-}dppp)]$	1.91(t) CH_2, 2.73(t) CH_2, 7.34 (m) C_6H_5, -10.13(t) Os*H*	Not measured	8.2

Chapter 5 Reactions of $[Os_3(CO)_{12}]$ and $[Ru_3(CO)_{12}]$ with (R)(+)–4–pyridylethanol, (S)–(-)–nicotine and pyridine

5.1 Introduction: metallation of pyridyl type ligands and the chirality of the products

Clusters may have one of three kinds of chirality:

a) inherent chirality, i.e. the cluster metal framework itself is chiral,

b) chirality resulting from the rigid attachment of a ligand that is itself not chiral to a cluster that is itself not chiral but together combining to form a chiral system, and

c) chirality as a result of the attachment of chiral ligand.

There are cases where, although two or more isomers exist, resolution is not possible as fluxionality within the cluster, for example a rapid hydride migration of a ligand prevents it.[114,115] Early resolution of diastereomers relied heavily on column chromatography or TLC (**t**hin **l**ayer **c**hromatography) for separation.[117] As its name implies, the widespread use of the higher resolution technique of HPLC (**h**igh **p**erformance **l**iquid **c**hromatography) has allowed this area to progress further than was previously possible.[116]

Some of the first diastereomeric triosmium clusters separated were those of $[Os_3(\mu\text{-}H)(CO)_{10}(\mu\text{-}RNHCO)]$, such as the diastereomers derived from (+)-1-phenylethylamine.[117,118] The separation was confirmed by the different ^1H NMR spectra of the diastereomers but essentially similar IR spectra. The two components were characterised by CD (**c**ircular **d**ichroism) but without the absolute stereochemistry of the $Os(CO)_3$ sub-units being determined.

The cluster $[FeCoMoS(C_5H_5)(CO)_8]$ has been resolved,[119] and the absolute stereochemistry determined by reaction it with an optically active phosphine and subsequent fractional crystallisation. The phosphine is then removed by reaction with methyl iodide and the pure enantiomers are recovered.[119] The absolute configuration has been determined for the phosphine containing cluster by single crystal X-ray methods and then by comparison of the CD spectra, by inference, the pure enantiomers of $[FeCoMoS(C_5H_5)(CO)_8]$.

The reaction of pyridine and $[Os_3(CO)_{12}]$ is characterised although there appears to be no X-ray structure of the enantiomeric products $[Os_3(\mu\text{-}H)(CO)_9(NC_5H_4)]$.[120] The reaction between $[Os_3(CO)_{12}]$ and pyridine or $[Os_3(CO)_{10}(MeCN)_2]$ and pyridine gives a series of products. By direct reaction, in a sealed glass tube, the following products are obtained $[Os_3(\mu\text{-}H)(CO)_{10}(NC_5H_4)]$, $[Os_3(\mu\text{-}H)(CO)_9(pyridine)(NC_5H_4)]$ two isomers; $[Os_3(\mu\text{-}H)_2(CO)_8(NC_5H_4)_2]$ and $[Os_2(CO)_6(NC_5H_4)_2]$ two isomers. The reaction sequence appears to be that $[Os_3(\mu\text{-}H)(CO)_{10}(NC_5H_4)]$, possibly formed from $[Os_3(CO)_{11}(py)]$ which is not observed, undergoes CO substitution to give $[Os_3(\mu\text{-}H)(CO)_9(py)(NC_5H_4)]$. Hydrogen transfer to the metal core on loss of CO then gives $[Os_3(\mu\text{-}H)_2(CO)_8(NC_5H_4)_2]$. The real significance of this reaction series lies in the reversibility of some steps and the non-reversibility of others. If CO is passed through a refluxing solution of $[Os_3(CO)_{12}]$ and pyridine in octane there is no reaction, if N_2 is used (thus purging the CO displaced) then there is an almost quantitative (in terms of the metal carbonyl) reaction to various clusters. However once the hydrogen has been transferred from the ligand to the metal core

the reaction is not reversible. CO is then lost followed by a further hydrogen transfer to allow the further substitution of a pyridine to give $[Os_3(\mu\text{-}H)_2(CO)_8(NC_5H_4)_2]$. However once again before the final step to the $[Os_3(\mu\text{-}H)_2(CO)_8(NC_5H_4)_2]$, where the hydrogen relocates to the M_3 framework from the ligand, the pyridine cannot be displaced. The cluster $[Os_3(\mu\text{-}H)(CO)_{10}(NC_5H_4)]$ may be separated by derivatisation with a chiral amine followed by crystallisation or TLC and finally the removal of the amine to yield the pure resolved cluster.[120] Extensive studies of the vibrational frequencies of the α-pyridyl moeity in $[Os_3(\mu\text{-}H)(CO)_{10}(\mu\text{-}\eta^2\text{-}NC_5H_4)_2]$, under pressurè, have been carried out by IR spectroscopy.[121] The observed pressure effects reflect both inter and intramolecular effects. The first order effect of pressure is the 'stiffening' of the force constant and a subsequent shift to higher energy, the magnitude of this effect can be considerably modified if significant van der Waals interactions are present. In the case of $[Os_3(\mu\text{-}H)(CO)_{10}(\mu\text{-}\eta^2\text{-}NC_5H_4)_2]$ this shift can be up to 30 cm^{-1} over a range of 60 Kbar.

It has been demonstrated that $[Os_3(CO)_{10}(MeCN)_2]$ reacts readily with 2-vinylpyridine to form $[Os_3(\mu\text{-}H)(CO)_9L(NC_5H_4CH{=}CH)]$ (where L = CO or PMe_2Ph) with an open Os structure.[122] The open structure has been exploited as it allows further reaction with $[Os_3(CO)_{10}(MeCN)_2]$ to give the unique hexanuclear cluster $[Os_6(\mu\text{-}H)(CO)_{20}(\mu\text{-}\eta^2\text{-}NC_5H_4CH{=}CH)]$ in which the osmium chain is fused to one edge of an osmium triangle through two Os-Os bonds and a hydride bridge.[123]

Isoquinoline reacts with $[Os_3(CO)_{12}]$ to give the two isomeric clusters $[Os_3(\mu\text{-}H)(CO)_{10}(NC_9H_6)]$ both metallated *ortho* to the nitrogen in a manner analogous to that of pyridine. However the yield of the two isomers (determined by NMR spectroscopy) were reported as being quite different with 1,1-$[Os_3(\mu\text{-}H)(CO)_{10}(NC_9H_6)]$ being favoured 2:1 over the other possible isomer.[120]

Bipyridyl reacts with $[Os_3(CO)_{12}]$ to give a black insoluble material $[Os_3(CO)_{10}(bipy)]$ which thermally loses a CO ligand at 150 °C to form a red solid species $[Os_3(\mu\text{-}H)(CO)_9(NC_5H_4NC_5H_3)]$ which has been characterised structurally revealing that one of the pyridyl rings is *ortho*metallated and the other is chelating.[124, 125] The $[Ru(bipy)_3]^{2+}$ system which has much studied catalytic properties.[126] The catalytic activity of $[Ru_3(CO)_{12}]$-bipyridine mixture has also been determined for the reduction of nitrobenzene to aniline with good conversion;[127] although it is far from clear what the catalytically active species is. However what is clear, is that a transition metal pyridyl cluster species does, in certain circumstances, have catalytic activity. $[Os_3(\mu\text{-}H)(CO)_9(bipy)]$ was the first cluster bipyridyl to be structurally characterised.

Peters and Deeming determined that the order of reactivity for pyridyl, vinyl and ethynyl groups with $[Os_3(\mu\text{-}H)_2(CO)_{10}]$ was ethynyl > pyridyl > vinyl.[124,128] They found that 2-vinylpyridine reacts with $[Os_3(\mu\text{-}H)_2(CO)_{10}]$ at room temperature to form $[Os_3(\mu\text{-}H)(CO)_{10}(NC_5H_4CHCH)]$ which had an unusual carbonyl distribution of 4,3,3 based on ^{13}CO NMR evidence.[129]

Objectives of the present work

The objectives of the work carried out in this chapter were:-

a) To prepare novel triosmium clusters with a variety of pyridines including, novel triosmium and triruthenium clusters with the chiral pyridine (R)-1-(4-pyridyl)ethanol,
b) To investigate and evaluate the various methods available for separating the diastereomers produced by (a),
c) To prepare the known diastereomers and positional isomers produced by the reaction of $[Os_3(CO)_{12}]$ with (s)-(-)-nicotine, which were previously inseparable,
d) To investigate and evaluate the various methods available for separating the diastereomers and positional isomers formed by (c),
e) To characterise the various forms of the clusters by X-ray or a combination of X-ray and CD spectroscopy.

5.2 Results and discussion

5.2.1 Reaction of $[Os_3(CO)_{10}(MeCN)_2]$ with (R)–1–(4–pyridyl)ethanol and with (S)–nicotine

The trinuclear cluster $[Os_3(CO)_{10}(MeCN)_2]$ reacts readily with the optically active compound (R)-1-methyl-(4-pyridyl)ethanol to give good yields of the simple substituted diastereomeric derivatives $[Os_3(\mu\text{-}H)(CO)_{10}\{(R)\text{-}NC_5H_3CH(OH)Me\text{-}4\}]$.

The known analogous cluster $[Os_3(\mu\text{-}H)(CO)_{10}(\mu\text{-}NC_5H_4)]$ exists as two distinct enantiomers. The reasoning behind using chiral analogues of pyridine is that they will form diastereomers which are physically different and therefore separable. Nicotine is a good example of a naturally occurring enantiomerially pure ligand which is commercially available as the natural form S–(–)–nicotine, a colourless, highly toxic liquid. Interest in nicotine dates back some twenty years initially on account of its availability as an enantiomerically pure ligand at a time when few others were available. The attractiveness of nicotine is in no way now reduced, in light of the many other enantiomerically pure ligands available, as it is one of the cheapest available.

Figure 5.1 The four isomers produced by the reaction of S–(–)–nicotine with $[Os_3(CO)_{12}]$ two positional isomers and two diastereomers.

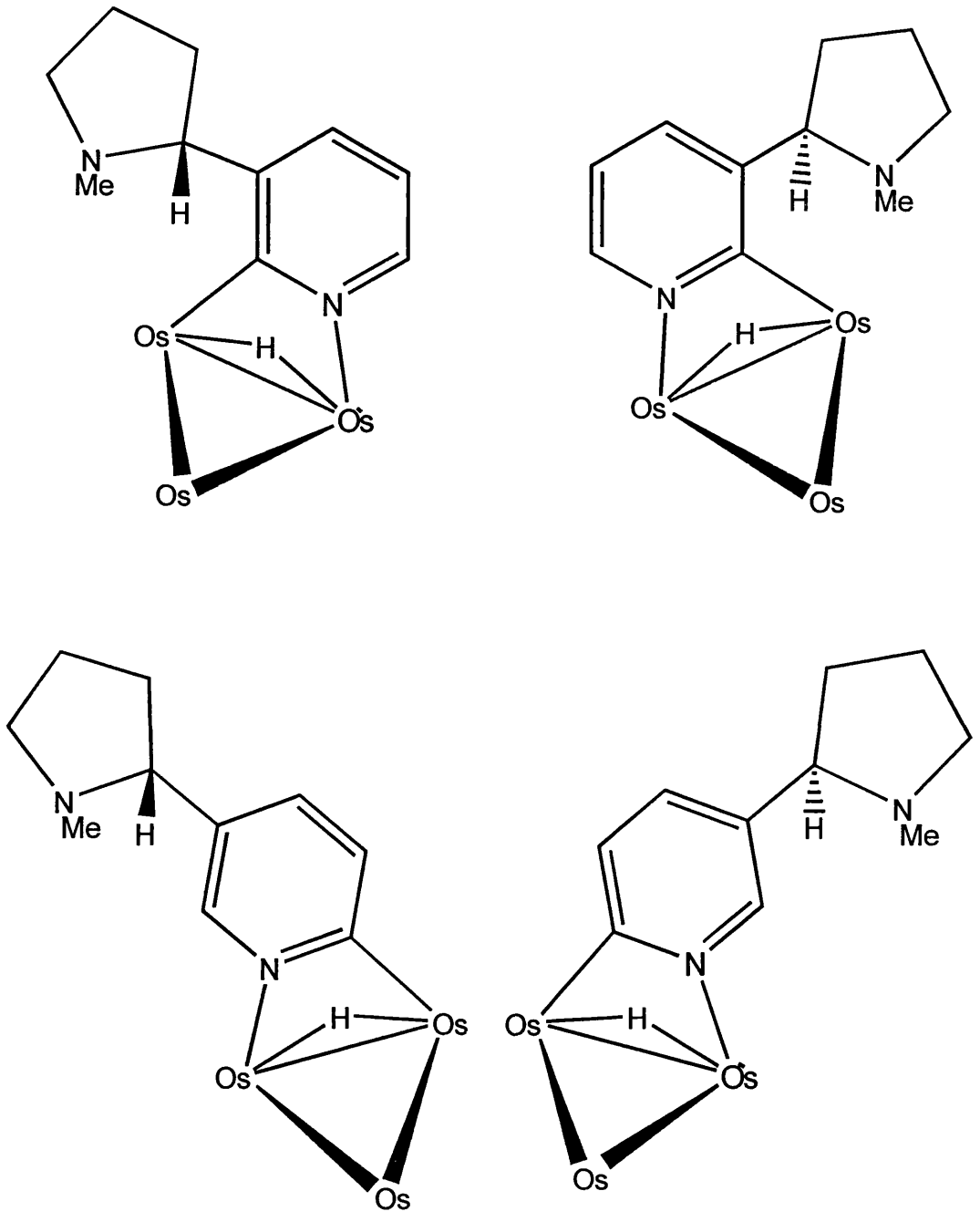

Initially our efforts to study the nicotinyl system were hampered by the difficulties surrounding the separation of the four isomeric forms (the two positional isomers each existing as a pair of diastereomers). The separation of pyridines and pyridyl derivatives is notoriously difficult, so much so that the separation of pyridines is used as the basis for the evaluation of HPLC columns by rival manufacturers.[130] However it has been pointed out that this may be the result of the exposed lone pair, which is of course, bound to the metal cluster in this case. One problematic feature of the HPLC of basic compounds is a characteristic tailing on HPLC columns. Even when separation was attained, significant tailing was experienced for two of the four isomers, indicating that there may be significantly different basicity for one of the positional isomers and its two diastereomers compared with the two diastereomers of the other positional isomer.

The cluster $[Os_3(\mu\text{-}H)(CO)_{10}(\mu\text{–nicotyl})]$ was synthesised some years ago by the reaction of $[Os_3(CO)_{10}(MeCN)_2]$ and (S)-nicotine, in our group.[131,132] The synthesis yields two positional isomers with two diastereomers for each of the positional isomers. Separation of the isomers was unsuccessfully attempted by TLC and column chromatography.[131] Whittacker achieved partial separations[132] using analytical HPLC but full separation and workable quantities were not achieved. We have now fully separated sufficient quantities, by semi-preparative HPLC followed by analytic HPLC, to characterise the four isomers by ^1H NMR and record clear CD spectra of all four species. This two-step separation process is necessary to get the high purity that is necessary for CD studies. In the first semi-preparative step the four isomer are separated into two pairs of isomers

which can than be handled with the higher resolution inherent to an analytical column (see Figure 5.6). We have been able to obtain essentially total separation of these four isomers of the cluster $[Os_3(\mu\text{-}H)(CO)_{10}(\mu\text{–nicotyl})]$ by these methods.

5.2.2 Separation and characterisation of the isomers of $[Os_3(\mu\text{–}H)(CO)_{10}\{(R)\text{–}NC_5H_3CH(OH)Me\text{–}4\}]$

Given the problems experienced in the separation of the nicotyl clusters, the cluster $[Os_3(\mu\text{-}H)(CO)_{10}\{(R)\text{-}NC_5H_3CH(OH)Me\text{-}4\}]$ was synthesised, yielding two diastereomeric forms. It had been hoped that the separation of these two diastereomers would be more tractable given the presence of the polar H–bonding hydroxyl groups. After evaluating a number of solvent systems, an essentially total separation of the two diastereomers was also achieved. Sufficient material was separated to allow ^1H NMR spectroscopy and for crystals to be grown. For one of the diastereomers, suitable crystals for a single crystal X-ray structure determination were obtained. The structure was needed to establish the relative configuration of the CH(OH)Me substituent at pyridine to that of Os_3(pyridyl) subgroup. Having established one absolute stereochemistry in this way, we expected to be able to establish all the others by comparison of the CD spectra. Interestingly the diastereomers were produced in the synthesis in a 1:1 ratio on the basis of integrated ^1H NMR hydride spectra. The IR spectra of the separated diastereomers in the 2000 cm^{-1} region are almost identical and indistinguishable from that of the unsubstituted pyridine derivative $[Os_3(\mu\text{-}H)(CO)_{10}(\mu\text{-}NC_5H_4)]$. The ^1H NMR spectrum of the initial unseparated mixture shows seven signals,

one for each proton environment as expected. The signals for the diastereomers are close and overlapping but are just resolved at 500 MHz. When we first recorded a ^{1}H NMR spectrum a distorted singlet was observed for the hydride ligands but, with careful shimming using the FID (**f**ree **i**nduction **d**ecay) area or field gradient shimming at 500 MHz we were able to observe two almost overlying singlets with matching patterns of ^{187}Os satellites (see Figure 5.4). This indicated that there is little chemical recognition between the CH(OH)Me substituent and the hydride ligand, which did not augur well for the usefulness of these materials in catalytic applications. In view of this, it was unsurprising that the TLC treatment gave only one band and that even with careful division of the band there was no enrichment of one isomer over another. However, as we have described above, HPLC was totally successful.

Figure 5.2 The two diastereomers of $[Os_3(\mu\text{-}H)(CO)_{10}\{(R)\text{-}NC_5H_3CH(OH)Me\text{-}4\}]$

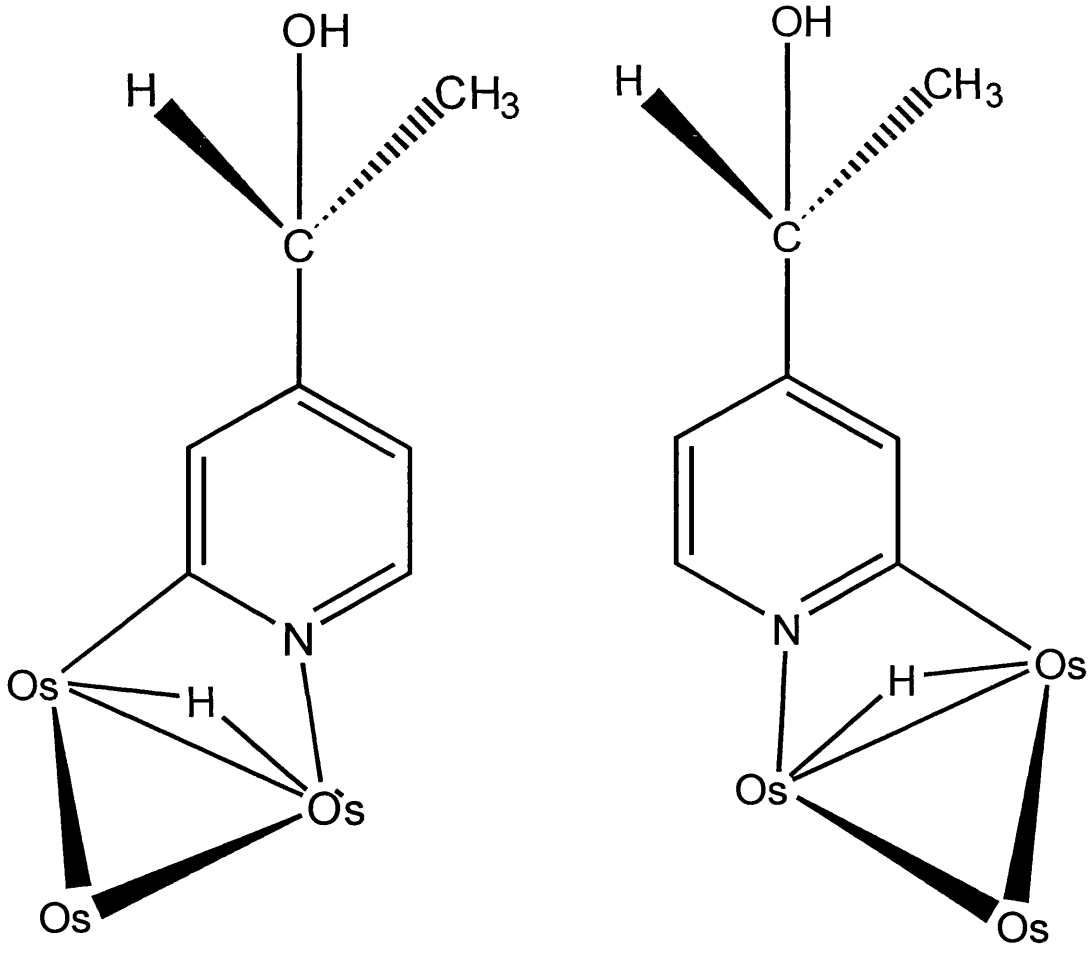

Figure 5.3 X-ray structure of $[Os_3(\mu\text{-}H)(CO)_{10}\{\mu\text{-}(R)\text{-}NC_5H_3CH(OH)Me\text{-}4\}]$ isomer **1B** with the hydride marked below the Os_3 plane. Note the considerable physical distance between the hydride ligand and the chiral carbon of the pyridyl ligand.

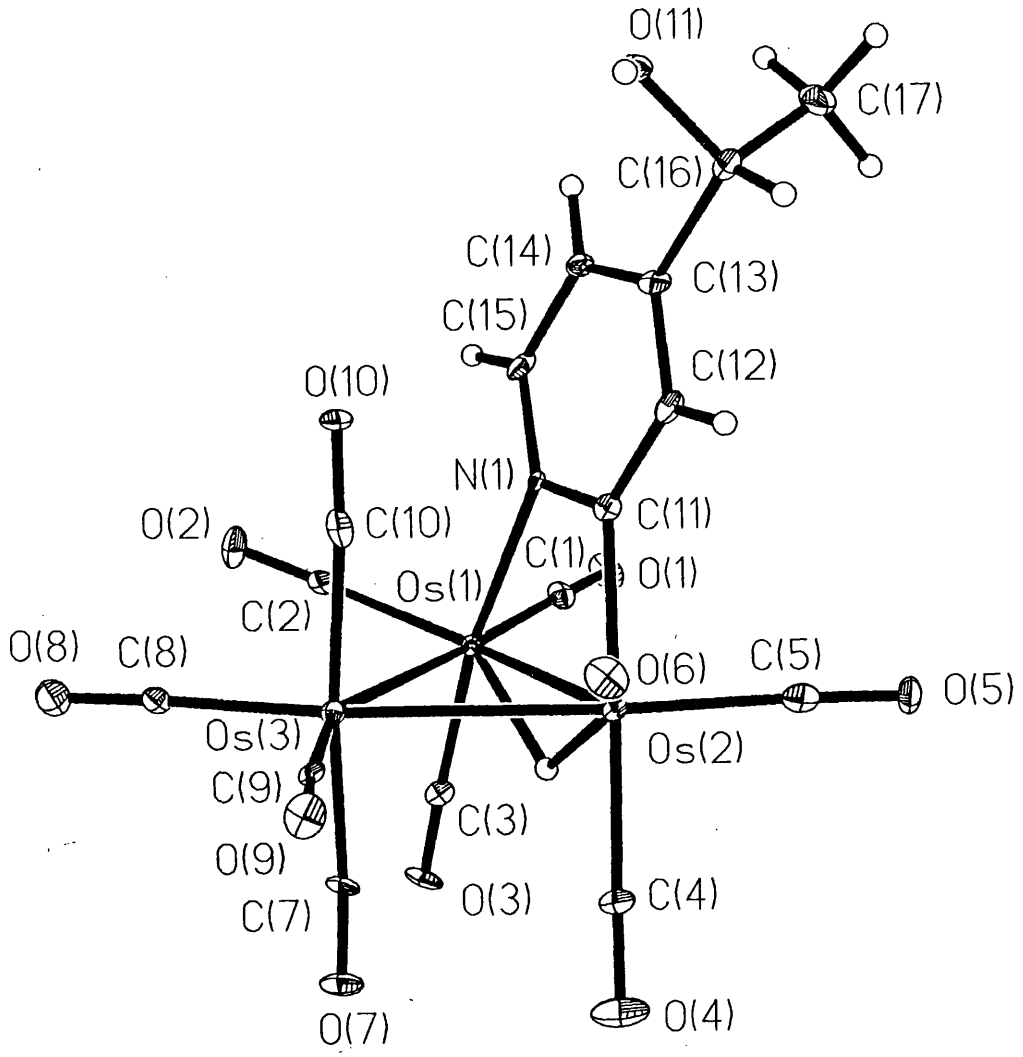

Table 1 Selected data for the X-ray structure of $[Os_3(\mu\text{-}H)(CO)_{10}\{\mu\text{-}(R)\text{-}NC_5H_3CH(OH)Me\text{-}4\}]$ carried out at King's College London by Dr. J. W. Steed.

crystal size (mm)	0.35 x 0.25 x 0.18
formula	$C_{19}H_9NO_{11}Os_3$
Fw	974
colour	yellow
crystal system	monoclinic
space group	C_2
Temp (K)	293(2)
a (Å)	21.9372(11)
b (Å)	11.7406(4)
c (Å)	9.1656(4)
β (deg)	93.680(3)
V (Å^3)	2355.8(8)
Z	4
d_{calc} (g cm^{-3})	2.814
μ(Mo Kα) (mm^{-1})	0.71070
F(000)	1784
2θ range (degrees)	2.23 to 27.49
no. independent reflections	5017
wR2 (all data)	0.0859
R1 [$I>2\sigma(I)$]	0.0847
goodness-of-fit on F^2	1.047
Data/parameters	5017/308
peak/hole eÅ^{-3}	1.344, -0.800

Figure 5.4 300 MHz ^{1}H (hydride region only) NMR of $[Os_3(\mu\text{-}H)(CO)_{10}\{\mu\text{-}(R)\text{-}NC_5H_3CH(OH)Me\text{-}4\}]$ showing the ^{187}Os satellites and the ^{13}CO satellites. The signals resulting from one of the two diastereomers are marked by •.

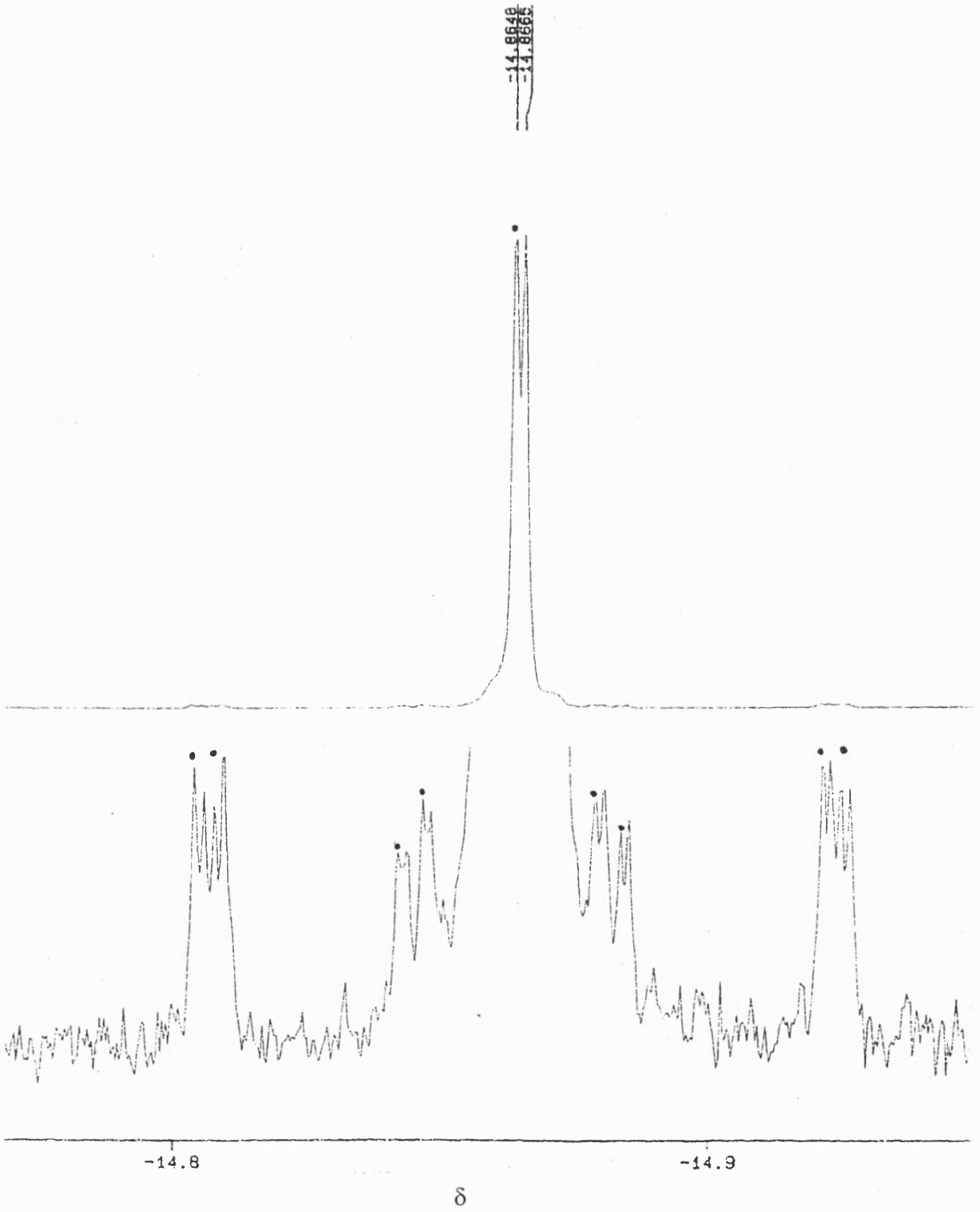

CD spectroscopy (see 5. 3) gave clear evidence of the effectiveness of the HPLC separation producing two almost perfect mirror image CD traces in the 230 – 450 nm range in which the Os_3 framework is the active chromaphore. These CD spectra confirm that the Os_3(μ–pyridyl) groups in the separated isomers have different configurations. The absolute structure of one isomer has been determined by X-ray crystallography. There were, however, problems with obtaining crystals of the appropriate size and quality for the determination from the small samples (5 mg) of each isomer available. Fortunately we did obtain small crystals suitable for the structural determination which was carried out on a CCD area detector diffractometer by Dr. J. W. Steed at King's College London. The small yellow crystals are of C_2 space group. The absolute configuration was determined using the Flack parameter. The result of the Flack determination is consistent with the absolute stereochemistry of the ligand as supplied by Aldrich. Hydride ligands are not often located by X-ray methods as they have low electron density by comparison with the heavy metal atoms, however, their positions can be estimated by using energy minimisation criteria. To this end the programme HYDEX was used to predict the location of the hydride which was found to be below the M_3 plane with the pyridyl bridging above it.

5.2.3 Reaction of $[Ru_3(CO)_{10}(MeCN)_2]$ with (R)-(+)-4-pyridylethanol

The cluster $[Ru_3(CO)_{10}(MeCN)_2]$ was reacted with (R)–1–(4–pyridyl)ethanol in refluxing dichloromethane for 30 minutes. After separation by TLC a single product was isolated in 70% yield as orange crystals which were spectroscopically characterised as the mixed diastereomers of $[Ru_3(\mu\text{-}H)(CO)_{10}\{(R)\text{-}$

$NC_5H_3CH(OH)Me\text{-}4\}]$. A carefully shimmed ^1H NMR spectrum revealed the presence of two singlets in the hydride region, one for each diastereomer. The FAB mass spectrum is consistent with the formulation given. Unsuccessful attempts were made to separate the diastereomers at IVIC in Venezuela both by TLC and HPLC.

5.2.4 Separation and characterisation of the (S)–nicotine derivatives of $[Os_3(CO)_{10}(MeCN)_2]$

The treatment of $[Os_3(CO)_{12}]$ with (S)-nicotine in refluxing octane for 30 minutes[132] gave the same mixture of four as we obtained by treating $[Os_3(CO)_{10}(MeCN)_2]$ with (S)-nicotine in refluxing dichloromethane.

Subsequent to the separation of the diastereomeric forms of $[Os_3(\mu\text{–}H)(CO)_{10}\{(R)\text{–}NC_5H_4CH(OH)Me\text{–}4\}]$ **1**, a further attempt to separate the $[Os_3(\mu\text{-}H)(CO)_{10}(nicotyl)]$ isomers **2A to 2D** was made. Similar chromatographic conditions proved, after some optimisation, to be effective and it was possible to scale to a semi-preparative scale. However fully preparative–scale HPLC did not prove effective at separating the four isomeric forms; instead isomers **2A** + **2B** could be separated from **2C** + **2D** which could then be handled individually under optimal conditions at a semi-preparative scale. That is to say the positional isomers were separated before the diastereomers. Strong tailing limited the loading of the columns we could use. However by careful control of the conditions, we were able to achieve greater than 95% isomeric purities after separation.

In spite of extensive shimming efforts two of the four observed hydride signals (figure 5.7) remained broad. These signals are also possibly broadened by quadrupolar interactions with the nitrogen ligand atoms causing a faster relaxation pathway. However, there is no direct evidence for this. The hydride singlets were found at δ –14.388, -14.474, -14.833 and –14.840 in an approximate ratio of 2:2:3:3. The two positional isomers are a result of metalled at the 2-position or metallation at the 6-position. The ^{1}H NMR hydride signals (Figure 5.7), allow a comparison to be made between the mixture and the separated products. On the basis of the HLPC fractions collected, the signals at δ -14.388 and -14.474 correspond to isomers **2C** and **2D** metallate at the 2–position of the pyridine ring. The signals δ - 14.833 and – 14.840 correspond to isomer **2A** and **2B,** which are metalled at the 6–position. It is significant that there is a larger chemical shift difference between isomers **2C** and **2D** ($\Delta\delta$ = 0.086) where the pyridine ring is closer to the Os_3. When the pyridyl ring is further away (**2A** and **2B**), the shift difference is smaller ($\Delta\delta$ = 0.007). However, anomalously, the small chemical shift difference is reflected in larger HPLC separations of **2C** and **2D** as opposed to **2A** and **2B,** which are relatively close together on the HPLC trace.

Figure 5.5 Circular Dichroism spectra for $[Os_3(\mu\text{-}H)(CO)_{10}\{\mu\text{-}(R)\text{-}NC_5H_3CH(OH)Me\text{-}4\}]$ (a) and for $[Os_3(\mu\text{-}H)(CO)_{10}\{\mu\text{-}(S)\text{-nicotyl}\}]$ (b) recorded at concentrations of 0.075 mg cm^{-1} in CH_2Cl_2.

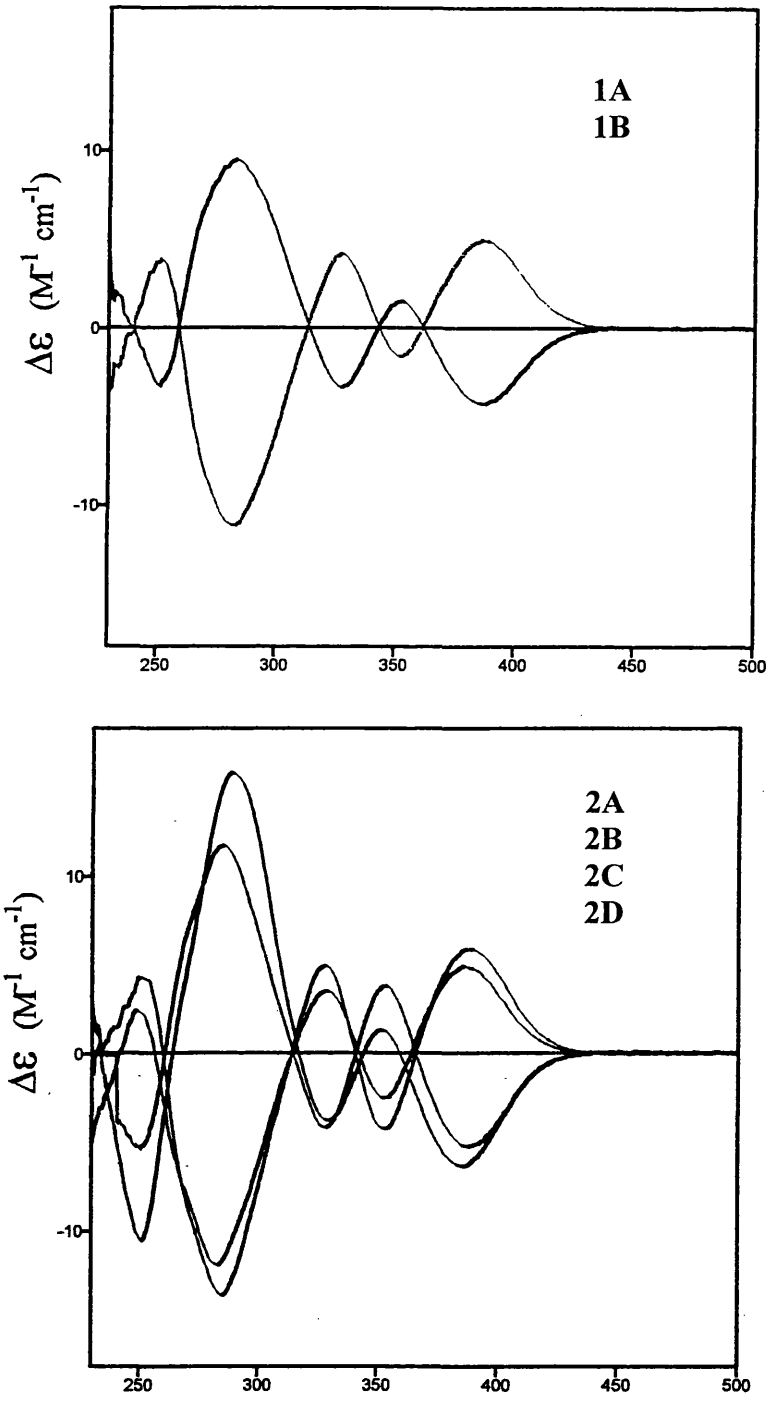

Figure 5.6 HPLC traces form the separation of $[Os_3(\mu\text{-}H)(CO)_{10}\{\mu\text{-}(S)\text{-nicotyl}\}]$ the isomers are marked with the same labelling scheme as in the text.

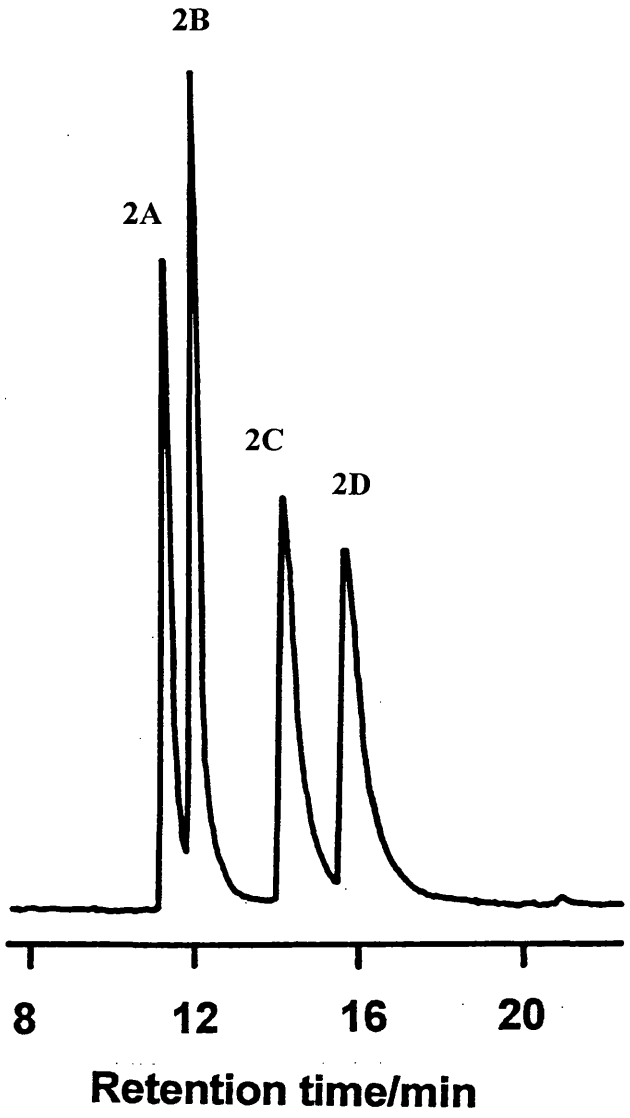

Figure 5.7 ^{1}H hydride region for the four $[Os_3(\mu\text{-}H)(CO)_{10}\{\mu\text{-}(S)\text{-nicotyl}\}]$ isomers separated 2A-D and the mixture is shown below. The two segments are shown at different horizontal expansions.

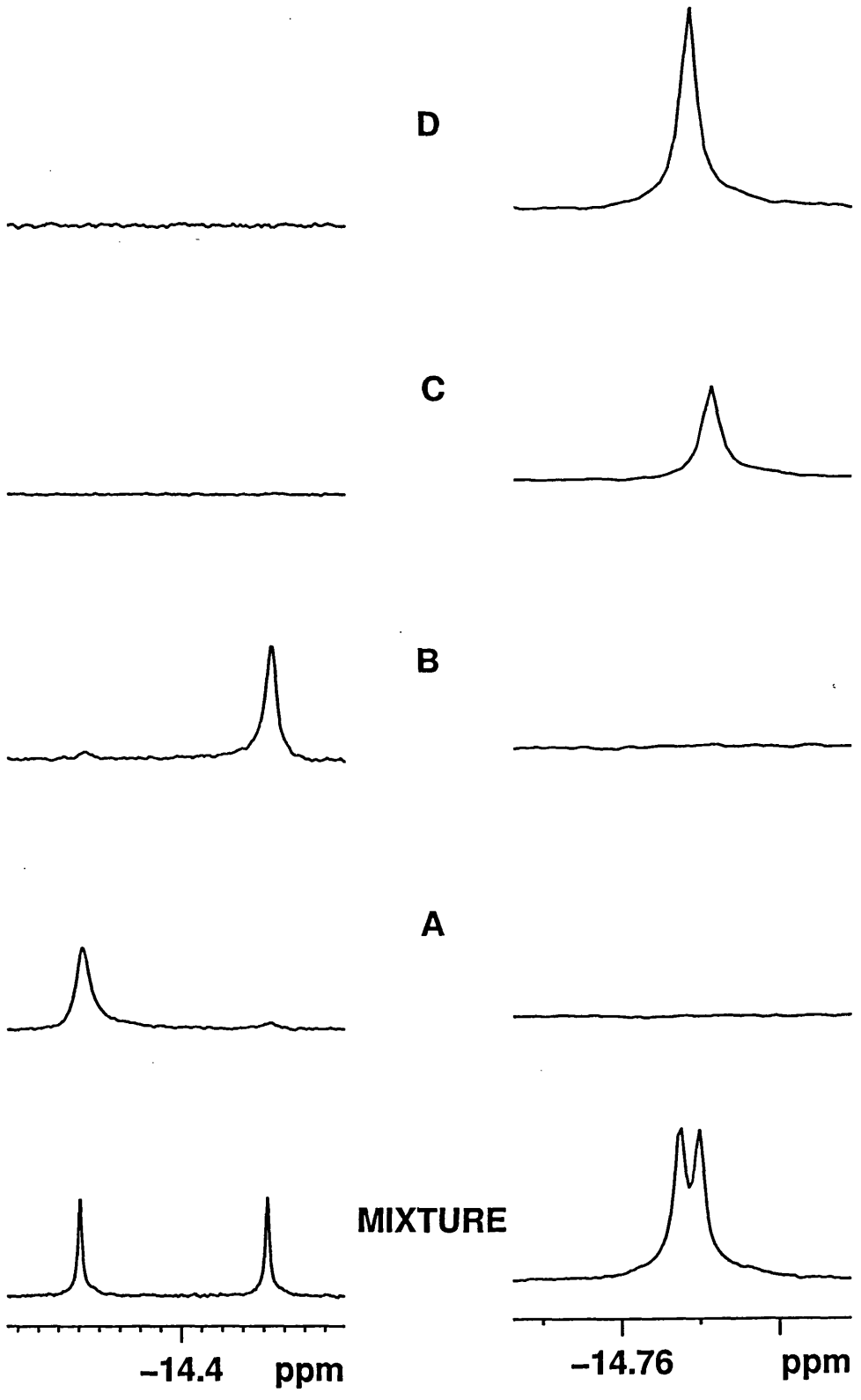

5.3 Conclusions

The following objectives were achieved:-

The diastereomers of the triosmium and triruthenium clusters derived from the chiral pyridine (R)-1-(4-pyridyl)ethanol were prepared and the Os cluster successfully separated.

The known diastereomers and positional isomers produced by the reaction of triosmium(s)-nicotine and $[Os_3(CO)_{10}(MeCN)_2]$ were re-prepared.

The four diastereomers and positional isomers of $[Os_3(\mu\text{-}H)(CO)_{10}(\mu\text{–nicotyl})]$ were separated by HPLC.

A diastereomer of $[Os_3(\mu\text{-}H)(CO)_{10}(C_5H_3NCHOHMe)$ was characterised by X-ray diffraction.

All the enantiomers produced in this work were characterised by CD spectroscopy and by the combined use of the CD and X–ray data, the absolute configurations of all the diastereomers were determined.

5.4 Experimental

The cluster $[Os_3(CO)_{12}]$ was prepared by published methods.[133] The cluster $[Ru_3(CO)_{12}]$ was purchased from Strem and used without further purification. The bisacetonitrile derivatives were prepared by published methods.[134,135] S(-)-Nicotine and the (R)-1-(4-pydridyl)ethanol were purchased from Aldrich and used without further purification. NMR spectra were acquired on a Bruker AC300 spectrometer and processed using XWIN-NMR and XWIN-PLOT and on a Bruker DRX500 spectrometer. FAB mass spectra were acquired on a ZAB instrument (MNBA matrix). IR spectra were recorded on a Nicolet 280 FT-IR spectrometer. Solvents were dried and distilled by standard methods prior to use.

5.4.1 Preparation of $[Ru_3(\mu\text{-}H)(CO)_{10}\{(R)\text{–}NC_5H_3CH(OH)Me\text{–}4\}]$

Equimolar quantities of $[Ru_3(CO)_{10}(MeCN)_2]$ (0.105 g) and (R)-1-(4-pyridyl) ethanol (0.028 g) in CH_2Cl_2 solution were refluxed under nitrogen for 30 minutes. The solvent was removed under reduced pressure to give an orange residue which was loaded on to a silica TLC plate (2 mm Merck 1045, eluent: dichloromethane/n-hexane, 3:7 by volume). One orange band was recovered which gave orange crystals. IR (ν/cm^{-1}, cyclohexane): 2098m, 2060vs, 2049vs, 2022s, 2013s, 1997m. FABMS: observed centre of the highest mass isotopic envelope is 680, calculated for the parent molecular ion is 708. The highest mass ion observed was the nonacarbonyl.

5.4.2 Preparation of $[Os_3(\mu\text{-}H)(CO)_{10}\{(R)\text{–}NC_5H_3CH(OH)Me\text{–}4\}]$

Equimolar quantities of $[Os_3(CO)_{10}(MeCN)_2]$ (0.130 g) and (R)-1-(4-pyridyl)ethanol (0.028 g) in CH_2Cl_2 solution were refluxed for 1 hour under nitrogen. The solvent was removed under reduced pressure and the yellow residue was loaded on to a silica TLC plate (2 mm Merck 1045) eluting with a solvent mixture of CH_2Cl_2/n-hexane (3:7 by volume). One yellow band was recovered. IR (ν/cm^{-1}, cyclohexane): 2104w, 2063vs, 2053s, 2022s, 2010s, 2003m, 1990m, 1975vw. FABMS: observed centre of the isotopic envelope 974, calculated for the parent molecular ion 974 (based on ^{192}Os). Analytical data: found C, 21.0; H, 0.8; N, 1.4%. Calculated for $Os_3C_{17}H_9NO_{11}$: C, 21.9; H, 1.0; N, 1.4%.

5.4.3 HPLC separation of the diastereomers of $[Os_3(\mu\text{-}H)(CO)_{10}\{(R)\text{-}NC_5H_3CH(OH)Me\text{-}4\}]$.

The yellow band from the TLC separation was dissolved in CH_2Cl_2 (50 mg/cm^3). A 5 μm mesh silica analytical column (length, 20 cm id, 0.5 cm) was used to determine separation parameters. A number of solvent mixtures were tried and the best separation was found using an isocratic 2.5 % propan-2-ol / 97.5 % n-hexane mixture at a flow rate of 0.7 cm^3/min with an injection volume of 5 μL. Excellent resolution was achieved. On scaling up, an identical isocratic solvent blend was used with a 5 μm mesh silica semi-preparative column (length, 20 cm; id, 1 cm). Excellent resolution (better than 95%) was achieved with injection volumes of 150 μL and an eluent flow rate of 4 cm^3/min.

5.4.4 Preparation of $[Os_3(\mu\text{-}H)(CO)_{10}\{(S)\text{-nicotyl}\}]$

Equimolar quantities of $[Os_3(CO)_{10}(MeCN)_2]$ (0.100 g) and (S)-nicotine (0.010 cm^3) were dissolved in 25 cm^3 of dichloromethane and the solution refluxed for 2 hours under nitrogen. The solvent was removed under reduced pressure and the yellow residue was loaded onto a silica TLC plate (2 mm Merck 1045), eluting with a solvent mixture of dichloromethane/n-hexane (3:7 by volume). One broad yellow band was recovered yielding a mixture of the four isomers 2A-2D. IR (ν/cm^{-1}, cyclohexane): 2082m, 2048s, 2029s, 2001s, 1993sh, 1986w, 1976s, 1960m. FABMS: observed centre of the isotopic envelope 975, calculated for the parent molecular ion 975 based on ^{192}Os. Analytical data: found C, 23.5; H, 1.55; N, 2.7%, calculated for $Os_3C_{17}H_9NO_{11}$: C, 23.7; H, 1.5; N, 2.7%.

5.4.5 HPLC separation of the diastereomers of $[Os_3(\mu\text{-}H)(CO)_{10}(S)\text{-nicotyl})]$.

The mixture from the TLC separation was dissolved in CH_2Cl_2 (50 mg/cm^3). A 5 μm mesh silica analytical column (length, 20 cm; id, 0.5 cm) was used to determine separation parameters. A number of solvent mixtures were tried. The best separation was found using an isocratic 3% propan-2-ol / 97% n-hexane mixture at a flow rate of 1cm^3/min with an injection volume of 10 μL. Excellent resolution was achieved. On scaling up, an identical isocratic solvent blend was used with a 5 μm mesh silica semi-preparative column (length, 20 cm; id, 1 cm). Fair resolution was achieved with injection volumes of 75 μL. This separation was scaled up to a fully preparative scale separation, using isocratic 3 % propan-2-ol / 97 % n-hexane at a flow rate of 14 cm^3/min with an injection volume of 500 μL. This method allowed a total separation of (**2A** + **2B**) from (**2C**

+ **2D**). These two mixtures were then further separated on semi-preparative scale (conditions above) to yield the four separated isomers (> 95% purity).

5.4.6 X-ray structure determination

This work was carried out by Dr. J. W. Steed, King's College London, using an area detector diffractometer to carry out the structural determination. Yellow crystals of **1A** were grown by cooling a mixed dichloromethane–hexane solution. A suitable crystal was mounted in an oil droplet which solidified at 100(2) K, the temperature at which the structure was determined. The crystal was indexed and the collected using Nonius 'Collect' software.[136] The data were integrated and merged and a Lorentz and polarization effect correction was applied using DENZO-SMN and Scalepack.[137] The structure was solved using direct methods (SHELXS-97).[138] All non-hydrogen atoms were refined anisotropically, while hydrogen atoms were included in calculated positions and allowed to ride on the atoms to which they were attached. Hydrogen atom thermal parameters were not refined directly. Instead those of the parent atom were superimposed on them. Some poorly defined solvent peaks were located and these are tentatively attributed to hexane.

Table 3 Selected bond lengths (Å)and angles (°) for the structure of $[Os_3(\mu\text{-}H)(CO)_{10}\{(R)\text{-}NC_5H_3CH(OH)Me\text{-}4\}]$ shown in Figure 5.3

Os(1)-Os(2)	2.9049(8)	Os(2)-C(4)	1.968(12)
Os(1)-Os(3)	2.8680(10)	Os(2)-C(5)	1.921(14)
Os(2)-Os(3)	2.8882(7)	Os(2)-C(6)	1.913(12)
Os(1)-N(1)	2.147(11)	Os(3)-C(7)	1.944(11)
Os(2)-C(11)	2.122(11)	Os(3)-C(8)	1.927(12)
Os(1)-C(1)	1.932(12)	Os(3)-C(9)	1.904(13)
Os(1)-C(2)	1.901(12)	Os(3)-C(10)	1.955(14)
Os(1)-C(3)	1.902(12)		

Os(1)-Os(2)-C(11)	68.3(3)
Os(3)-Os(2)-C(11)	88.3(3)
Os(2)-Os(1)-N(1)	68.5(2)
Os(3)-Os(1)-N(1)	88.2(2)
Os(1)-N(1)-C(11)	110.3(7)
Os(1)-N(1)-C(15)	126.9(8)
Os(2)-C(11)-N(1)	112.7(8)
Os(2)-C(11)-C(12)	128.4(8)

5.4.7 NMR data tables 500 MHz ^{1}H NMR data for the diastereomers 1A and 1B $[Os_3(\mu\text{-}H)(CO)_{10}\{(R)\text{-}NC_5H_3CH(OH)Me\text{-}4\}]$ in $CDCl_3$.

Compound	OsH	H^2	H^4	H^3	CH	CH_3
1A	-14.837(s)	7.280(d) (2.0)	6.707(dd) (5.8,2.0)	8.052(d) (5.8)	4.700(dq) (6.5,2.6)	1.403(d) (6.5)
1B	-14.834(s)	7.302(d) (2.0)	6.682(dd) (5.8,2.0)	8.046(d) (5.8)	4.704(dq) (6.5,2.7)	1.411(d) (6.5)

The J values shown in parentheses are number with the Os-C carbon as C^1.

The free ligand shows the following signals δ 8.48 (complex multiplet H^2 andH^6), 7.30 (complex multiplet H^3 andH^5), 4.89 (q, J = 6.6 CH), 3.35 (broad, OH), 1.49 (d, CH_3, J = 6.6)

Chapter 6 Study of hydride migrations and exchange within various hydrido cluster systems

6.1 Introduction

Interest has always been strong in the properties of unsaturated triosmium clusters, particularly those of the cluster $[Os_3(\mu\text{-}H)_2(CO)_{10}]$ which is one of the most reactive stable clusters. Of the order of a hundred papers have explored the reactivity of this cluster. The original synthesis of $[Os_3(\mu\text{-}H)_2(CO)_{10}]$ was reported some time ago.[139] Its crystal structure has been determined[148] and interestingly the data shows that it does not have precise C_{2v} symmetry since there are some differences in Os–H bond distances. Whether this is reflected in the solution structure was only resolved recently.[140] Clearly if there were two different hydride environments, two slightly different sets of signals would be seen from the partially deuterated adduct. T_1 measurements have also established the H-D distance.[140]

The principle purpose of our investigations into the reactivity of $[Os_3(\mu\text{-}H)_2(CO)_{10}]$ has been to study migration reactions with unsaturated systems, and to compare behaviour with that of BINAP–substituted clusters. Various substituted forms of $[Os_3(\mu\text{-}H)_2(CO)_{10}]$ have been shown to have reactivity with alkenes showing specifically either α or β eliminations or both. In reactions with alkenes, reversible insertion would lead to hydrido–alkyl intermediates which may also be obtained from diazoalkanes.

For example, the reaction of $[Os_3(\mu\text{–}H)_2(CO)_{10}]$ with CH_3CHN_2 gives $[Os_3(\mu\text{–}H)(CH_2CH_3)(CO)_{10}]$[141] which readily undergoes β–elimination. This

would lead to $[Os_3(\mu\text{–}H)_2(CH_2{=}CH_2)(CO)_{10}]$ but this readily loses C_2H_4 and regenerates $[Os_3(\mu\text{–}H)_2(CO)_{10}]$.[155] So effectively the dihydride cluster catalyses the conversion of CH_3CHN_2 to dinitrogen and ethene.

$[Os_3(\mu\text{-}D)_2(CO)_{10}]$ is prepared by standard methods except that deuterium is used in place of hydrogen gas.[142] $[Os_3(\mu\text{-}D)_2(CO)_{10}]$ reacts with a range of alkenes to form $[Os_3(\mu\text{-}H)_2(CO)_{10}]$ and the deuterated alkene (by ^2H NMR spectroscopy).[143] However, stable alkyl cluster are not formed in stark contrast to the situation with the insertion of C_2H_2 (and other alkynes) into $[Os_3(\mu\text{-}H)_2(CO)_{10}]$ which leads to stable vinyl complexes.

Addition of a two–electron donor monodentate ligand L (L = CO, MeCN, PPh_3, PMe_2Ph, $AsMe_2Ph$) to $[Os_3(\mu\text{-}H)_2(CO)_{10}]$ leads to the stable adducts $[Os_3(\mu\text{–}H)(H)(CO)_{10}L]$ which shows considerable reactivity. These complexes $[Os_3(\mu\text{–}H)(H)(CO)_{10}L]$ contain bridging and terminal hydride ligands which are in rapid exchange. There are difficulties associated with exploring the exchange mechanism fully by dynamic NMR methods, as the samples tend to be thermally sensitive (i.e. *ortho*metallation and other reactions at higher temperatures) and giving very broad signals at room temperature. However this has not prevented studies at lower temperatures (-60 °C) which clearly show two well-defined hydride signals that, in chemical shift, correspond with two terminal and bridging hydride positions.[144] This has been confirmed by IR observations on both $[Os_3(\mu\text{–}H)_2(CO)_{11}]$ and $[Os_3(\mu\text{–}D)_2(CO)_{11}]$. $[Os_3(\mu\text{–}H)_2(CO)_{10}]$ shows bands at 1930 and 1525 cm^{-1} in the solid state IR spectrum, shifting to 1410 and 1110 cm^{-1} for the deuterated analogue. Shapley[144] assigns the higher frequency band to the

terminal Os-H(D) and the lower frequency band to the bridging Os-H(D)-Os entity. Shapley further speculates that there is an intermediate state between the known structures of $[Os_3(\mu\text{–}H)_2(CO)_{10}]$ and $[Os_3(\mu\text{–}H)_2(CO)_{11}]$ with both H ligands bound to one osmium. There, is however, no direct evidence presented for this intermediate state.

Brown and Evans[145] reported that the treatment of $[Os_3(\mu\text{-}H)_2(CO)_9(PPh_3)]$ with acetylene provides two isomers of $[Os_3(\mu\text{-}H)(\mu\text{-}\eta^2\text{-}CH{=}CH_2)(CO)_9(PPh_3)]$. Shapley[146] has produced X-ray structures of both of these isomeric clusters. The major isomer has the hydride ligand bridging the same cluster edge as the vinyl ligand with the vinyl forming a σ-bond to Os(1) and a π-bond to Os(2) which also bears the PPh_3 ligand. The minor isomer has the vinyl forming a σ-bond to Os(1) and a π-bond to Os(2) with the PPh_3 bound to the Os(3). In this case the hydride is between the π-bonded and the PPh_3–bound osmium centres. Interestingly the two isomers slowly interconvert with a half life of 85 minutes. ^{13}C spin–saturation–transfer experiments on enriched samples supported the view that there was π/σ bond interchange in the bridging vinyl groups and that the solid state structures were indeed the same as the solution structures.[144]

The related cluster $[Os_3(\mu\text{-}H)(\mu\text{-}OH)(CO)_{10}]$[147] was reported before that of the dihydride $[Os_3(\mu\text{-}H)_2(CO)_{10}]$ and its structure has been determined.[83] Both the H and OH ligands bridge the same edge of the cluster. The Os-Os distance between the osmium atoms bearing the bridged ligands is 2.8061(5) Å, considerably longer than the distance between the bridged metal atoms in $[Os_3(\mu\text{-}H)_2(CO)_{10}]$ [2.681

(1) Å].[148] The metal–metal bond lengths in $[Ru_3(\mu\text{-}OH)_2(CO)_8\{\mu\text{-}(R)\text{-}BINAP\}]$[109] are 3.023(2) Å for the bridged edge as opposed to 2.812(2) Å for the other edges, while the length of the bridged edge in $[Os_3(\mu\text{–}H)_2(CO)_8\{\mu\text{–}dppm\}]$ is 2.675(9) as opposed to 2.812(10) for the unbridged face. This demonstrates that the effect of bridging hydrides is to shorten the metal–metal bond length while the effect of bridging hydroxides is to elongate the bond so $[Os_3(\mu\text{-}H)(\mu\text{-}OH)(CO)_{10}]$, the bridges having an essentially neutral effect on bridged Os....Os distance. Another view is that $[Os_3(\mu\text{–}H)_2(CO)_{10}]$, $[Os_3(\mu\text{–}OH)(\mu\text{–}H)(CO)_{10}]$ and $[Os_3(\mu\text{–}OH)_2(CO)_{10}]$ are 46, 48 and 50 valence electron systems and hence will support four, three and two Os–Os bonds respectively.

Catalytic hydrogenations of diethyl fumarate and ethyl acrylate by $[Os(\mu\text{-}H)_2(CO)_{10}]$ are observed under very similar conditions, however, the number of catalytic cycles is limited by side reaction which consume the catalyst. The reaction of 100 equivalents of 1-hexene with H_2 under pressure catalysed by $[Os_3(\mu\text{-}H)_2(CO)_{10}]$ leads to 31 equivalents of hexane and 69 equivalents of internal hexenes with full recovery of all the catalyst (see Figure 6.1).[155]

Figure 6.1 Scheme showing the interaction of $[Os_3(\mu\text{-}H)_2(CO)_{10}]$ with alkenes reproduced from reference 155.

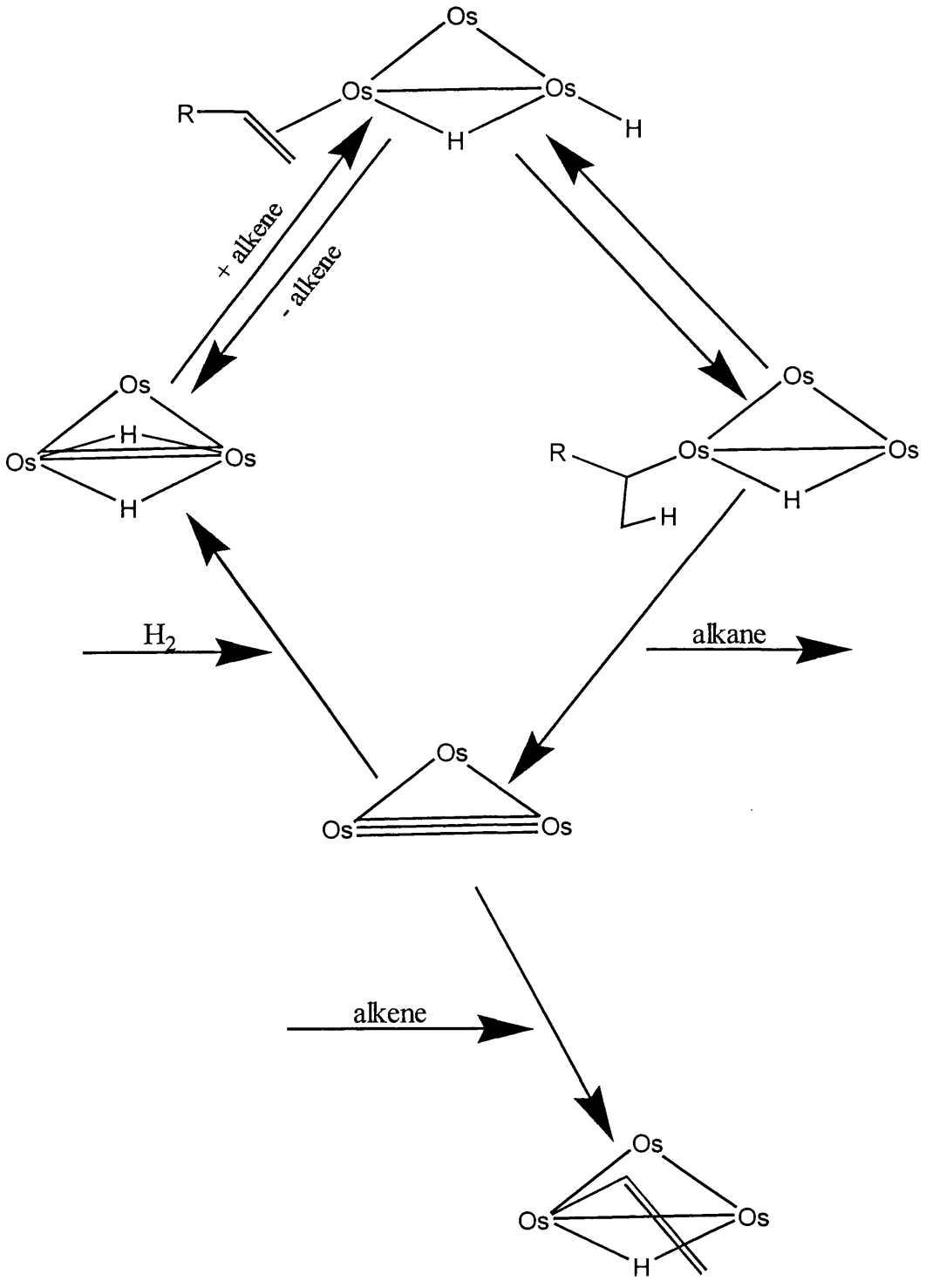

The clusters $[Os_3H_2(CO)_{10}L]$ where L = PPh_3, $P(Pr^i_3)$ and $POPh^i_3$ have been studied extensively.[149] It has been shown by ^{13}C NMR spectroscopy that the exchange of the two hydride ligands is also accompanied by the exchange of two carbonyl ligands. The clusters in the series $[Os_3H_2(CO)_{10}L]$ are easily formed by adding L to $[Os_3(\mu\text{–}H)(CO)_{10}]$. A solid state X-ray structure has been carried out for $[Os_3H_2(CO)_{10}(PPh_3)]$ including direct location of the hydride ligands.[150] It has been proposed that $[Os_3(\mu\text{-}H)(H)(CO)_{11}]$ is an intermediate in the conversion of $[Os_3(CO)_{12}]$ to $[Os_3(\mu\text{-}H)_2(CO)_{10}]$ on reaction with H_2 and it was further suggested that the transition state for hydride exchange (in which both hydrides are equivalent) between might be on the reaction path for activation of dihydrogen. Because of this background, the barrier to the bridge–terminal exchange was investigated for a number of substituted clusters $[Os_3(\mu\text{-}H)_2(CO)_{10}]$. It was found that the activation energy for the bridge–terminal hydrogen exchange increased with the cone angle of the ligand L.[151] It was also found that the more basic ligands of similar cone angle produced the lower activation energy. This, however, could not be generalised to different rows in the periodic table. Shapley therefore concluded that the value of the free energy of activation decreases as the polarizability of the donor atom of L increases and increases as the size of L increases. Pearson and Kresge also noted analogous effects for iridium.[152] Lau and his co-workers[153] reported similar results for a series of one pot autoclave reactions. However, unusually they chose to add the ligand to the cluster $[Os_3(\mu\text{-}H)_2(CO)_{10}]$ or to $[Os_3(CO)_{12}]$ *in situ* and then simultaneously react the product with the unsaturated substrates under hydrogen. The effects were found to be strongly pressure dependent and the overall findings with regards to basicity

appear to correspond to those of Shapley. However some caution should be exercised as the 'catalytic' species were never isolated but these were considered to be a complex mixture. Also there were no precautions taken against heterogeneous catalysis (i.e. mercury metal present as a control experiment to form an amalgam with any traces of metal). High hydrogen pressures were used (45 atm.), and the suspicion must be that, if the catalytic effect is real, some transient species was formed at these pressures, possibly one of the known species discussed before.

The reactions of alkenes with $[Os_3(\mu\text{–}H)_2(CO)_{10}]$, whether leading to alkene isomerisation, alkene hydrogenation or H/D exchange, all involve intermediates of the type $[Os_3H(alkyl)(CO)_{10}]$ and crucial work on the simplest example $[Os_3(\mu\text{–}H)(\mu\text{–}CH_3)(CO)_{10}]$, has been carried out. ^1H and ^{13}C NMR spectroscopy and associated T_1 relaxation studies were undertaken to investigate the solution structures of the tautomeric complexes $[Os_3(\mu\text{–}H)(\mu\text{–}CH_3)(CO)_{10}]$ and $[Os_3(\mu\text{–}H)_2(\mu\text{–}CH_2)(CO)_{10}]$.[154] These are derived from the reaction of $[Os_3(\mu\text{-}H)_2(CO)_{10}]$ with diazomethane. The cluster $[Os_3(\mu\text{-}H)_2(\mu\text{-}CH_2)(CO)_{10}]$ has had its structure determined by X-ray and neutron diffraction studies which establish that one hydride bridges the same edge as the methylene ligand and the other hydride bridges an adjacent edge. In the absence of any X-ray data, the methyl compound was assigned a related structure. The structure (see Figure 6.3) established on the basis of the NMR evidence is now accepted.

Figure 6.2 (a) A proposed structure of $[Os_3(\mu\text{-}H)(\mu\text{-}CH_3)(CO)_{10}]$[98] (b) the now accepted structure based on NMR studies (see reference 154).

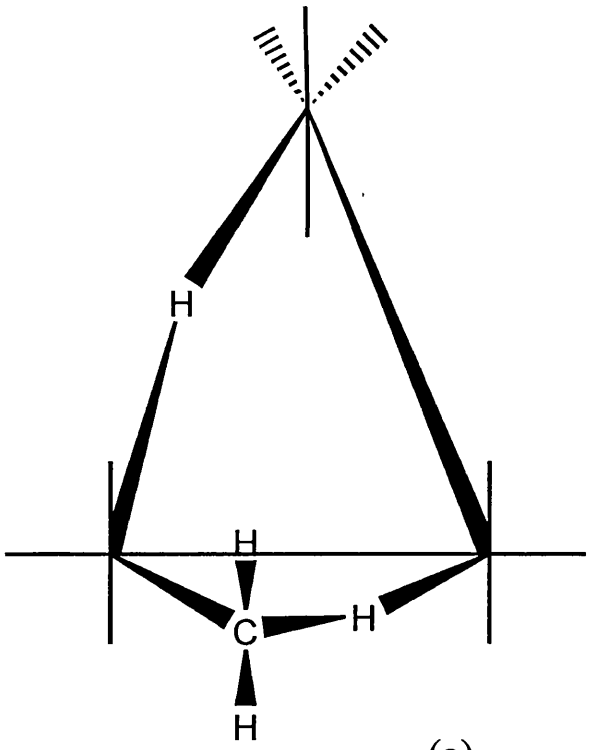

(a)

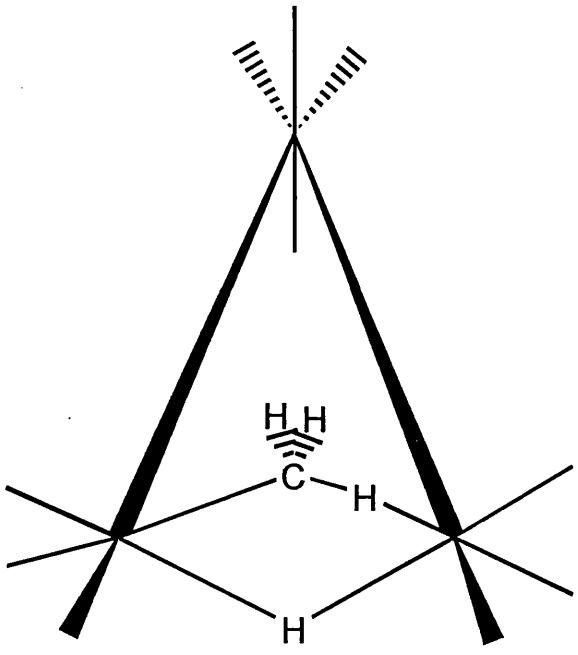

(b)

6.2 Objectives

The objectives of the work carried out in this chapter were:

a) To reproduce the basic know chemistry of the parent dihydride $[Os_3(\mu\text{-}H)_2(CO)_{10}]$ with a number of reagents specifically acetylene and trifluoroacetic acid.

b) To investigate the reaction of the parent dihydride $[Os_3(\mu\text{-}H)_2(CO)_{10}]$ with styrene–d^8 leading to H/D exchange.

c) To investigate possible mechanisms for the reaction with trifluoroacetic acid by monitoring ^1H NMR spectra over a period of time.

d) In light of the above, to evaluate the reactivity of the clusters synthesised in Chapter 4 of the general form $[Os_3(\mu\text{-}H)_2(CO)_{10-x}L_x]$ (where x = 0 or 2).

6.3 Reaction of $[Os_3(\mu\text{-}H)_2(CO)_{10}]$ with styrene-d^8

Shapley alludes to a reaction between styrene and $[Os_3(\mu\text{-}H)$ (alkyl)] $(CO)_{10}]$ but gives no details save that it appears to go to 80% of completion and that the product is $[Os_3(\mu\text{-}H)(\mu\text{–}CH{=}CHPh)(CO)_{10}]$.[155] We have investigated in this work the reaction of styrene–d^8 with $[Os_3(\mu\text{-}H)_2(CO)_{10}]$ in order to get some understanding of the mechanism(s) of reversible insertion. A tenfold excess of styrene–d^8 was added to a solution of $[Os_3(\mu\text{–}H)_2(CO)_{10}]$ in CD_2Cl_2 in an NMR tube and the reaction was monitored by ^1H NMR spectroscopy.

6.3.1 Study of exchange by ^1H NMR spectroscopy

The reaction was followed over time and no net reaction other than the H/D exchange between the metal hydrides and the D atoms on the styrene was observed. It was clear by inspection of the ^1H NMR spectra (see Figure 6.4) that initial ^1H transfer from the metal cluster was occurring predominantly at the vinyl CH_2 site of the styrene in the early stages of the reaction, followed by subsequent exchange at the vinyl CH position. Exchange into the two non-equivalent CH_2 sites occurred equally. It seemed probable from these results H–transfer into the CH_2 site was kinetically controlled but that slower process led to exchange at the CH site so that after a long period there was a statistical distribution of H and D over the $CHCH_2$ group and the metal hydride sites. There is no evidence of any incorporation of ^1H into the ring of the styrene–d^8 even after extended reaction times.

6.3.2 Discussions of the mechanisms of H/D exchange between $[Os_3(\mu\text{–}H)_2(CO)_{10}]$ and styrene–d^8

In view of the inability of $[Os_3(\mu\text{-}H)_2(CO)_{10}]$ to catalyse the addition of hydrogen to internal hexenes,[155] it is unsurprising that it does not promote H/D migration into the cyclic part of styrene. We believe that this would require orthometallation at an intermediate phenylethyl complex but there is no evidence that this reaction occurs. The results may be interpreted in terms of styrene insertion into M–H bonds, together with α– and then β-elimination (see Figure 6.4). If insertion and β-elimination were the dominant processes, then H would be largely incorporated at the α position to give $PhCH{=}CD_2$. This is not observed. We also prefer to rule out insertion to give a secondary alkyl intermediate as the predominant route.

More likely is a scheme based on the formation of a primary alkyl followed by facile α-elimination leading to H incorporation at the terminal carbon. Probably the α-elimination would occur via an agostic bridging alkyl, as found with CH_3 bridging an Os-Os bond in $[Os_3(\mu\text{–}H)(\mu\text{–}CH_3)(CO)_{10}]$,[146] with one D transferred if only temporarily, to another edge of the cluster. Following this rapidly reversible α-elimination there would need to be a second slower β-elimination step and hydrogen transfer strongly preferred over D transfer. We therefore propose that there is a kinetic preference for the formation of the styrenes shown at the bottom left of Figure 6.5.

Figure 6.3 ^{1}H NMR spectrum of the reaction of styrene d^{8} with $[Os_3(\mu\text{-}H)(CO)_{10}]$, the elapsed time is marked in minutes.

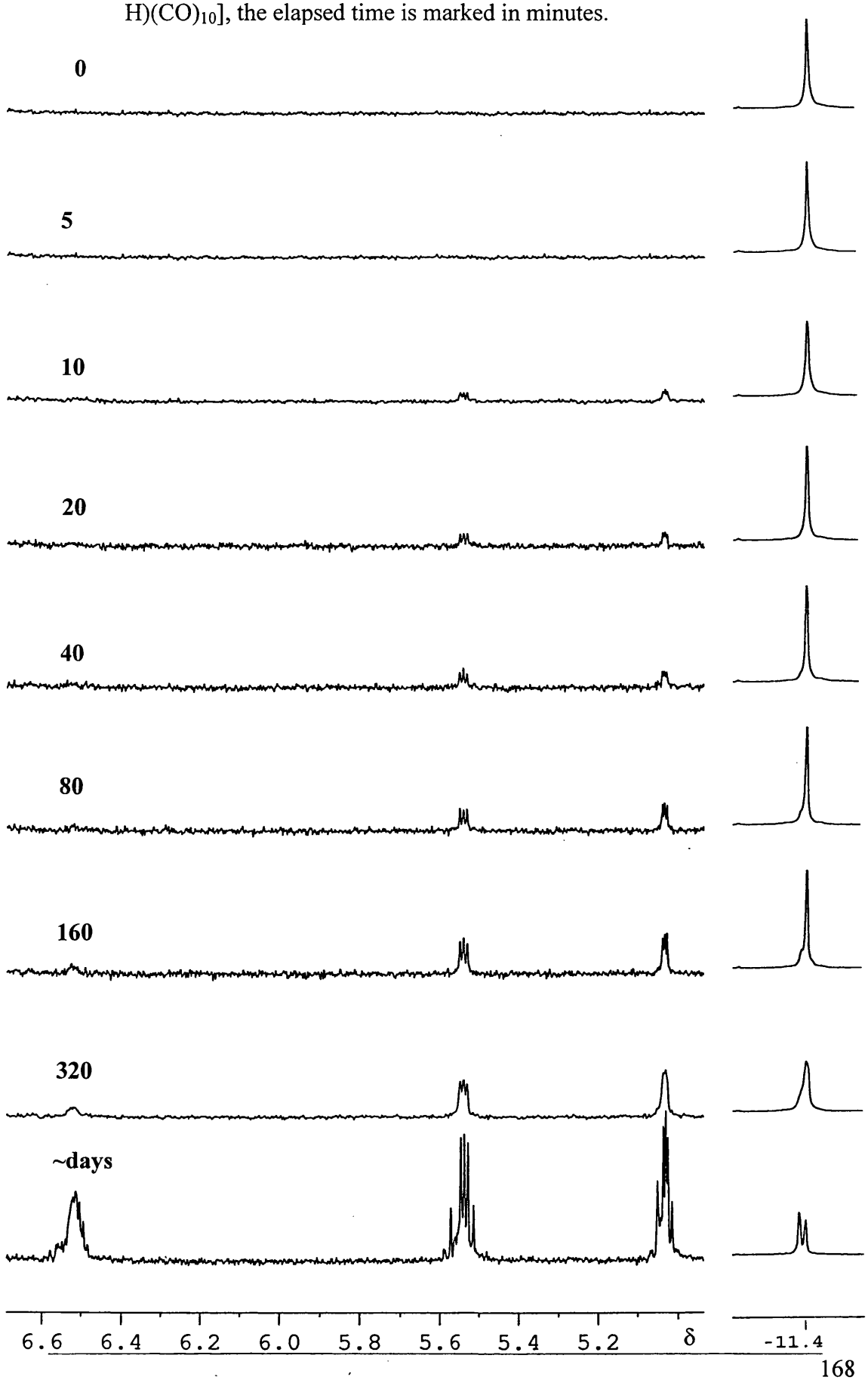

This scheme fits in with the pattern of the couplings observed in the ^1H spectra (see Figure 6.3). It would be interesting to repeat this experiment using smaller amounts of styrene d^8 and see if any H/D exchange occurred at the β-site and also to repeat this using the more sensitive NMR equipment now available.

6.4 Reaction of $[Os_3(\mu\text{-}H)_2(CO)_8$tolBINAP] with styrene-$d^8$

Having produced a chiral triosmium dihydride isostructural with the parent dihydride $[Os_3(\mu\text{-}H)_2(CO)_{10}]$, we were keen to see if it shared the same reactivity as the parent dihydride because this would provide the potential for chiral H/D exchange with substituted substrates. We chose to investigate this by the reaction of styrene–d^8 with $[Os_3(\mu\text{-}H)_2(CO)_8$(tolBINAP)] to establish whether exchange would occur. A tenfold excess of styrene–d^8 was added to $[Os_3(\mu\text{-}H)_2(CO)_8$(tolBINAP)] in CD_2Cl_2 solution in an NMR tube and the reaction was monitored by ^1H NMR spectroscopy. No change was observed in the ^1H NMR spectra over a period of weeks. Similar experiments were attempted with the other clusters synthesised in Chapter 4, but none of these clusters reacted or exchanged D/H with styrene–d^8. Therefore we can conclude that reversible alkene coordination and insertion into the Os–H bonds is totally suppressed by incorporating a diphosphine ligand into the cluster. This could be a steric effect but also the greater electron richness of the cluster might prevent alkene coordination and/or alkene insertion into M–H bonds.

Figure 6.4 Preferred scheme for H/D exchange between styrene-d^8 and $[Os_3(\mu\text{-}H)(CO)_{10}]$

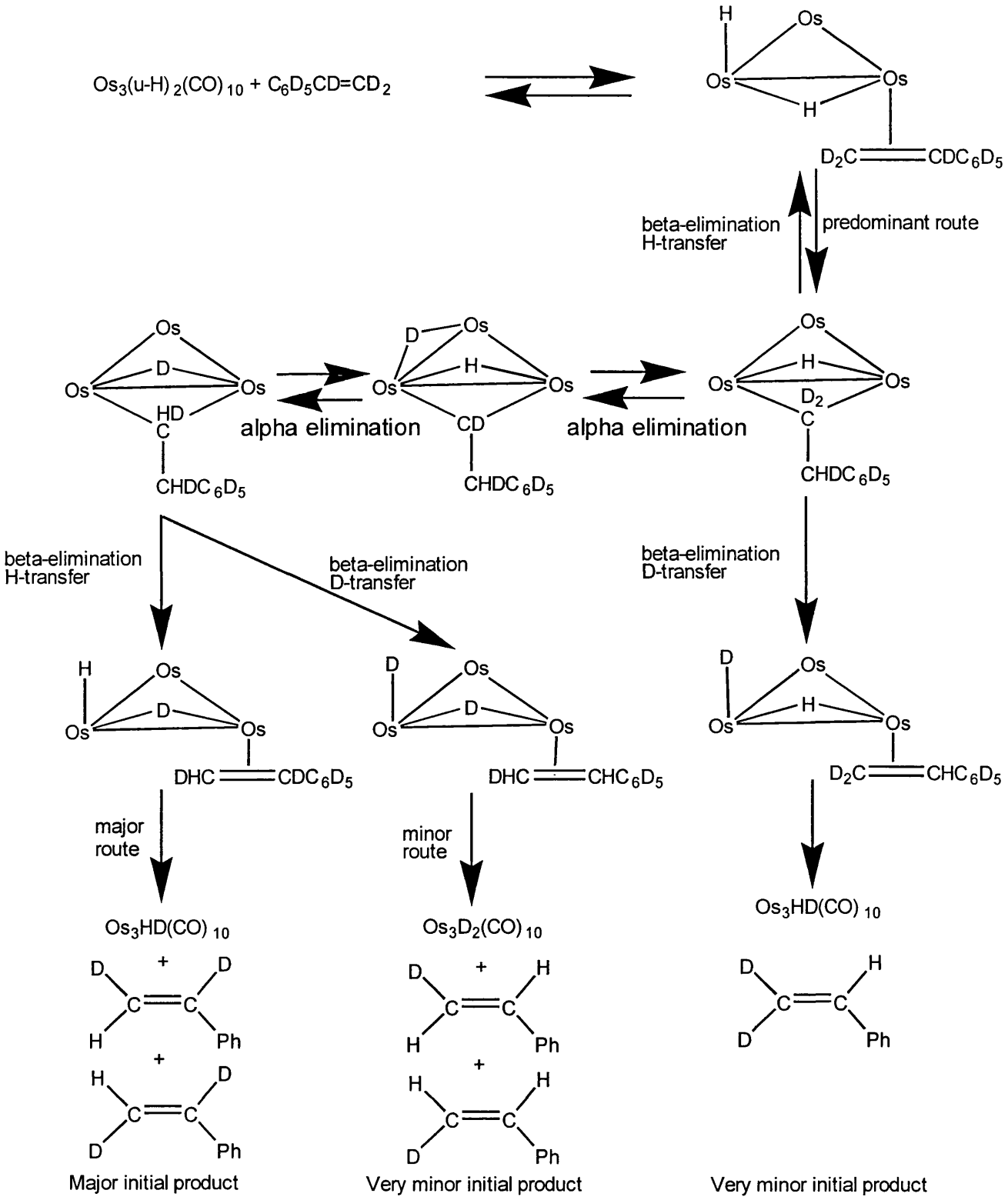

6.5 Conclusions

Conclusions for the work in this chapter were;

a) There was no exchange of H from $[Os_3(\mu\text{–}H)_2(CO)_{10}]$ into the C_6H_5 ring of styrene–d^8 even over a period of weeks, that is orthometallation of intermediate phenylethylene complexes does not occur.

b) There is an significant substitution into the α and β-sites of the vinyl portion of styrene-d^8.

c) However, there is an significantly faster rate of exchange into the CD_2 vinyl site of the styrene–d^8 than into the CD-vinyl site.

d) Taking (b) and (c) together points either towards secondary alkyl formation as the dominant process over primary alkyl formation which is unlikely, or that rapidly reversible α–elimination occurs at a primary alkyl intermediate.

e) The second interpretation requires a significant H/D isotope effect in the β–elimination step favouring H rather than D transfer from C to Os.

f) Disappointingly we were unable to find any evidence of H-D migration in the reaction of the clusters produced in Chapter 4 with styrene d^8.

6.6 Experimental

Spectral data acquired using a Bruker AC300 spectrometer were transferred to a Silicon Graphics O2 from the Aspect3000 computer using NMRLINK and processed using XWINMR and XWINPLOT. Styrene–d^8 was purchased from Aldrich and used without any further purification and without the removal of the t-butylcatechol inhibitor. Trifluoroacetic acid was purchased form Aldrich and used without further purification. $[Os_3(\mu\text{-}H)_2(CO)_{10}]$ was synthesised using standard methods.

6.6.1 The reaction of $[Os_3(\mu\text{-}H)_2(CO)_{10}]$ with styrene–d^8

A solution of 30 mg of $[Os_3(\mu\text{-}H)_2(CO)_{10}]$ in 0.7 cm^3 of CD_2Cl_2 was placed in a 5 mm NMR tube and the parameters, specifically the tuning and matching of the probe and receiver gain, were carefully optimised and a ^1H spectrum acquired from δ 10 to – 25. A tenfold excess of styrene d^8 (0.04 cm^3) was then added to the tube by a microlitre syringe. The tube was then shaken and a spectrum was acquired five minutes after the styrene was added. Further spectra were acquired at 10, 20, 40, 80 (etc) minute intervals.

6.6.3 Attempted reaction of $[Os_3(\mu\text{-}H)_2(CO)_8(tolBINAP)]$ with styrene-d^8

A solution of 30 mg of $[Os_3(\mu\text{-}H)_2(CO)_8(tolBINAP)]$ in 0.7 cm^3 of CD_2Cl_2 was placed in a 5 mm NMR tube and the parameters, specifically the tuning and matching of the probe and receiver gain, were carefully optimised and a ^1H spectrum acquired from δ 10 to – 25. A tenfold excess of styrene-d^8 (0.05 cm^3) was then added to the tube by a microlitre syringe, the tube was then shaken and spectrum acquired five minutes after the styrene was added. Further spectra were acquired at 10, 20, 40, 80, etc minute intervals. This procedure was also used with all the other dihydrido clusters synthesised in Chapter 4 i.e. $[Os_3(\mu\text{-}H)_2(CO)_8(dppm)]$, $[Os_3(\mu\text{-}H)_2(CO)_8(dppe)]$ and $[Os_3(\mu\text{-}H)_2(CO)_8(dppp)]$.

Chapter 7 NMR studies of the low γ nucleus ^{187}Os

7.1. Introduction

If one is to accept the cluster surface analogy and then pursue its full potential for catalytic use, a means of identifying and screening metal sites for potential catalytic activity needs to be developed. In this respect NMR spectroscopy has much to offer. Although it is generally accepted that ^{187}Os is the least sensitive spin ½ nucleus, even less sensitive than ^{57}Fe [175] (initial studies of ^{57}Fe systems were carried out using ^{57}Fe enrichment)[156] more recent studies of ^{57}Fe have used 2D HMQC (**h**eteronuclear **m**ultiple **q**uantum **c**oherence)techniques[157,158] extended to detection via ^{31}P as opposed to ^{1}H which have offered tractable levels of sensitivity.[175]

It has been shown that the performance of Ziegler-Natta type catalysts depends on the nature of the metal-ligand interaction which may be described in terms of the stability of the metal-alkyl bond and the metal-olefin coordination as well as more general steric effects.[159] von Philipsborn and his co-workers have established an impressive body of data correlating the reactivity of known rhodium,[160,161,162] cobalt,[163] manganese[164] and iron[165] systems with the chemical shifts of the metal nuclei by both direct and indirect detection NMR methods.

For example the ligand effects in cyclopentadienyl-iron complexes were studied by ^{57}Fe NMR.[165] For the series $CpFe(CO)_2R$, ^{57}Fe shielding was found to decrease with the bulkiness of the alkyl ligand R (where R = Me, ^{n}Bu, ^{i}Bu, ^{neo}Pe, ^{i}Pr and ^{s}Bu). The reaction rate of $CpFe(CO)_2R$ with PPh_3 in refluxing THF was

determined using a large excess of PPh_3 so as to provide pseudo first order conditions.[166] The chemical shift was found to correlate with the rate of CO insertion rate into the Fe-R bond (r = 0.976 based on six points of data).[165] Steric factors were also quantified by nOe effects between the ligands R and Cp for the above systems.

Ramsey divided the shielding constant σ into two components, the paramagnetic component (σ_{para}) and the diamagnetic component (σ_{dia}).[167] Others have shown that variation in σ_{dia} is small, being limited to about 5%, for heavy metal nuclei.[168] On this basis the large observed δ shifts of heavy metal nuclei are usually attributed to variations in the σ_{para} term.[169] von Philipsborn goes further and using the Popple assumption[170] equates the radial distance of the valence *d* electrons to the σ_{para} term for these heavy metal nuclei .

7.1.1. Direct detection

Kaufman and Schwenk[57] reported the first, and to our knowledge, the only report of a signal from direct detection of ^{187}Os, using molten osmium tetroxide. OsO_4 has therefore by default become used as a primary standard in spite of the difficulties associated with handling it.[171] Brevhard and Grainger[172] re-determined the frequency of this resonance more accurately, this time for a solution in CCl_4. It is unsurprising that there are no other references to direct detection given that the sensitivity assigned to ^{187}Os is generally of the order of 10^{-3} compared to ^{13}C, both at natural abundances. We have succeeded in reproducing Brevhard and Grainger's original measurements on OsO_4, but we have been unable to observe

any signals of other materials possibly due to long relaxation times. There appear to be no reports of any ^{187}Os NMR spectroscopy applied to clusters and that the relaxation properties of ^{187}Os in clusters are unknown. von Philipsborn[173] has developed an inverse technique to measure ^{187}Os T_1 via ^{31}P and applied it to mononuclear systems. However, we have not evaluated this method for clusters.

7.1.2. Polarisation transfer

INEPT (**i**nsensitive **n**uclei **e**nhanced by **p**olarization **t**ransfer) was developed to increase the signal strength of nuclei with low γ.[174] Polarization transfer achieves considerable sensitivity enhancement usually for low γ nuclides coupled to ^{1}H, although in practice ^{1}H can be replaced by any suitable sensitive nuclei such as ^{19}F or ^{31}P. The sensitivity gain is γ^{H}/γ^{X} and is independent of the sign of γ. INEPT is one of the most important building blocks of the sequences used in the following sections. For ^{1}H detected ^{187}Os INEPT spectroscopy the enhancement given by INEPT is γ^{H}/γ^{Os} 26.75/0.61 = 43.19.[54]

Long before the birth of fully developed inverse NMR spectroscopy it was possible to identify the approximate chemical shift of spin ½ nuclei that could not be observed directly. This can be accomplished in a number of ways, most simply by applying a ^{1}H $\pi/2$ pulse followed by a $\pi/2$ pulse for the X nucleus after a delay equal to 1/2*J*(X-H) and observing an ^{1}H signal (adjusted so that the satellites are in anti-phase) that shows a coupling to the nucleus in question. The $\pi/2$ pulse width of the nucleus under investigation is initially set to the $\pi/2$ pulse of the nucleus nearest in frequency that has a known $\pi/2$ pulse for that probe if the

nuclide under investigation has not been determined on that probe before. The frequency of the X is then varied in small increments (1 kHz) until a disturbance is seen in the phase or intensity of the X satellites. Once the frequency has been identified in this way the experiment is repeated, this time with the frequency fixed and the $\pi/2$ pulse width varied until the satellites are not visible.[175] After initial optimisation the process is usually repeated using smaller steps to obtain more refined values. This method is widely used to calibrate inverse pulses and is relatively easy to carry out. Now that this information has been obtained more informative experiments may be attempted.

7.1.3. Two dimension inverse methods

Definition of terms used:

F1 is the indirect dimension in 2D NMR

F2 is the direct dimension in 2D NMR

f1 is the observe channel on a spectrometer

f2 is the X decouple/pulse channel on a spectrometer

f3 is the Y decouple/pulse channel on a spectrometer

$\mathbf{T_1}$ is the spin-lattice relaxation time

$\mathbf{T_2}$ is the transverse relaxation

t_1 is the evolution time delay in 2D sequences to differentiate the increments, in the indirect dimension

Correlation techniques such as COSY (**co**rrelation **s**pectroscop**y**) are a familiar part of NMR spectroscopy. The principle was quickly extended to cover C-H detection by sequences such as HETCOR (**het**eronuclear **cor**relation

spectroscopy). However whilst such sequences show the same enhancement as INEPT they still depend on the detection of the X nucleus so preventing their application to really insensitive nuclei.

The HMQC (**h**eteronuclear **m**ultiple **q**uantum **c**orrelation) sequence may be understood (at a basic level) as an elision of the INEPT sequence and the COSY sequence. This is not an attempt at a rigorous explanation of the sequence only at an explanation that gives a feel for the significance of the various pulses and delays. Using the basic COSY sequence as a basis for the explanation, then the initial HMQC magnetisation is generated by a $\pi/2$ ^{1}H pulse and is then allowed to transfer via $^1J_{X\text{-}H}$ during a delay equal to $1/2(J_{H\text{-}X})$ to the X nuclei of interest. An X $\pi/2$ pulse is then applied that is analogous to the first pulse of the COSY sequence. Now the problem is that correlation information of both ^{1}H,^{1}H and ^{1}H,X exists in F1: the ^{1}H,X spin-spin coupling information is then purged by the use of a π ^{1}H pulse half way through the t_1 period. A $\pi/2$ X pulse is then applied after an incremented delay to develop t_1 (to differentiate the t_1 slices in the 2D) and to transfer the magnetisation back to ^{1}H. The FID is then acquired after a small delay, according to the hardware used, and during the acquisition period the ^{1}H-X coupling evolves again. As an additional refinement broad band decoupling may be applied on the X channel to prevent the ^{1}H-X spin coupling evolving again in F2. Whilst this increases the signal intensity it makes it very hard to distinguish between real signals and artefacts. We have found it better not to use this optional decoupling at all, as the coupling allows direct comparison with the satellites in the ^{1}H projection and therefore the ability to distinguish instantly between artefacts and real signals.

HMQC: **$\pi/2(^1H)$ - d2 - $\pi/2(X)$ - $t_1/2$ - $\pi(^1H)$ - $t_1/2$ - $\pi/2(X)$-acquire FID**

where d2 = $1/2J_{X-H}$

This sequence can then be modified to provide HMBC[158] (**h**eteronuclear **m**ultiple **b**ond **c**orrelation) an analogous method based on $^{2-3}J_{H-X}$ couplings. This sequence operates in essentially the same way as the HMQC sequence discussed above except that an optional pulse or pulses is sometimes added to suppress the $^1J_{H-X}$ couplings. Decoupling is not conventionally applied during the acquisition period. Two main problems with HMQC are that the magnitude of the $^{2-3}J_{H-X}$ couplings is often unknown and is not usually observable from the 1D proton spectra nor is the chemical shift of X often known. This can lead to apparent non-detection. One approach is the so called ACCORDION principle[179] in which the delays responsible for selecting $^{2-3}J_{H-X}$ are cycled through a defined range so allowing the detection of a range of coupling constants. This is implemented in the sequence ACCORD-HMBC.[54]

The use of pulsed field gradients is now widespread. Field gradients essentially provide a means of reducing or eliminating the need for time-consuming phase cycling to suppress unwanted magnetisation.[176] They also have the benefit that add/subtract phase errors are almost totally eliminated. Also experimental time is often reduced by a factor of up to eight. Significantly though, sensitivity is increased, at the same time, because all that is observed at the detection of the FID is the required signals and not, the often relatively intense, centre lines. This

allows the receiver gain to be set substantially higher resulting in a better use of the analogue to digital converter. Pulsed field gradients represent a major step forward in this area. Whilst a detailed discussion of gradients is beyond the scope of this work, there are a few factors that need to be considered when using gradients. The selection of the coherence pathway depends on the relative magnitudes of the gradient pulses, which in turn depend on the relative magnitudes of γ. As the γ of the X nuclides varies widely, it is necessary to calculate the gradient ratios for each and every pair of nuclides separately. How this is done depends on the specific sequence used. In our work we have evaluated a number of ^{1}H-detected gradient selected sequences and found pulsed field gradients to be a great advantage once the initially somewhat more complex set-up was established. Since this was a new area of cluster NMR spectroscopy, non-gradient studies (on account of their simplicity) were undertaken in all cases to optimise the basic parameters. Only once a reasonable non-gradient spectrum was obtained were gradient experiments attempted. However in the longer term, now that these methods are fully established, gradient sequences are those of choice.

Apart from the construction of a suitable pulse sequence, there are a few other experimental requirements that must be met.[179] A measurable spin-spin coupling must exist. This implies that the nuclei must not be more than three bonds apart. The spin-lattice and spin-spin relaxation times must allow the magnetisation to be persistent for long enough to be measured. This often makes quadrupolar nuclei unobservable by these methods.

Referencing of non-standard nuclei has until recently been a major area of contention. Widely varying reference chemical shifts are quoted and the instrument manufacturers often use widely differing reference frequencies in their software. In more recent work, the use of actual physical standards has been abandoned in favour of using Ξ values based on the frequency of operation. On this basis the Ξ value for TMS (Ξ_{TMS}) is defined as 100 MHz and the Ξ values for all other nuclei are calculated relative to this using the equation:[169]

$$\Xi_x = (\Xi_{TMS} / \nu_{TMS}) \nu_X$$

where ν_{TMS} = the operating frequency of TMS on the spectrometer used

Ξ_{TMS} = the standard frequency of TMS (100.00 MHz)

Ξ_x = the standard operating frequency of nucleus X

ν_X = the operating frequency of nucleus X on the spectrometer

In this work the Ξ convention has been used with Ξ_{Os} taken as 2.282343 MHz.

7.1.4. Hardware developments

Until recently probes were tuned in the range ^{31}P to ^{15}N (50–200 MHz on 500 MHz instruments) on the X coil with a second coil doubly tuned to $^{1}H/^{19}F$ and ^{2}H. Such design necessitated the use of specific low frequency probes. Newer probe designs have extended the tuning range and some probes are now able to cover the range ^{187}Os to ^{31}P (11.5-200 MHz on 500 MHz instruments). Commercial triply tuned probes were introduced in the late 1980's with the $^{1}H/^{19}F$ and ^{2}H coil able to be tune to another fixed frequency, commonly that of ^{15}N, ^{13}C or ^{31}P.[177]

Also in the late 1980's the drive towards protein NMR lead to the development of commercial inverse probes with the $^{1}H/^{19}F$ and ^{2}H coil in the centre of the probe and X-coil on the outside. These probes offered ^{1}H sensitivity improvements about twice that of probes with a conventional coil orientation. Probes tend to be less efficient at lower frequencies and therefore require longer radio frequency pulses,[55] which in turn, limits the ultimate observable frequency range. Inverse probes offer the advantage of not being designed for X-nucleus detection but for X-decoupling and therefore the X-coil is somewhat more robust and capable of handling higher power levels and therefore covering larger frequency ranges. Older spectrometers have restricted amplifier power such as 75 W on the X channel with newer spectrometers having up to 500 W. Triple inverse probes ^{1}H, ^{13}C on the inner coil and ^{15}N on the outer coil are now common in biological NMR.

Although the first sequences that allowed inverse detection (published in 1979-1983[158,157]), and are the basis of our experiments, it was not possible to use these on commercial spectrometers until the late 1980's. This was because the relative phases of the two (or three) channels were not fixed to one common reference which is essential for these sequences.

7.2. Aims and objectives

The aims and objectives the work in this chapter were to:-

a) To examine and evaluate means of determining the chemical shift of ^{187}Os.

b) To determine the viability of indirect detection (via $J_{M\text{-}L}$) using hydride or phosphine ligands in a similar manner to that used previously to determine ^{57}Fe and ^{103}Rh chemical shifts by HMQC.

c) To modify pulse programs appropriately to allow decoupling of other 'spectator' nuclei and thereby increase sensitivity and possibly add nOe enhancement.

d) To quantify the chemical shifts of ^{187}Os and determine whether there was a significant phosphine shift effect.

e) To evaluate the shift effect in light of the known reactivity of $[Os_3(\mu\text{-}H)_2(CO)_{10}]$.

f) To examine the possibility of using ^{31}P-detected HMQC.

g) To examine the possibility of detecting ^{187}Os, utilising long range couplings via $^2J_{M\text{-}L}$ with HMBC detected by either ^{1}H or ^{31}P.

7.3. Methods of observation

7.3.1. Direct observation

Using a sample of 100 mg of OsO_4 dissolved in CCl_4, observation connotations were identical to those used by Brevhard and Grainger[172] in their observation. A signal of poor intensity was observed after 100,000 transients. We did not pursue this method of observation further.

7.3.2. One dimensional inverse detection ^{1}H-^{187}Os

Using the procedure described in the introduction, the frequency and $\pi/2$ pulse length were determined for a sample of $[Os_3(\mu\text{-}H)_2(CO)_8(tolBINAP)]$, which was chosen for the investigation as it was highly soluble and had two equivalent osmium nuclei bridged by two hydrides. The ^{187}Os satellites from this cluster were readily observed in one transient without the use of line broadening on both the spectrometers used. Additionally, as a check of these results, a one-dimensional HMQC experiment was performed to check that the satellites were enhanced and the centre lines suppressed (see Figure 7. 1). The total experiment time was about 10 minutes and shows clearly the effectiveness of this approach. The residual centre signals are due to imperfections in the phase cycling and T_1 noise and can be reduced further by allowing a longer relaxation delay. All the data was now at hand to perform the two-dimensional version of the experiment.

Figure 7.1 1D HMQC ^{1}H-^{187}Os uses the standard Bruker pulse programme ***inv4nd1d***. 64 transients were acquired with a recycle time of five seconds, total acquisition time 5 minutes.

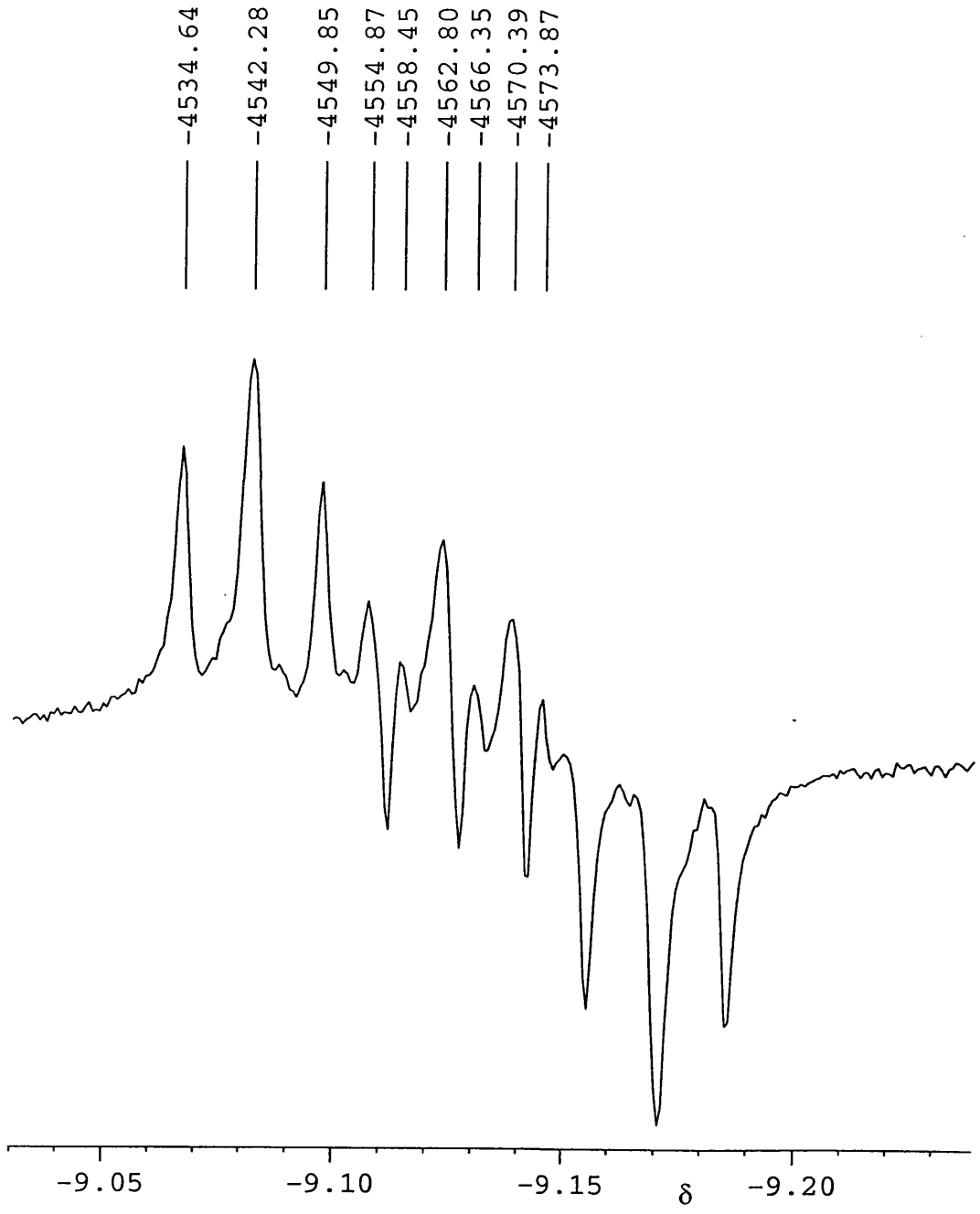

7.3.3. Two dimensional inverse detection ^{1}H-^{187}Os

The standard Bruker HMQC programme was used with ^{1}H detection. Using the parameters determined in the previous experiments and the standard Bruker pulse programme inv4nd the ^{1}H-^{187}Os HMQC spectrum of $[Os_3(\mu\text{-}H)_2(CO)_8(tolBINAP)]$ was recorded and gave δ ^{187}Os 11345 ± 2 (see Figure 7.2). It is believed that this is the first observation of such a signal for triosmium systems. The veracity of the signal is confirmed by the measurement of the couplings that are shown in the two-dimensional experiment these accord with those from standard one-dimensional experiments: $J_{Os\text{-}P}$ = 204 ± 2 Hz, $J_{Os\text{-}H}$ = 38 ± 1 Hz and $J_{P\text{-}H}$ = 15 ± 1 Hz (see Figure 7.2). The chemical shift of the parent dihydride $[Os_3(\mu\text{-}H)_2(CO)_{10}]$ was determined as $\delta^{187}Os$ 11302 ± 2. All chemical shifts are relative to OsO_4 at 0 ppm however in this work the Ξ convention has been used with Ξ_{Os} taken as 2.282343 MHz as the absolute reference.

7.3.4. Simplifying the spectrum by decoupling a third nucleus ^{1}H-^{187}Os $\{^{31}P\}$

Most of our experiments described in this chapter have been on clusters containing phosphine ligands. Whilst having the ^{1}H-^{187}Os couplings is useful, the ^{31}P-^{187}Os and ^{31}P-^{1}H couplings severely diminish the signal intensity. A signal of two cross peaks is divided into a signal of eight cross peaks. As an example, a ^{1}H-^{187}Os spectrum has been recorded with and without ^{31}P decoupling (see Figure 7.3 and 7.4). The basic HMQC pulse program was modified to provide continuous ^{31}P GARP decoupling on the f3 channel.[178]

Figure 7.2a ^{1}H-^{187}Os HMQC low resolution spectrum of $[Os_3(\mu\text{-}H)_2(CO)_8(tolBINAP)]$ showing $J_{Os\text{-}P}$ = 204 ± 2 Hz, $J_{Os\text{-}H}$ = 38 ± 1 Hz and $J_{P\text{-}H}$ = 15 ± 1 Hz at 400 MHz without z-gradients.

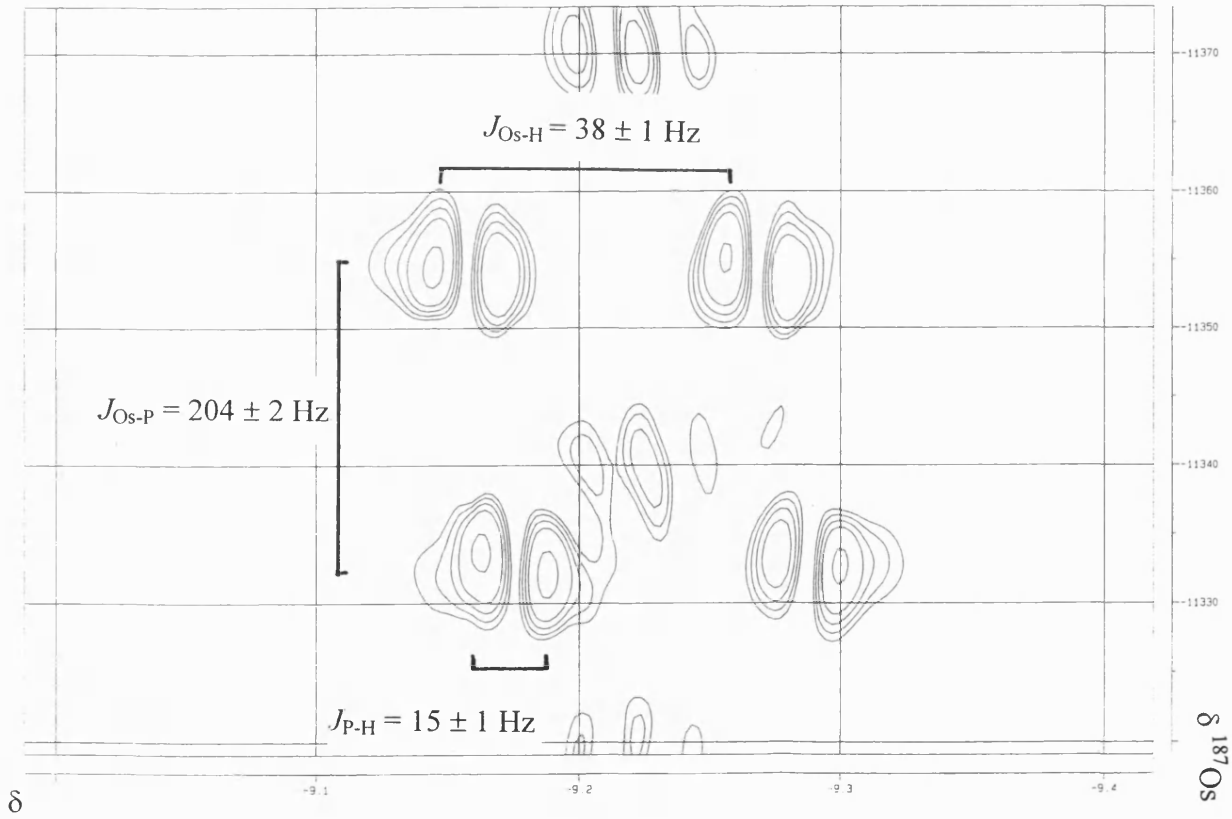

Figure 7.2b ^{1}H-^{187}Os HMQC spectrum of $[Os_3(\mu\text{-}H)_2(CO)_8(tolBINAP)]$ showing $J_{Os\text{-}P} = 204 \pm 2$ Hz, $J_{Os\text{-}H} = 38 \pm 1$ Hz and $J_{P\text{-}H} = 15 \pm 1$ Hz at 500 MHz using z-gradients at very high F1 resolution. The ^{187}Os spectrum shown to the right is an internally calculated summed projection.

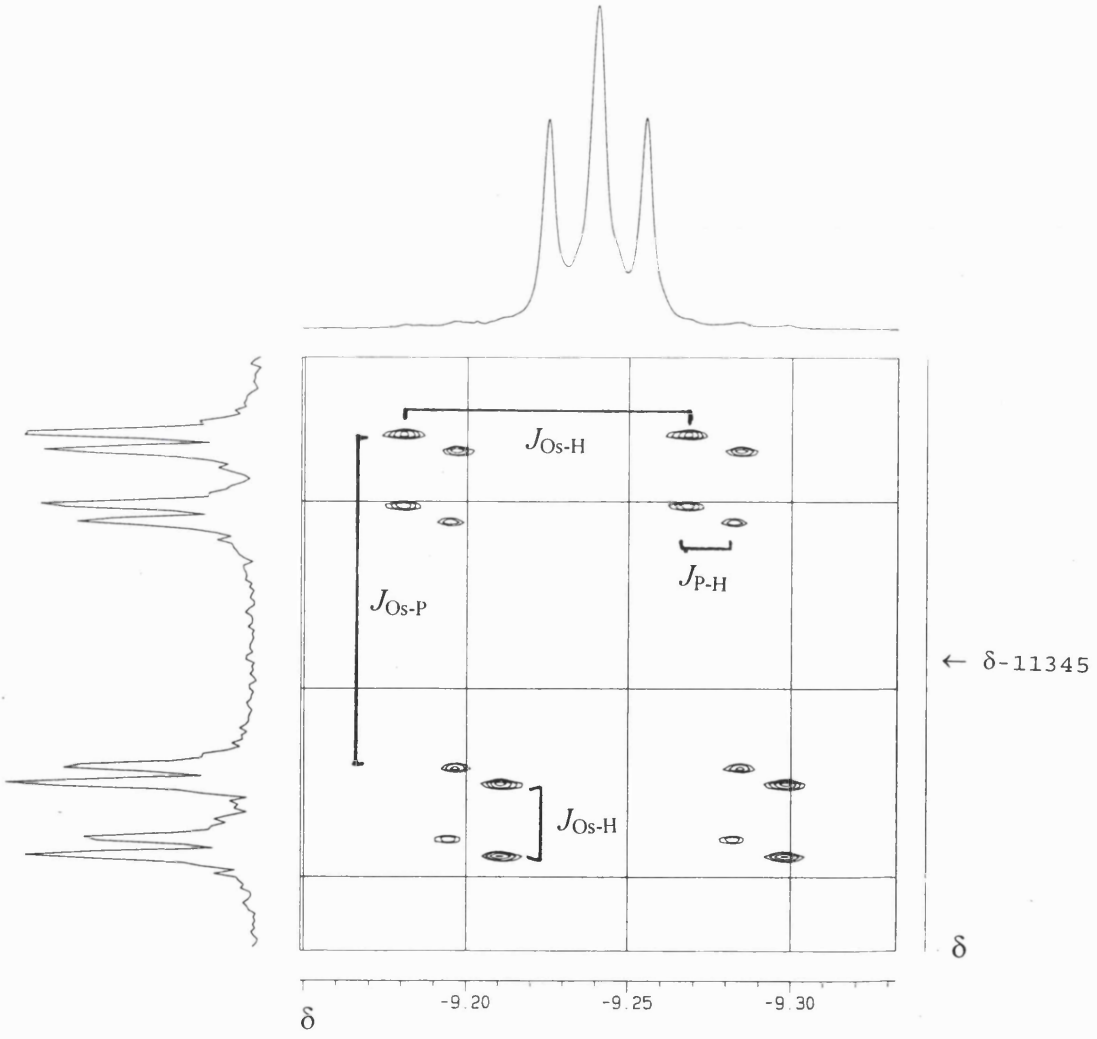

Figure 7.3 ^{1}H-$^{187}Os\{^{31}P\}$ HMQC spectrum of $[Os_3(\mu\text{-}H)_2(CO)_8(tolBINAP)]$ showing $J_{Os\text{-}H}$ = 38 ± 1 Hz and the elimination of $J_{P\text{-}H}$ and $J_{Os\text{-}P}$.

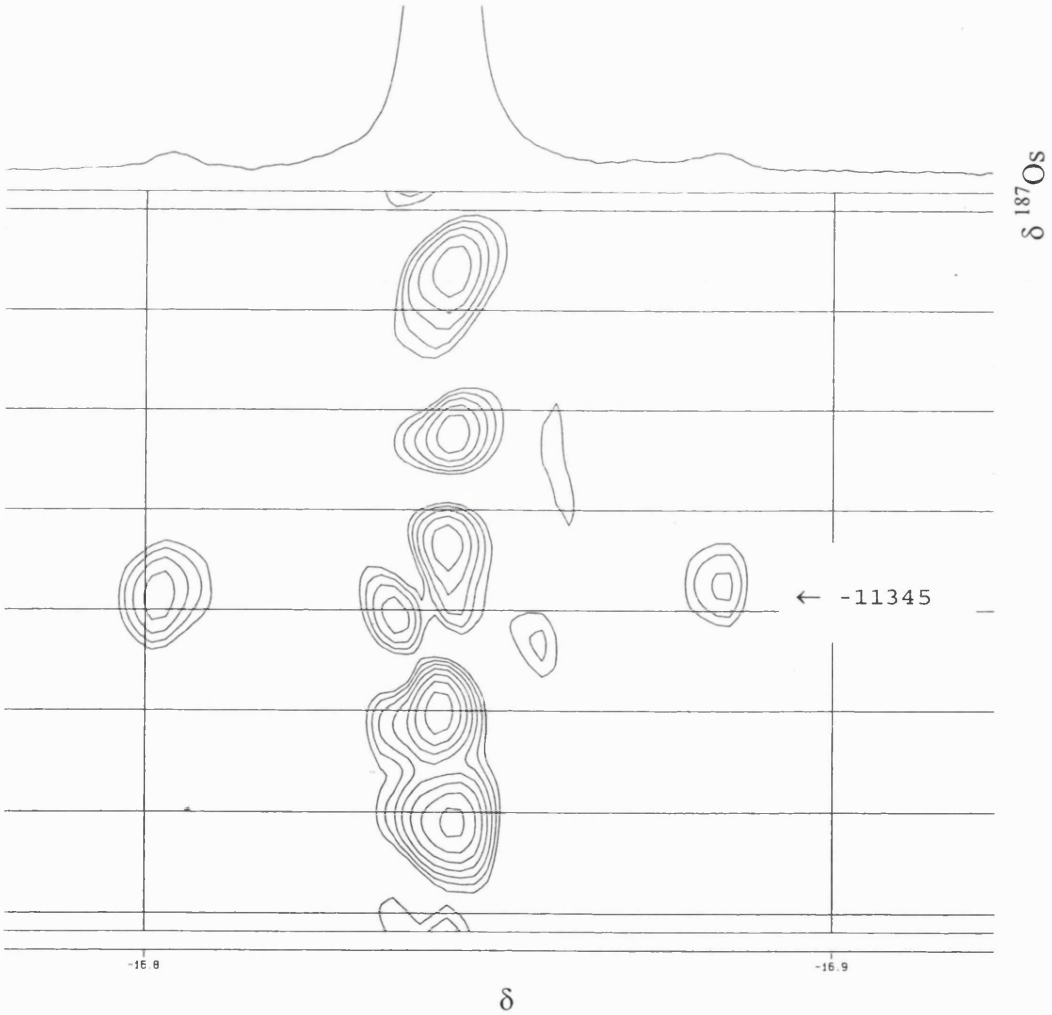

On the Bruker naming convention of the channels, f1 is always the observe channel, f2 is decoupler A and f3 is decoupler B. The decoupler channels can also provide hard (i.e. π) pulses.

The ^{1}H-^{187}Os{^{31}P} HMQC spectra of [$Os_3(\mu\text{-}H)_2(CO)_8$(tolBINAP)] and[$Os_3(\mu\text{-}H)(CO)_8$(BINAP-H)] were recorded giving δ ^{187}Os –11345 ± 5 for [$Os_3(\mu\text{-}H)_2(CO)_8${*tol*BINAP}] δ ^{187}Os –13150 ± 20 and δ ^{187}Os –12720 ± 20 for [$Os_3(\mu\text{-}H)(CO)_8${BINAP-H}]. Interestingly both ^{187}Os ($^{1}J_{Os\text{-}H}$) signals were observed for [$Os_3(\mu\text{-}H)(CO)_8${BINAP-H}]. This is believed to be the first observation of such signals for osmium systems (see Figure 7.4); $J_{H\text{-}Os}$ = 30.7 and 33.7 ± 2 Hz. This observation is consistent with the ^{1}H NMR spectrum previously observed. It is likely that the smaller coupling is that for the osmium with the phosphine ligand attached and that the larger coupling is that for to the osmium with only the hydride (and carbonyls) attached. The signal from [$Os_3(\mu\text{-}H)(CO)_8${BINAP-H}] at δ ^{187}Os –13150 is approximately twice as intense as that at δ ^{187}Os –12720, possibly reflecting an nOe enhancement from the ^{31}P decoupling applied. We have not confirmed which signal is which by acquiring a non ^{31}P decoupled experiment as we did nor have sufficient sample for this inherently less sensitive experiment in the time available.

Figure 7.4 ^{1}H-$^{187}Os\{^{31}P\}$ HMQC spectrum of $[Os_3(\mu\text{-}H)(CO)_8(BINAP\text{-}H)]$showing two ^{187}Os ($^{1}J_{Os\text{-}H}$) signals for $^{a}J_{H\text{-}Os}$ = 30.7 ± 2 Hz, $^{b}J_{H\text{-}Os}$ = 33.7 ± 2 Hz. The signal at δ ^{187}Os –13150 is approximately twice as intense as that at δ ^{187}Os –12720 (see text).

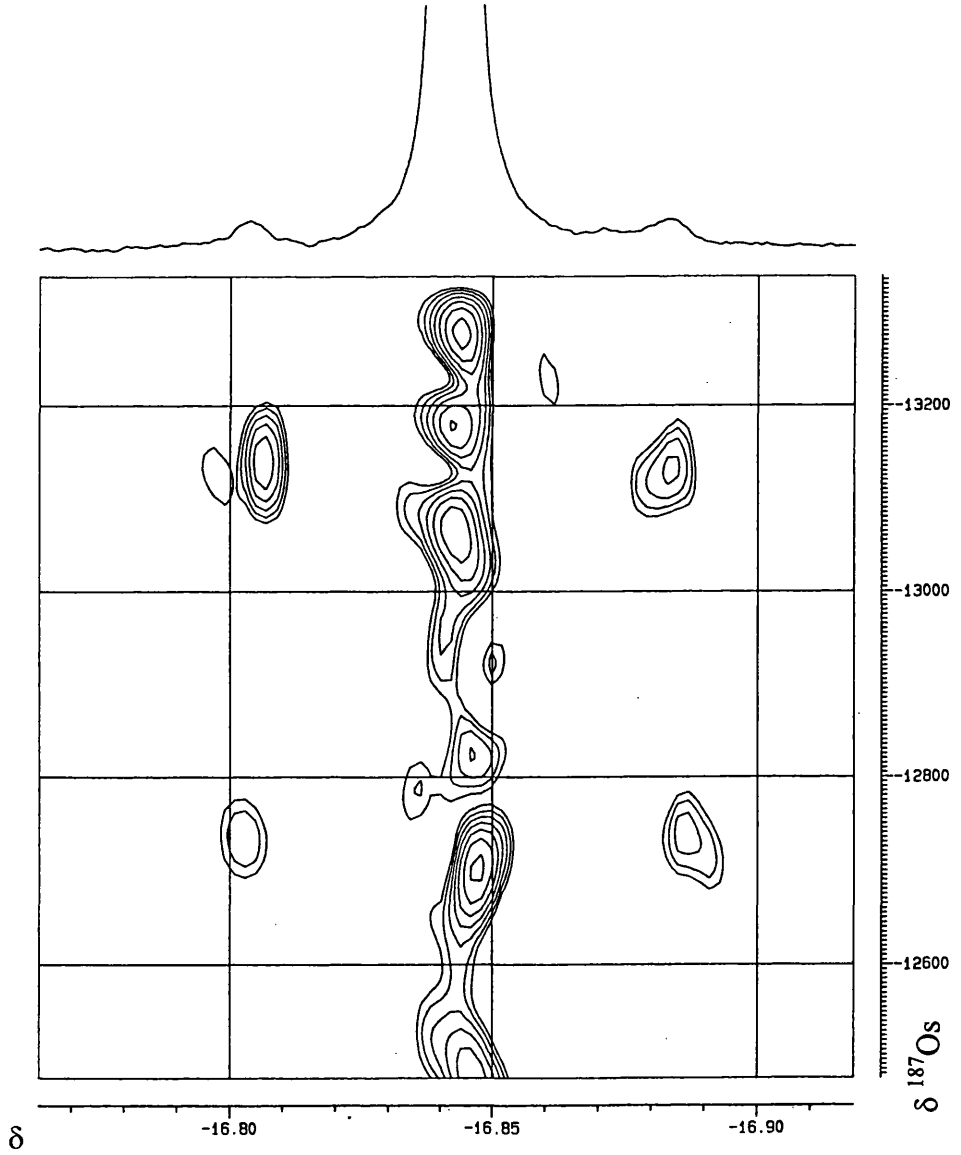

7.3.5. Two dimensional inverse detection ^{31}P-$^{187}Os\{^{1}H\}$

As mentioned previously, the detection nucleus can be any nucleus with a high γ and a high natural abundance.[179] In practice, however, the detection nucleus is usually selected on the basis of the available probe(s) since this 'third nucleus' is usually fixed. In this work we have evaluated ^{31}P as the detection nucleus. The pulse program used is identical to that for ^{1}H detected HMQC except that the channels are redefined. X (^{187}Os) pulses are moved to the f3 channel, the f1 (observe) channel is defined as ^{31}P and continuous ^{1}H decoupling is applied using WALTZ16[55] on the f2 channel. Based on the ratios of γ, the enhancement factor for ^{31}P-detected HMQC over direct detection is 1281.5 as opposed to 12,264.3 for ^{1}H-detected HMQC. However it is worth considering that if T_2 was short and relaxation fast then the following condition may be considered to apply:-

a) The delay d2 is set to 1/2(J) seconds therefore the larger the coupling ($J_{Os\text{-}H} \approx$ 40 Hz $J_{Os\text{-}P} \approx$ 205 Hz) the shorter is the delay that can be used.

b) The shorter the delay, the lower are the relaxation losses.

c) The lower the relaxation losses, the more magnetisation is transferred through to the FID and so a stronger signal is observed.

Alternatively it is possible that the nOe from the ^{1}H decoupling is responsible for the enhancement. As γ for all the nuclei in these systems is positive, then decoupling is highly advantageous as it will lead to a positive enhancement. Negative enhancements, as for ^{29}Si, are quite possible leading to disappearing signals! All the usual authorities mention this possibility, however, all equally skirt round the issue of calculating the magnitude such enhancements. However,

an enhancement factor of 7 times the non-decoupled signal intensity is observed. This gives an effective sensitivity of 8963.5 for ^{31}P detection with ^{1}H decoupling assuming the enhancement is 'seen' by both the ^{31}P and the ^{187}Os nuclei. This raises the ^{31}P-detected sensitivity to the same order of magnitude as that for ^{1}H-detection. This coincides with the observed high sensitivity even on a non-optimal probe (^{31}P on the outer coil) found in this work.

The ^{187}Os chemical shift of the two ligand-bound osmium nuclei in $[Os_3(\mu\text{-}H)_2(CO)_8(tol\text{BINAP})]$ has been evaluated to be δ 11345 in agreement with the value obtained by analogous methods previously (see Figure 7.5).

Figure 7.5 ^{31}P-$^{187}Os\{^{1}H\}$ HMQC acquired in 1.5 hours showing that the sensitivity of this method is much greater than that expected on the basis of the γ values (see text).

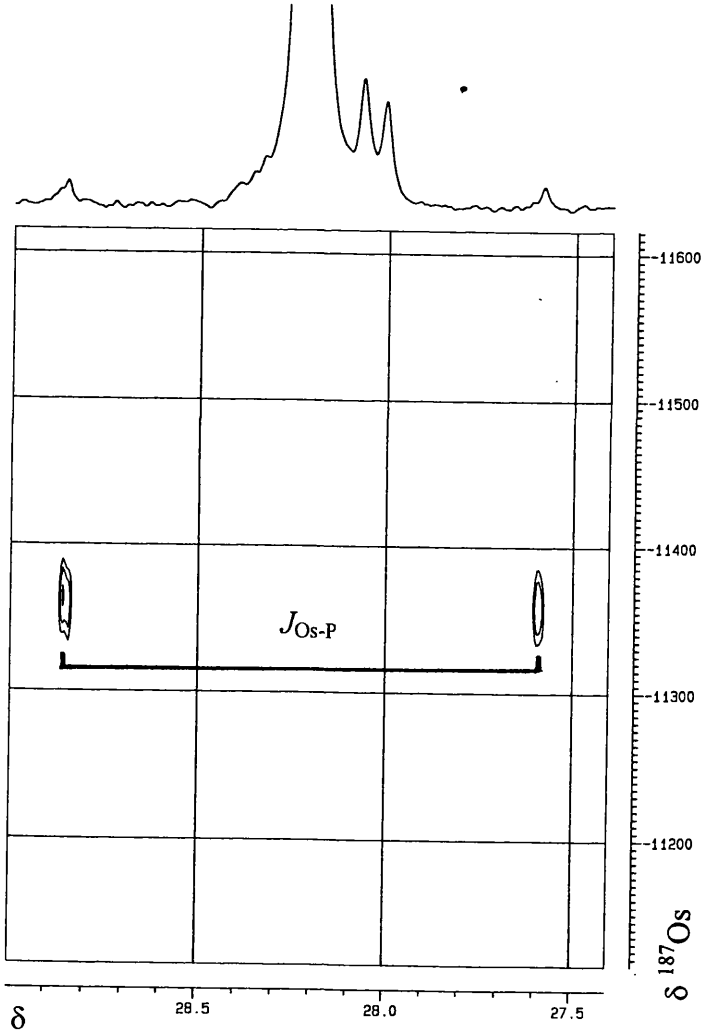

7.3.6. Attempted two dimensional inverse detection ^{1}H-^{187}Os of long range couplings using HMBC

As previously mentioned, although the HMQC sequence can be used for this type of experiment, the more specialised HMBC sequence has been employed. The sequence we used is simply the HMQC sequence with an extra pulse added to nullify the $^{1}J_{Os\text{-}H}$ magnetisation and is a standard Bruker pulse programme. The largest problem with these experiments is that the magnitude of $^{2}J_{Os\text{-}H}$ is unknown as is the relative chemical shift of the $Os(CO)_4$ subunit. This required a repeated search over a range of chemical shift values with the experiment optimised for a number of different coupling constants. We were unable to identify any signals from the data acquired.

Note added in proof

Recently however the signals from osmium nuclei not directly bonded to hydrides have been detected by HMBC via both ^{31}P at 400 MHz and ^{1}H at 600 MHz for a number of trinuclear species. It was found that there was little variation in the chemical shift of the remote metal site despite large shift differences in the shift of the directly hydride bonded metal sites. Thus it is likely that the Os-Os coupling is extremely small and indeed using an ^{187}Os enriched sample provided by Prof. A. A. Koridze the coupling appears to be less than 7 Hz (the limit of measurement) in this one case.[180]

7.3.7. Attempted two dimensional inverse detection ^{31}P-$^{187}Os\{^1H\}$ of long range couplings using HMBC

Given the arguments advanced in section 7.3.5 concerning delay lengths, detection of the $Os(CO)_4$ subunit via $^2J_{Os\text{-}P}$ was attempted. The pulse programme used in section 7.3.6 was modified such that f1 was ^{31}P and f3 was ^{187}Os, and continuous WALTZ16 decoupling was applied to ^1H on f2. The same experimental procedure was adopted as in section 7.3.6 except that larger values of $^2J_{Os\text{-}P}$ (2-50) Hz were tried. We were unable to observe any signals from the data acquired.

7.4. Experimental

7.4.1. General

The compounds used were synthesised as previously described in this thesis. All spectra were recorded in $CDCl_3$. Before all experiments the probehead was matched and tuned to the precise experimental conditions of that experiment. $\pi/2$ values were determined once for the probehead and checked at periodic intervals and there was found to be no significant variation in these values. Care was taken to optimise the shim set and receiver gain so as to maximise the signal-to-noise obtained. It was found that careful adjustment of these parameters considerably reduced the necessary experimental times.

All basic 1D ^{1}H, ^{13}C and ^{31}P spectra were obtained on either a Bruker DRX500 (B_0 = 11.7 T) or a Bruker AMX400 (B_0 = 9.4 T) referenced against the internal digital standards in the case of the DRX500 and against TMS in the case of the AMX400. All samples except [$Os_3(\mu\text{-H})(CO)_9(\mu\text{-BINAP-H})$] were not degassed or sealed. Several samples were run at lower temperatures to establish the variation in shift with temperature. These temperature shifts were found not to be insignificant confirming the results of von Philipsborn.[171]

All triple resonance experiments were carried out using a Bruker AMX400 (B_0 = 9.4 T) three-channel spectrometer with a specially constructed three-channel probehead, a TBO probehead, inner coil X, outer coil ^{1}H and ^{31}P. Both the X and Y channels on the AMX400 are equipped with BSV-10 300 W amplifiers; the ^{1}H

channel is equipped with a 50 W amplifier. Pulse widths were found to be of the order of $\pi/2$ ^{1}H, 9 μs: $\pi/2$ ^{31}P, 24 μs: $\pi/2$ ^{187}Os, 90 μs. Optimal GARP conditions were found to be ^{31}P, 75 μs @ 20 dB on the fixed outer coil; ^{187}Os, 105 μs @ 20 dB. The optimal ^{1}H WALTZ16 pulse was found to be 55 dB at 100 μs. Data were processed using XWINNMR on a Silicon Graphics O2 computer.

All gradient selected experiments were carried out using a Bruker DRX500 (B_0 11.4 T) equipped with a 300 W linear amplifier and GAB 10A (52 G cm^{-1}) gradients amplifier. Appropriate RF pass and stop filters were inserted into the transmitter lines to prevent breakthrough of the decoupler pulses. A standard 5 mm BBO probehead (inner coil X, outer coil $^{1}H/^{19}F$) equipped with self-shielding z-gradients was used. Pulse widths were found to be $\pi/2$ ^{1}H, 11 μs: $\pi/2$ ^{187}Os, 45 μs. Real-time digital filtering was applied to the incoming signals to eliminate folding in the F2 (direct) dimension. ^{1}H sensitivity was at least twice as good as that found on the AMX400. With the replacement of the phase cycling by the use of the gradients, experiment times were reduced to 10-20 minutes to give clear results for normal HMQC spectra for 50 mg of sample (Fw ≈ 1500) in 0.7 cm^3 of $CDCl_3$.

7.4.2. Initial determination of frequency of $\pi/2$ pulses for ^{187}Os

Using an AMX400 spectrometer:

The determination was carried out using the a standard Bruker pulse programme observing ^{1}H and pulsing on X after a delay of $1/2J_{Os\text{-}H}$. The FID was then acquired. A starting value of 9.128 MHz (^{1}H 400 MHz) was used for the

frequency of ^{187}Os and an initial π pulse of 30 μs was applied. The sample used was 50 mg of $[Os_3(\mu\text{-}H)_2(CO)_8(tolBINAP)]$ in 0.7 cm^3 $CDCl_3$ in a 5mm NMR tube. The observation window was optimised to 800 Hz (^1H) and the receiver gain appropriately adjusted. The ^1H signal was adjusted into antiphase with one satellite pointing up on screen and the other down. An automated series of experiments was run using the Bruker AU programme PAROPT varying the frequency in 1 kHz steps. For each experiment four transients were accumulated and transformed without any window function. A disturbance in the phase of the satellites was found at 9.115 MHz. The X frequency was moved to 9.115 MHz and the ^{187}Os pulse adjusted until the satellites were not visible. This was then taken as the starting value for the following experiments. $\pi/2$ ^{187}Os = 90 μs.

Using a DRX500 spectrometer

The same procedure as above was followed. However, the value of the chemical shift was calculated from the ratio of the exact field strengths so that only the $\pi/2$ pulse needed to be determined. $\pi/2$ ^{187}Os = 45 μs.

7.4.3. Direct detection of ^{187}Os

The $\pi/2$ ^{187}Os pulse was known and the frequency had previously been determined[172] as well as the other critical parameters: recycle time 0.2 s acquisition time 0.17 s and line broadening 5 Hz. Using these parameters a signal for OsO_4 was observed after ten hours and 100,000 transients. The signal observed had poor signal to noise characteristics even though more than 100 mg of OsO_4 had been used dissolved in CCl_4.

7.4.4. Detection of ^{187}Os by INEPT

The standard Bruker sequence INEPT was used. The $\pi/2$ pulses and the frequency used were those previously determined in 7.4.1. A recycle time of 2 s was used with an acquisition time of 1.2 s and a sweep width of 20 kHz. Even after 15,000 transients we were unable to observe any signals for a sample of 50 mg of $[Os_3(\mu\text{-}H)_2(CO)_8(tolBINAP)]$ in 0.7 cm^3 of $CDCl_3$.

7.4.5. 1D inverse detection ^{1}H-^{187}Os by HMQC

The standard Bruker sequence ***inv4nd1d*** was used on a DRX500 as a quick check of the essential parameters before the 2D experiment was carried out. The $\pi/2$ pulses and the frequency used were those previously determined in 7.4.1. A relaxation delay of 5 s was used with an acquisition time of 1.3 s and a sweep width of 2 ppm in ^{1}H, set on resonance to the hydride ligand. 64 transients were acquired. For a sample of 50 mg of $[Os_3(\mu\text{-}H)_2(CO)_8(tolBINAP)]$ in 0.7 cm^3 of $CDCl_3$, we were able to observe a strong signal. The satellites showed considerably more strongly than the residual unsurpressed parent signals. This confirmed the validity of the observations in section 7.4.1.

7.4.6. 2D inverse detection by ^{1}H-^{187}Os HMQC

The standard Bruker AMX sequence ***inv4nd*** (HMQC) was used on an AMX400 with a magnitude calculation in F1. Sample concentrations of 30 mg/0.7 cm^3 were required for experimental times of 45 min. The $\pi/2$ pulses and the frequency

used were those previously determined in 7.4.1. Typical parameters were relaxation delays of 1.4 s was used with an acquisition time of 0.5 s and a sweep width of 2 ppm in F2 (^{1}H), set on resonance to the hydride ligand and 50 kHz in the F1 (^{187}Os). With 16 transients per t_1 increment, 128 increments were acquired. This was zero-filled to a 1k by 1k matrix and transformed using a shifted QSINE function. For a sample of 50 mg of $[Os_3(\mu\text{-}H)_2(CO)_8(tolBINAP)]$ in 0.7 cm^3 of $CDCl_3$, we were able to observe a strong signal at δ ^{187}Os -11300 ± 200. For a sample of 30 mg of $[Os_3(\mu\text{-}H)_2(CO)_{10}]$ in 0.7 cm^3 of $CDCl_3$, we were able to observe a strong signal at δ ^{187}Os -11302 ± 2. Typically the F1 window was then narrowed to 5 kHz and the experiment repeated with otherwise the same parameters to obtain a more accurate determination of δ ^{187}Os. In the case of $[Os_3(\mu\text{-}H)_2(CO)_8(tolBINAP)]$ δ ^{187}Os -11343 ± 2.

7.4.7. 2D inverse detection ^{1}H-^{187}Os{^{31}P} by HMQC

The standard Bruker AMX sequence ***inv4nd*** was modified to include continuous ^{31}P GARP decoupling. The $\pi/2$ pulses and the frequency used were those previously determined in 7.4.1. A relaxation delay of 1.4 s was used with an acquisition time of 0.5 s and a sweep width of 2 ppm in F2 (^{1}H), set on resonance to the hydride ligand and 50 kHz in the F1 (^{187}Os). The ^{31}P GARP was set on resonance for the observed ^{31}P signals. With 16 transients per t_1 increment, 128 increments were acquired. This was zero-filled to a 1k by 1k matrix and transformed using a shifted QSINE function. For a sample of 50 mg of $[Os_3(\mu\text{-}H)_2(CO)_8(tolBINAP)]$ δ ^{187}Os -11345 ± 5 and for 30 mg of $[Os_3(\mu\text{-}H)(CO)_8(BINAP\text{-}H)]$ δ ^{187}Os -13150 ± 20 and -12720 ± 20 in 0.7 cm^3 of

$CDCl_3$ were determined. We were able to observe a strong signal with this experiment. Typical experimental times were 45 min. Typically the F1 window was then narrowed to 5 kHz and the experiment repeated to obtain a more accurate determination of δ ^{187}Os.

7.4.8. 2D inverse detection ^{31}P-^{187}Os{^{1}H} by HMQC

The standard Bruker AMX sequence ***inv4nd*** was modified to include continuous WALTZ16 decoupling on the f2 channel and the pulses previously on the f2 channel were move to the f3 channel. The $\pi/2$ pulses and the frequency used were those previously determined in 7.4.1. A relaxation delay of 1.4 s was used with an acquisition time of 0.5 s and a sweep width of 5 ppm in F2 (^{31}P), set on resonance to the ligand signal and 100 kHz in the F1 (^{187}Os). f2 (as distinct from F2) was set on resonance with the hydride ligand. With 32 transients per t_1 increment, 128 increments were acquired. This was zero-filled to a 1k by 1k matrix and transformed using a shifted QSINE function. For a sample of 50 mg of $[Os_3(\mu\text{-}H)_2(CO)_8(tolBINAP)]$, in 0.7 cm^3 of $CDCl_3$ we were able to observe a strong signal. Typical experiment times were 1-2 hours. Typically the F1 window was then narrowed to 5 kHz and the experiment repeated to obtain a more accurate determination of δ ^{187}Os – 11300 ± 5.

7.4.9. Attempted 2D inverse detection ^{1}H-^{187}Os by HMBC of long range couplings

The standard Bruker AVANCE sequence ***inv4lrnd*** was used. The $\pi/2$ pulses and the frequency used were those previously determined in 7.4.1. A relaxation delay

of 2 s was used with an acquisition time of 0.5 s and a sweep width of 2 ppm in F2 (^{1}H) set on resonance to the hydride ligand and 10 kHz in the F1 (^{187}Os). With 128 transients per t_1 increment, 128 increments were acquired. This was zero-filled to a 1k by 1k matrix and transformed using a shifted QSINE function. For a sample of 50 mg of $[Os_3(\mu\text{-}H)_2(CO)_8(tolBINAP)]$ in 0.7 cm^3 of $CDCl_3$, we were unable to observe any signals. Typical experiment times were 6 hours. The experiment was repeated for five different $^{2}J_{Os\text{-}H}$ couplings in the range 2-20Hz in 4 Hz steps. Each step was repeated for five different offsets in the F1 dimension so covering 50 kHz.

7.4.10. Attempted two dimensional inverse detection ^{31}P-^{187}Os{^{1}H} of long range couplings using HMBC

The standard Bruker AVANCE sequence ***inv4lrnd*** was modified such that f1 was ^{31}P and f3 was ^{187}Os, continuous WALTZ16 decoupling was applied to ^{1}H on f2. f2 was set on resonance to the hydride ligand. The $\pi/2$ pulses and the frequency used were those previously determined in 7.4.1. A relaxation delay of 2 s was used with an acquisition time of 0.5 s and a sweep width of 5 ppm in F2 (^{31}P), set on resonance to the ligand and 10 kHz in the F1 (^{187}Os). With 128 transients per t_1 increment, 128 increments were acquired. This was zero-filled to a 1k by 1k matrix and transformed using a shifted QSINE function. For a sample of 50 mg of $[Os_3(\mu\text{-}H)_2(CO)_8(tolBINAP)]$ in 0.7 cm^3 of $CDCl_3$, we were unable to observe any signals. Typical experiment times were 6 hours. The experiment was repeated for five different $^{2}J_{Os\text{-}H}$ couplings in the range 2-50 Hz in 9.5 Hz steps. Each step was repeated for five different offsets in the F1 dimension so covering 50 kHz.

7.5. Conclusions

a) Direct detection of ^{187}Os has proved, as expected, not to be viable.

b) INEPT has proved not to be a tractable method for detecting ^{187}Os chemical shifts.

c) 2D HMQC (^{1}H detected) has proved to be a tractable method for determining ^{187}Os chemical shifts with or without ^{31}P decoupling.

d) 2D HMQC (^{31}P detected) has proved to be a tractable method for determining ^{187}Os chemical shifts with ^{1}H decoupling.

e) The ^{187}Os chemical shifts of a number of compounds described earlier in this thesis have been evaluated.

f) There is clear evidence of a phosphine effect in the ^{187}Os chemical shifts evaluated.

g) The reactivity of these compounds with ligands such as PPh_3 has not been evaluated so no conclusions concerning the relationship between chemical shift and reactivity can be made. However the reactivity of the parent dihydride $[Os_3(\mu\text{-}H)_2(CO)_{10}]$ with ligands such as acetylene, CO and hydrogen is well characterised and the clusters evaluated in this work show no such reactivity and considerable differences in chemical shift to that of $[Os_3(\mu\text{-}H)_2(CO)_{10}]$.

References

1 S. R. Drake and P. A. Loveday, *Inorg. Synth.*, 1990, **28**, 230.

2 C. W. Bradford and R. S. Nyholm, *Chem. Commun.*, 1967, 384.

3 M. I. Bruce, C. M. Jensen and N. L. Jones, *Inorg. Synth.*, 1990, **28**, 216; *Inorg. Synth.* 1989, **26**, 259.

4 N. Masciocchi, M. Moret, P. Cairati, F. Ragaini and A. Sironi, *J. Chem. Soc., Dalton Trans.*, 1993, 471.

5 E. Corey and L. Dahl, *Inorg. Chem.*, 1962, **1**, 521.

6 I. A. Oxton, D. B. Powell, N. Sheppard, K. Burgess, B. F. G. Johnson, J. Lewis, *Chem. Commun.*, 1982, 719.

7 A. J. Deeming, in *Trinuclear Clusters of Ruthenium and Osmium, Comprehensive Organometallic Chemistry II*, Ed. E. W. Abel, F. G. A. Stone and G. Wilkinson, Pergammon, Elsevier Science, Oxford, 1995.

8 R. Peters, *PhD Thesis*, University of London, 1981.

9 B. F. G. Johnson (ed), *Transition Metal Clusters*, Wiley-Interscience, NY, 1980.

10 M. I. Bruce, M. P. Cifuentes and M. G. Humphrey, *Polyhedron*, 1991, **10**, 277.

11 A. J. Deeming, D. M. Speel and M. J. Stchedroff, *Organometallics*, 1997, **16**, 6004.

12 S. E. Kabir and M. B. H. Howlander, *Ind. J. Chem. Sect. A.*, 1989, **28**, 47.

13 B. Ambwani, S. K. Chawla, A. J. Pöe, *Polyhedron*, 1988, **7**, 1939.

14 A. J. Deeming and M. J. Stchedroff, *J. Chem. Soc., Dalton Trans.*, 1998, 3819.

15 N. E. Leadbeater, *J. Chem. Soc., Dalton Trans.*, 1995, 2923.

16 M. I. Bruce and M. Williams, *Inorg. Synth.*, 1990, **28**, 219.

17 H. Nagashima, A. Suzuki, M. Nobata, K. Aoki, K. Itoh, *Bull. Chem. Soc. Jpn*, 1998, **71**, 2441.

18 A. J. Deeming and S. Donovan-Mtunzi, *J. Chem. Soc., Dalton Trans.*, 1988, 579.

19 Y. Chi and J. R. Shapley, *ACS Abstracts*, 1985, **190**, 246.

20 G. A. Foulds, B. F. G. Johnson and J. Lewis, *J. Organomet. Chem.*, 1985, **296**, 147.

21 B. F. G. Johnson, J. Lewis, M. Martinelli, A. H. Wright, D. Braga and F. Grepioni, *J. Chem. Soc., Dalton Trans.*, 1990, 364.

22 A. J. Edwards, N. E. Leadbeater, J. Lewis and P. R. Raithby, *J. Chem. Soc., Dalton Trans.*, 1995, 3785.

23 M. A. Gallop, M. P. Gomez-Sal, C. E. Housecroft, B. F. G. Johnson, J. Lewis, S. M. Owen, P. R. Owen, P. R. Raithby and A. H. Wright, *J. Am. Chem. Soc.*, 1992, 2502.

24 S. L. Ingham, B. F. G. Johnson and J. G. M. Nairn, *J. Chem. Soc., Chem. Commun*, 1995, 189.

25 S. E. Kabir, A. Miah, L. Nesa, K. Uddin, K. I. Hardcastle, E. Rosenberg and A. J. Deeming, *J. Organomet. Chem*, 1995, **492**, 41.

26 A. J. Deeming, S. Donovan-Mtunzi and S. E. Kabir, *J. Organomet. Chem.* 1987, **333**, 253.

27 A. J. Pöe and V. Sekhar, *J. Am. Chem. Soc.*, 1984, **106**, 5034.

28 M. P. Brown, P. A. Dolby, M. M. Harding, A. J. Matthews and A. K. Smith, *J. Chem. Soc., Dalton Trans.*, 1993, 1671.

29 M. P. Brown, P. A. Dolby, M. M. Harding, A. J. Mathews, A. K. Smith, D.

Osella, M. Arbrun, R. Gobetto, P. R. Raithby and P. Zanello, *J. Chem. Soc., Dalton Trans.*, 1993, 827.

30 M. A. Gallop, M. P. Gomz-Sal, C. E. Housecroft, B. F. G. Johnson, J. Lewis, S. M. Owen, P. R. Raithby and A. H. Wright, *J. Am. Chem. Soc.*, 1992, **114**, 2502.

31 D. Braga, F. Grepioni, B. F. G. Johnson, J. Lewis, M. Martinelli and M. A. Gallop, *J. Chem. Soc., Chem. Commun.*, 1990, 53.

32 Z. Dawoodi, M. J. Mays and P. R. Raithby, *J. Chem. Soc., Chem. Commun.*, 1979, 721.

33 S. E. Kabir, A. Miah, K. Uddin and A. J. Deeming, *J. Organomet. Chem.*, 1994, **476**, 121.

34 A. J. Deeming, B. F. G. Johnson and J. Lewis, *Inorg. Phys. Theor.*, 1970, 2967.

35 M. M. Harding, B. Kariuki, A. J. Mathews, A. K. Smith and P. Braunstein, *J. Chem. Soc., Dalton Trans.*, 1994, 33.

36 A. J. Deeming, S. Donovan-Mtunzi, S. E. Kabir, M. B. Hursthouse, K. M. A. Malik and N. P. C. Walker, *J. Chem. Soc., Dalton Trans.*, 1987, 1869.

37 A. J. Deeming, S. Donovan-Mtunzi, K. I. Hardcastle, S. E. Kabir, K. Hendrick and M. McPartlin, *J. Chem. Soc., Dalton Trans.*, 1988, 579.

38 E. Bryan, W. Jackson, B.F. G. Johnson, J. Kelland, J. Lewis and K. Schorpp, *J. Organomet. Chem.*, 1976, **108**, 385.

39 H. K. Sanati, A. Becalska, A. K. Ma and R. K. Pomeroy, *J. Chem. Soc., Chem. Commun.*, 1990, 197.

40 H. D. Kaesz, *Chem. Brit.*, 1973, 344.

41 R. Broach and J. Williams, *Inorg. Chem.*, 1979, **18**, 314.

42 A. J. Deeming and S. E. Kabir, *J. Organomet. Chem.*, 1988, **340**, 359.

43 J. A. Clucas, M. M. Harding and A. K. Smith, *J. Chem. Soc., Chem. Commun.*, 1985, 1280.

44 A. J. Deeming and M. J. Stchedroff, *Unpublished Results.*

45 M. R. Churchill, F. J. Hollander and J. P. Hutchison, *Inorg. Chem.*, 1977, **16**, 2697.

46 P. Dawson, B. F. G. Johnson, J. Lewis, J. Puga, P. R. Raithby and M. Rosales, *J. Chem. Soc., Dalton Trans.*, 1982, 233.

47 S. R. Drake and R. Khattar, *Organomet. Synth.*, 1988, **4**, 234.

48 R. K. Alex and R. K. Pomeroy, *Organometallics*, 1987, **6**, 2437.

49 B.F. G Johnson and A. Bott, *J. Chem. Soc., Dalton Trans.*, 1990, 2437.

50 G. E. Hawkes, E. W. Randall, S. Aime, D. Osella and J. E. Elliot, *J. Chem. Soc., Dalton Trans.* 1984, 279.

51 M. A. Gallop, B. F. G. Johnson and J. Lewis, *J. Chem. Soc., Chem. Commun.*, 1987, 1831.

52 A. J. Deeming, M. B. Smith, *J. Chem. Soc., Chem. Commun.*,1993, 844.

53 A. Schwenk and G. Zimmerman, *Phys. Lett.*, 1968, **26A**, 258; H. R. Loeinger and L. R. Sarles, *Phys. Lett.*, 1954, 291.

54 S. Braun, H-O. Kalinowski and S. Berger, *150 and More Basic NMR Experiments*, Wiley-VCH, Weinheim, 1998.

55 A. E. Derome, *Modern NMR techniques in Research Chemistry,* 2nd Ed., Pergammon, Oxford, 1995.

56 R. J. Goodfellow, *Multinuclear NMR, ed. J. Mason*, Plenum Press, N. Y.,

1987, 532.

57 R. Kaufmann and A. Schwenk, *Phys. Lett.*, 1967, **24a**, 115.

58 A. A. Koridze, O. A. Kizas, N. M. Astakhova, P. V. Petrovskii and Yu. K. Grishin, *J. Chem. Soc., Chem. Commun.*, 1981, 853.

59 B. F. G. Johnson and A. Bott, *J. Chem. Soc., Dalton Trans.*, 1990, 2437.

60 G. R. Frauenhoff, J-C. Liu, S. R. Wilson, J. R. Shapley, *J. Organomet. Chem.*, 1992, **437**, 347.

61 D. Bragga, C. E. Anson, A. Bott, B. F. G. Johnson, E. Marseglia, *J. Chem. Soc., Dalton Trans.*, 1990, 3517.

62 B. F. G. Johnson, A. Bott, D. Hugh-Jones and A. Rodger, *Polyhedron*, 1990, 14, 1769.

63 D. Braga, C. E. Anson, A. Bott, B. F. G. Johnson and E. Marseglia, *J. Chem. Soc., Dalton Trans.*, 1990, 3517.

64 G. R. Desiraju (ed.), *Solid State Chemistry Techniques*, Elsevier, New York, 1987.

65 I. Ojma, N. Clos and C. Bastos, *Tetrahedron*, 1989, **45**, 6901.

66 G. Proctor, *Asymmetric Synthesis*, Blackwell: Oxford, 1994.

67 R. Noyori and T. Ohkuma, *J. Synth. Org. Chem.*, 1996, **54**, 553.

68 S. Otsuka and K. Tani, *Synthesis-Stutgart,* 1991, **9**, 665.

69 F. Prespotino, R. Persson, M. Monari, N. Focci and E. Nordlander, *Inorg. Chem. Comm.*, 1998, **18**, 302.

70 K. Mashima, T. Hino and H. Takaya, *J. Chem. Soc., Dalton Trans.*, 1992, 2099.

71 K. Toriumi, T. Ito, H. Takaya, T. Souchi and R. Noyori, *Acta. Crystallogr.*,

Sect. B 1982, **38**, 807.

72 A. S. Chan, S. A. Laneman and C. X. Day, *Inorg. Chim. Acta,* 1995, **228**, 159.

73 X. Zang, K. Mashima, K. Koyano, N. Sayo, H. Kumobayashi, S. Akutagawa and H. Takaya, *J. Chem. Soc., Perkin Trans. 1*, 1994, 2309.

74 D. Braga, U. Matteoli, P. Sabatino and A. Scrivanti, *J. Chem. Soc., Chem. Commun.,* 1988, 466.

75 A. Ashimoori, T. Matsuura, L. E. Overman and D. J. Poon, *J. Org. Chem.*, 1993, **58**, 6949.

76 W. G-Y. Ho and W.-T. Wong, *Polyhedron*, 1995, **14**, 2849.

77 K. Azam , R. Dilshad, S. E. Kabir, R. Miah, E. Rosenberg, K. I. Hardcastle, M. B. Hursthouse and K. M. A. Malik, *J. Clust. Chem.,* 1996, **7**, 49.

78 B. F. G. Johnson, J. Lewis and D. A. Pippard, *J. Chem. Soc., Dalton Trans.*, 1981, 407.

79 S. R. Drake and R. Kattar, *Organomet. Synth.*, 1988, **4**, 234.

80 K. Azam, R. Dilshad, S. E. Kabir, R. Miah, M. Shahiduzzaman, E Rosenburg, K. Hardcastle, M. Hursthouse and M. Malik, *J. Clust. Chem.*, 1996, **7**, 49.

81 E. Ditzel, M. Gomez-Sal, B. F. G. Johnson, J. Lewis and P. R. Raithby, *J. Chem. Soc., Dalton Trans.*, 1987, 1623.

82 S. Hodge, B. F. G. Johnson, J. Lewis and P. R. Raithby, *J. Chem. Soc., Dalton Trans.*, 1987, 931.

83 D. W. Knoeppel, J-H. Chung and S. G. Shore, *Acta. Cryst.*, 1995, **C51**, 42.

84 D. S. Bohle, V. F. Breidt, A. K. Powell and H. Vahrenkamp, *Chem. Ber.*, 1992, **125**, 1111; C. Santini, J. Basset, B. Fontal, J. Krauss, S. G. Shore and C. Charrier, *J. Chem. Soc., Chem. Commun*, 1987, 512.

85 J. Clucas, D. Foster, M. R. Harding and A. K. Smith, *J. Chem. Soc., Chem. Commun.*, 1984, 949.

86 A. J. Deeming, S. Donovan-Mtunzi, S. E. Kabir and P. J. Manning, *J. Chem. Soc., Dalton Trans.*, 1985, 1037.

87 A. J. Pöe and V. C. Sekhar, *J. Amer. Chem. Soc.*, 1984, 5034.

88 F. A. Cotton and B. E. Hanson, *Inorg. Chem.*, 1977, **16**, 3369.

89 S. E. Kabir, *PhD Thesis*, University of London, 1986.

90 S. Malik and A. J. Pöe, *Inorg. Chem.*, 1979, **18**, 1241.

91 A. Shojaie and J. L. Atwood, *Organometallics*, 1985, **4**, 187.

92 A. J. Deeming, S. Donovan-Mtunzi and S. E. Kabir, *J. Organomet. Chem.*, 1987, **333**, 253.

93 B. F. G. Johnson, J. Lewis and D. A. Pippard, *J. Organomet. Chem.*, 1985, **296**, 147.

94 E. Nordlander, F. Prestopino, M. Monari, *Unpublished Results.*

95 S. E. Kabir, *PhD thesis*, University of London, 1986.

96 S. Aime, D. Osella, L. Milone and E. Rosenberg, *J. Organomet. Chem.*, 1981, **213**, 207.

97 E. Rosenberg, E. Anslyn, C. Barner-Thorsen, S. Aime, D. Osella, R. Gobetto and L. Milone, *Organometallics*, 1984, **3**, 1970.

98 A. J. Deeming, *Adv. Organomet. Chem.*, 1986, **26**, 1.

99 M. R. Churchill, F. Hollander and J. Hutchinson, *Inorg. Chem.*, 1977, **16**, 2696.

100 R. Broach and J. R. Williams, *Inorg. Chem.*, 1979, **18**, 314.

101 S. Aime, R. Gobetto and E. Valls, *Inorg. Chim. Acta,* 1997, **254**, 63.

102 A. J. Deeming and S. Hasso, *J. Organomet. Chem.*, **88**, 1975, C21; J. R. Shapley, J. B. Keister, M. R. Churchill and B. DeBoer, *J. Amer. Chem. Soc.*, 1975, **97**, 4145.

103 A. J. Clauss, M. Tachikawa, J. R. Shapley and C. Pierpont, *Inorg. Chem.*, 1981, **20**, 177; A. J. Deeming, S. Hasso and M. R. Underhill, *J. Chem. Soc., Dalton Trans.*, 1975, 1641.

104 S. Y. W. Hung and W. T. Wong, *J Organomet. Chem.*, 1998, **566**, 237.

105 J. Clucas, M. R. Harding and A. K. Smith, *J. Chem. Soc., Chem. Commun.*,1985, 1280.

106 R. Gobetto, C. G. Arena, D. Drommi and F. Faraone, *Inorg. Chim. Acta*, 1996, **248**, 257.

107 J.B. Keister and J. R. Shapley, *Inorg. Chem.*, 1982, **21**, 3304.

108 S. Aime, R. Gobetto and E. Valls, *Organometallics,* 1997, **16**, 5140.

109 A. J. Deeming, D. M. Speel and M. J. Stchedroff, *Organometallics*, 1997, **16**, 6006.

110 J. B. Keister, J. R. Shapley, M. R. Churchill and B. DeBoer, *J. Am. Chem. Soc.*, 1975, 4146.

111 J. B. Keister and J. R. Shapley, *J. Am. Chem. Soc.*, 1976, 1056; M. Koike, D. H. Hamilton, S. R. Wilson and J. R. Shapley, *Organometallics*, 1996, **15**, 4930.

112 S. R. Drake and P. Loveday, *Inorg. Synth.*, 1990, **28**, 230. Identical to reference 1

113 H. D. Kaesz, S. A. R. Knox, J. Koepke and R. Saillant, *J. Chem. Soc., Chem. Commun.*, 1971, 477.

114 A. J. Deeming and M. Underhill, *J. Chem. Soc., Dalton Trans.*, 1974, 1415.

115 A. J. Deeming and M. B. Smith, *J. Chem. Soc., Dalton Trans.*, 1993, 844.

116 A. J. Deeming, M. J. Stchedroff, C. Whittaker, A. J. Arce, Y. De Sanctis and J. W. Steed, *J. Chem. Soc., Dalton Trans.*, in press.

117 A. J. Deeming and A. J. Arce, *J. Chem. Soc., Chem. Commun.*, 1982, 820.

118 A. J. Deeming and A. J. Arce, *J. Chem. Soc., Chem. Commun.*, 1980, 1102.

119 F. Richter and H. Vahrenkamp, *Angew. Chem., Int. Ed. Engl.*, 1980, **19**, 65.

120 C. Choo Yin and A. J. Deeming, *J. Chem. Soc., Dalton Trans.*, 1975, 2091.

121 J. L. Coffer, H. G. Drickamer and J. R. Shapley, *J. Phys. Chem.*, 1990, **94**, 5208.

122 K. Burgess, B. F. G. Johnson and J. Lewis, *J. Organomet. Chem.*, 1982, **233**, 55.

123 W-Y. Wong and W-T. Wong, *J. Organomet. Chem.*, 1996, **513**, 27.

124 A. J. Deeming, R. Peters, M. B. Hursthouse and J. D. J. Baker-Dirks, *J. Chem. Soc., Dalton Trans.*, 1982, 787.

125 T. Venäläinen, J. Pursianinen and T. A. Pakkanen, *J. Chem. Soc., Chem. Commun.*, 1985, 1348.

126 D. Choudhury and D. J. Cole-Hamilton, *J. Chem. Soc., Dalton Trans.*, 1982, 1885.

127 E. A. Alession, G. Clauti and G. Mrestrroni, *J. Mol. Catal.*, 1985, **29**, 77.

128 A. J. Deeming D. Nuel, N. I. Powell and C. Whittaker, *J. Chem. Soc., Chem. Commun.*, 1990, 68.

129 K. Burgess, H. D. Holden, B. F. G. Johnson, J. Lewis, M. B. Hursthouse, N. P. C. Walker, A. J. Deeming, P. J. Manning and R. Peters, *J. Chem. Soc., Dalton Trans.*, 1985, 85.

130 F. Fyfield and D. Kealy, *Analytical Chemistry 3rd Ed.*, Blackie, London, 1990.

131 A. J. Arce, *personal communication*,1997.

132 C. Whittaker, PhD thesis, University of London, 1994.

133 S. R. Drake and P. A. Loveday, *Inorg. Synth.*, 1990 **28**, 230.

134 B. F. G. Johnson, J. Lewis and D. A. Pippard, *J. Chem. Soc., Dalton. Trans.*, 1981, 407.

135 G. A. Foulds, B. F. G. Johnson and J. Lewis, *J. Organomet. Chem.*, 1985, **296**, 147.

136 "Collect" data collection software, Nonius B., 1998.

137 Z. Otwinowski and W. Minor, Processing of X-ray Diffraction Data Collected in Oscillation Mode, *Methods in Enzymology*, Volume 276: *Macromolecular Crystallography*, Eds. C. Carter and R. Sweets, Academic Press 1997, Part A, 307.

138 SHELX-97, G. M. Sheldrick, University of Göttingen, 1997.

139 A. J. Deeming, S. Hasso and M. Underhill, *J. Chem. Soc., Dalton Trans.*, 1975, 1614.

140 R. Gobetto, *personal communication*, 1999 and results presented to the TMR group meeting, Torino, Italy, 1999.

141 R. Calvert, J. R. Shapley, A. Schultz, J. Williams, J. Suib and S. Stucky, *J. Am. Chem. Soc.*, 1978, **100**, 620.

142 S. A. R. Knox, J. Koepke, M. Andrews and H. D. Kaesz, *J. Am. Chem. Soc.*, 1975, **97**, 3942.

143 A. J. Deeming, D. Nuel and Y. Fuchita, *Unpublished Results*.

144 J. R. Shapley, J. B. Keister, M. R. Churchill and B. DeBoer, *J. Am. Chem. Soc.*, 1975, 4146.

145 S. Brown and J. Evans, *J. Chem. Soc. Dalton Trans.*, 1982, 1049.

146 M. Koike, D. H. Hamilton, S. R. Wilson and J. R. Shapley, *Organometallics*, 1996, **15**, 4930.

147 B. F. G. Johnson, J. Lewis and P. Kilty, *J. Chem. Soc. A.*, 1965, 2859.

148 M. R. Churchill, F. Hollander and J. Hutchinson, *Inorg. Chem.*, 1977, **16**, 2697.

149 S. Aime, D. Osella, L. Milone and E. Rosenberg, *J. Organomet. Chem.*, 1981, **213**, 207.

150 M. R. Churchill and B. DeBoer, *Inorg. Chem.*, 1977, **16**, 2397.

151 C. A. Tolman, *Chem. Rev.*, 1977, **77**, 313.

152 R. Pearson and C. Kresge, *Inorg. Chem.*, 1981, **20**, 1878.

153 C. P.Lau, C. Y. Ren, C. H. Yeung and M. T. Chu, *Inorg. Chim. Acta.*, 1992, **191**, 21.

154 M. Koike, D. G. VanderVelde and J. R. Shapley, *Organometallics*, 1994, **13**, 1404.

155 J. B. Keister and J. R. Shapley, *J. Am. Chem. Soc.*, 1976, **98**, 1056.

156 A. A. Koridze, P. Petrovskii, S. Gubin, and E. Fedin, *J. Organomet. Chem.*, 1975, **C26**, 93.

157 A. Bax, R. H. Giffrey and B. L. Hawkins, *J. Mag., Reson.*, 1983, **55**, 301.

158 L. Müller, *J. Am. Chem. Soc.*, 1979, **101**, 4481.

159 G. Henrici-Olivé and S. Olivé, *Angew. Chem. Int. Ed. Eng.* , 1971, **83**, 121.

160 B. R. Bender, M. Koller, D. Nanz and W. von Philipsborn, *J. Am. Chem. Soc*,

1993, **115**, 5889.

161 V. Tedesco and W. von Philipsborn, *Organometallics*, 1995, **14**, 3600.

162 M. Koller and W. von Philipsborn, *Organometallics*, 1992, **11**, 467.

163 H. Bönnman, W. Brijoux, R. Brinkmann, W. Meurers, R, Mynott, T. Egolf, W. von Philipsborn, *J. Organomet. Chem.*, 1984, **272**, 231.

164 M. E. Dowler, T. X. Le, P. DeShong W. von Philipsborn, M. Vöhler and D. Rentsch, *Tetrahedron*, 1993, **49**, 5673.

165 E. J. M. Meier W. Koźmiński, A. Linden, P. Lustenberger and W. von Philipsborn, *Organometallics*, 1996, **15**, 2469.

166 A. Wojcicki, *Adv. Organomet. Chem.*, 1973, **11**, 87.

167 N. Ramsey, *Phys. Rev.*, 1950, **78**, 699.

168 G. Webb, in *NMR of Newly Accessible Nuclei,* Academic Press, ed. P. Laszlo, N.Y., 1993, **1**, 79.

169 J. Mason, In *Multinuclear NMR,* Plenum Press, N.Y., 1987.

170 A. Popple. *J. Chem. Phys.* 1962, **37**, 53.

171 A. G. Bell, W. Koźmiński, A. Linden and W. von Philipsborn, *Organometallics,* 1996, **15** 3124; R. Benn, H. Brenneke, E. Joussen, H. Lehmkuhl and F. Lopéz Ortiz, *Organometallics*, 1990, **9**, 756.

172 C. Brevhard and P. Grainger, Handbook of Multinuclear NMR, Wiley: N.Y., 1981.

173 W. Koźmiński and W. von Philipsborn, *J. Magn. Reson. A.*, 1995, **116**, 262; D. Nanz, A. Bell, E. Meir, V. Tedesco and W. von Philipsborn, *Bruker*

Report, 1996, **143**, 29

174 G. A. Morris and R. Freeman, *J. Am. Chem. Soc.* 1979, **101**, 760.

175 R. Benn and C. Brevhard, *J. Am. Chem. Soc.*, 1986, **108**, 5622.

176 W. Willker, D. Leibfritz, R. Kerssebaum and W. Bermel, *Magn. Reson. Chem.*, 1993, **31**, 287.

177 Andrew Cadman, *Personal Communication*, Bruker, Switzerland, 1997.

178 A. Bax, *J. Magn. Reson.*, 1983, **52**, 76.

179 S. Berger, T. Fäcke, R. Wagner, *Magn. Reson. Chem.*, 1996, **34**, 4; L. D. Sims, L. R. Soltero, G. E. Martin, *Magn. Reson. Chem.*, 1989, **27**, 599.

180 M. J. Stchedroff, S. Aime and E. Nordlander, *Unpublished Results,* 1999.